2020

ENERGY CONSUMPTION AND SAVINGS ANALYSIS OF A PHEV IN REAL WORLD DRIVING THROUGH VEHICLE CONNECTIVITY USING VEHICLE PLATOONING, BLENDED MODE OPERATION AND ENGINE START-STOP OPTIMIZERS

Pruthwiraj Santhosh
Michigan Technological University, psanthos@mtu.edu

ENERGY CONSUMPTION AND SAVINGS ANALYSIS OF A PHEV IN REAL WORLD DRIVING THROUGH VEHICLE CONNECTIVITY USING VEHICLE PLATOONING, BLENDED MODE OPERATION AND ENGINE START-STOP OPTIMIZERS

By

Pruthwiraj Santhosh

A REPORT

Submitted in partial fulfillment of the requirements for the degree of

MASTER OF SCIENCE

In Mechanical Engineering

MICHIGAN TECHNOLOGICAL UNIVERSITY

2020

This report has been approved in partial fulfillment of the requirements for the Degree of MASTER OF SCIENCE in Mechanical Engineering.

Department of Mechanical Engineering-Engineering Mechanics

Report Advisor: *Dr. Darrell L. Robinette*

Committee Member: *Dr. Jeffrey D. Naber*

Committee Member: *Dr. Bo Chen*

Department Chair: *Dr. William W. Predebon*

Contents

List of Figures

List of Tables

Author Contribution Statement

This report contains a technical paper presented at the 2020 SAE World Congress. The contributions of authors to the paper are presented below:

Morgan, C., Robinette, D., Santhosh, P., and Bloom-Edmonds, J., "Utilization of Vehicle Connectivity for Improved Energy Consumption of a Speed Harmonized Cohort of Vehicles," SAE Technical Paper 2020-01-0587, 2020, https://doi.org/10.4271/2020-01-0587.

C. Morgan and D. Robinette conceptualized and designed the experiment. The paper reports three different sets of experiments. P. Santhosh and J. Bloom-Edmonds conducted experimentation and data acquisition for one set of tests. P. Santhosh processed and analyzed the acquired data for this set. C. Morgan drafted the manuscript and D. Robinette provided critical feedback and contributed to the revision of the manuscript. Only the results of the set of experiments to which P. Santhosh contributed is included in this report.

Acknowledgments

Pursuing a Masters degree at Michigan Tech has been equally exciting and challenging for me. It made me push the limits of my abilities and emerge with a whole new outlook on facing and solving problems. A number of people played a major role in helping me achieve this.

First and foremost, I am indebted to my advisor Dr. Darrell Robinette for guiding me through this endeavor and also for believing in me. Christopher Morgan for entrusting me with one of the most exciting vehicle testing processes. Neeraj Rama, for laying the foundation for most of the work I did. Joshua Orlando and Joe Oncken for helping me find solutions to some of the technical problems encountered in the project. John Bloom-Edmonds and Ahammed Basha Dudekula for being my test partners. I would also like to thank my committee members, Dr. Jeffrey Naber and Dr. Bo Chen, for their time and effort in helping me improve my work. Brandon Narodzonek, my colleague on the NEXTCAR team, for his support.

I want to acknowledge the Department of Energy's (DoE) Advanced Research Projects Agency - Energy (ARPA-E) and General Motors for providing financial and technical support for the NEXTCAR Project. Also, the Advanced Power Systems Labs at Michigan Tech for allowing the usage of its resources for this project.

Finally, I am indebted to all my friends, family and teachers for their unrelenting support in all my decisions and helping me become the person I am today.

List of Abbreviations

ANN	Artificial Neural Network
APS	Advanced Power Systems
ARPA-E	Advanced Research Projects Agency - Energy
BEV	Battery Electric Vehicle
CACC	Cooperative Adaptive Cruise Control
CAFE	Corporate Average Fuel Economy
CAN	Controller Area Network
CD	Charge Depleting
CFD	Computational Fluid Dynamics
CS	Charge Sustaining
DEFCO	Deceleration Fuel Cut Off
DoE	Department of Energy
DP	Dynamic Programming
ECMS	Equivalent Consumption Minimization Strategy
EPA	Environmental Protection Agency
EV	Electric Vehicle
FG	Fixed Gear Ratio
FTP	Federal Test Procedure

GPS	Global Positioning System
HER	High Extended Range
HEV	Hybrid Electric Vehicle
HMI	Human Machine Interface
HWFET	Highway Fuel Economy Driving Schedule
ICE	Internal Combustion Engine
LER	Low Extended Range
LIDAR	Light Detection and Ranging
MPC	Model Predictive Control
MPG	Miles per Gallon
MPGe	Miles per Gallon equivalent
MTU	Michigan Technological University
MTUDC	Michigan Technological University Drive Cycle
NEDC	New European Drive Cycle
NEXTCAR	Next-Generation Energy Technologies for Connected and Automated On-Road Vehicles
NHTSA	National Highway Traffic Safety Administration
NMPC	Non-linear Model Predictive Control
NYCC	New York City Cycle
PHEV	Plug-in Hybrid Electric Vehicle
PMP	Pontryagin's Minimum Principle

RDE	Real Driving Emissions
R-MTUDC	Reverse MTU Drive Cycle
SC03	Southern California 03
SOC	State of Charge
UDDS	Urban Dynamometer Driving Schedule
V2C	Vehicle to Cloud
V2I	Vehicle to Infrastructure
V2V	Vehicle to Vehicle
V2X	Vehicle to Everything

Abstract

This report presents an analysis on energy consumption of a Gen II Chevrolet Volt PHEV and its energy savings potential in Real World Driving scenarios with the help of vehicle connectivity. The research on the energy consumption analysis and optimization using connectivity will focus on four main areas of contribution which includes 1.) vehicle testing on a pre-defined drive cycle and alternative routing near the Michigan Tech campus and APS research center that is a continuation of previous students' works, 2) the energy savings potential of vehicle platooning and various vehicle platoon configurations, 3) the updating of a PHEV implementation of a charge depleting-charge sustaining energy blending optimization algorithm and 4) the development of an IC Engine start-stop prediction algorithm for HEV and PHEV's using connectivity data. The first part of the report discusses the development of a Real World Drive Cycle called Reverse MTU Drive Cycle which is the successor of MTU Drive Cycle, a drive cycle previously developed local to the Michigan Technological University. The energy consumption of the PHEV on the R-MTUDC is analyzed and the baseline characteristics of the drive cycle is setup. A set of baseline drive cycle characteristics was developed and tests on the drive cycle proved that the energy consumption on the real-world drive route is consistent with variability less than 3%. The next part of the report investigates the energy savings potential of the cars when they are travelling in a platoon rather than independently. Various tests have

been conducted to investigate energy savings under different platoon scenarios, like variable gap settings, variable speeds, inclusion of a vehicle with aero-modifier and effect of moving collinearly in a platoon. A platoon wide savings as high as 8.3% was achieved in the study. After that, the report discusses the on-road implementation of a Route Based Blended Mode Optimizer, in PHEVs, which comes up with an optimal control matrix using Dynamic Programming and Cost-To-Go matrix, to make use of the Hold mode capability of the Volts, to operate the cars in Charge Sustaining mode at sections of Drive Cycles where it is most efficient to be operated. Upto, 5% savings in energy was obtained using the optimizer. Some of the runs didn't provide the desired results and this is also investigated. Finally, the report presents the development of two kinds of Engine Start-Stop Optimizers, which utilizes vehicle connectivity and vehicle energy consumption model to come up with an optimal control map of regions on the predicted driving route where the engine should be turned On and Off for minimising energy consumption in HEVs and PHEVs. The first optimizer uses vehicle and route characteristics to predict engine starts and stops and then optimizes these signals based on decisions made from energy calculations. The second optimizer uses Dynamic Programming to create a matrix of engine On and Off signals based on route characteristics. These controllers are shown to provide energy savings as high as 8% on some routes.

Chapter 1

Introduction

In the past couple of decades, since the movement for reducing the human impact on environment and climate change took off, various regulatory agencies worldwide has implemented stringent programs and goals to reduce Green House Gas emissions and dependency on depleting oil reserves. The beginning of the US emissions regulatory move can be traced back to 1965 with the passing of 'Motor Vehicle Air Pollution Control Act' and the 'Environment Protection Agency (EPA)', the primary organization in the US responsible for emission regulations, was officially set up in 1970 [5].

In US, the EPA and NHTSA has set up a system called Corporate Average Fuel Economy (CAFE), by which each vehicle manufacturer must meet an average fuel

economy for its entire fleet of vehicles or otherwise attract penalties. Figures 1.1 and 1.2 show the emission targets of some of the world's countries. The European Union has set goals to reduce CO_2 emissions from cars by 37.5% by 2030 compared to 2021 levels [6]. While, India is also set to adopt the Bharat Stage VI emission regulations in April of 2020, which will align the country's emission standards with that of Europe's [7].

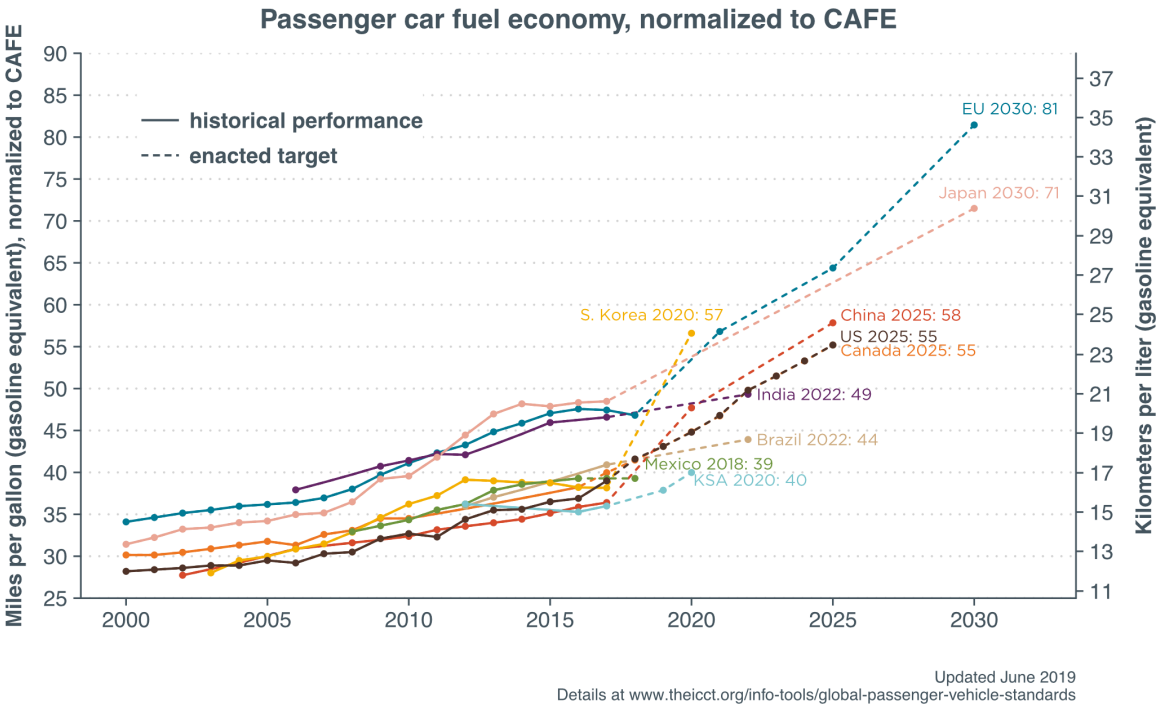

Figure 1.1: Historical and Target Emission standards for passenger cars of major countries normalized to CAFE [1]

Most of the agencies responsible for emissions certification tests the vehicle under different drive cycles. US's EPA uses different drive cycles to simulate different driving conditions like the Urban Dynamometer Driving Schedule (UDDS) for city driving conditions, the Federal Test Procedure (FTP), the Highway Fuel Economy Driving

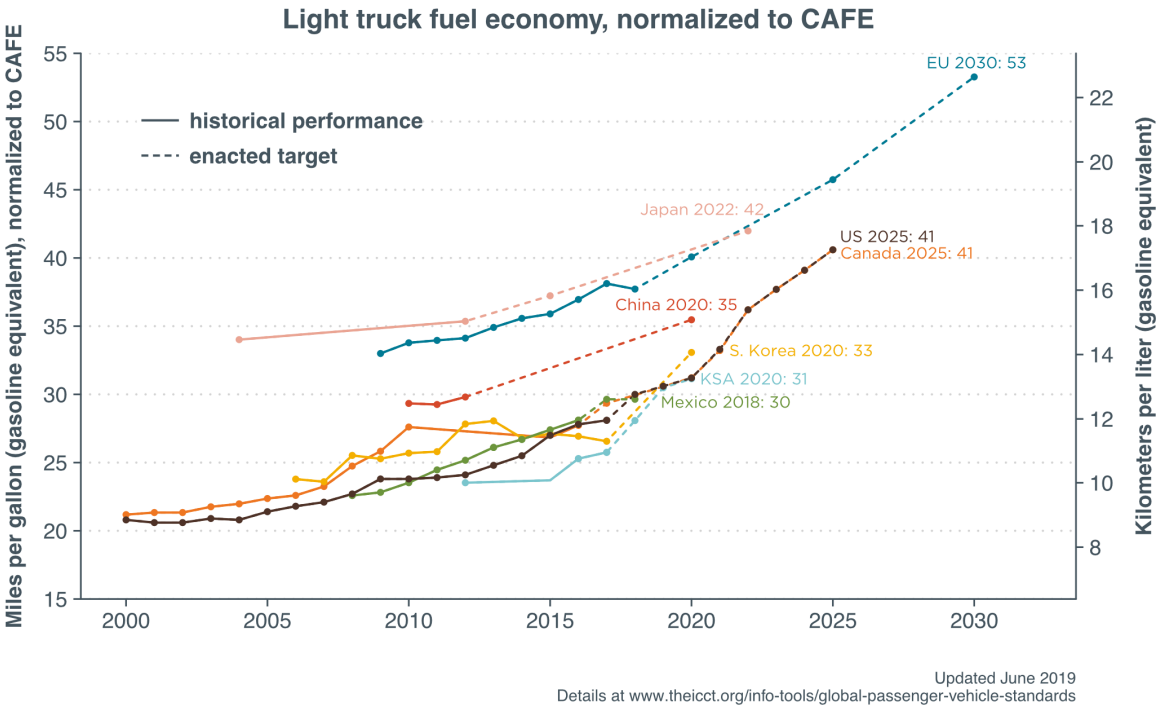

Figure 1.2: Historical and Target Emission standards for Light Trucks of major countries normalized to CAFE [1](Image Source License: https://theicct.org/legal, Creative Commons Attribution-ShareAlike 3.0 Unported License.)

Schedule (HWFET) to represent highway driving conditions under 60 mph, the New York City Cycle (NYCC) for low speed stop and go conditions, the US06 drive cycle for high speed (above 60 mph) and aggressive driving style and the SC03 drive cycle to represent driving in hot weather conditions [8]. Since these drive cycles are carried out on a dynamometer, it does not represent emissions produced on road. The fuel economy numbers from these test cycles might not be achievable in real world driving scenarios, since the driving conditions are predefined and vehicles can be prepared for that. So, a new set of emission testing procedure has been proposed which is called

the Real Driving Emissions (RDE) Test. In this method, the vehicle is tested on-road and is certified only if the emissions are within a threshold. Europe has started implementing the RDE test along with their traditional New European Driving Cycle (NEDC) [9][10][11].

All these targets and regulations means that the average energy consumption per mile for a passenger car or light truck must go up drastically in the near future. In order to meet these increasing demands, the industry has moved towards electrification of the vehicle powertrain since electric motors complements the shortcomings of an Internal Combustion (I.C) Engines. There are mainly two kinds of vehicles with electrified powertrain in the market – Battery Electric Vehicles (BEVs) and Hybrid Electric Vehicles (HEVs).

A BEV has a fully electrified powertrain, i.e. it does not have an I.C engine. Compared to I.C engines, an electric motor is more efficient and has a high starting torque and consumes very less energy during idling. But, these vehicles have lesser range because of its batteries' limited energy storage capacity and has to carry around heavy batteries because of its lesser energy density and once the batteries are depleted, it would take hours to recharge it. Also, the electric motors' efficiency starts decreasing at higher vehicle speeds. Even though solutions to these problems are being developed, it may not be fast enough to match the regulations of the near future. While, an HEV is a vehicle that derives power from both an in-house battery as well as an

I.C engine. It takes the best of a traditional vehicle and a BEV and combines it. Most of the HEVs are designed such that it can run on its I.C engine alone after the battery has been depleted, hence it does not have to carry heavy batteries and spend long hours recharging between trips. At the same time, the electric motors assist in low speed starting and peak torque demands. The downside of an HEV is its complex powertrain architecture and cost. Hence, HEVs have the ability to meet the strict emission regulations without compromising user comfort.

The operation of e-motors and I.C engine in an HEV is governed by control algorithms. These algorithms can be rules-based algorithms, instantaneous optimization algorithms or Global Optimization algorithms. Rules based algorithms are those in which a set of operations are executed when a set of pre-defined conditions are met. These types of algorithms are comparatively easier to implement on a vehicle's system and does not require huge computational power. Instantaneous optimization algorithms try to optimize the performance of the vehicle at a particular instant based on the current operating conditions. These algorithms require more time and computational power to execute. With enough testing and experience, some of these instantaneous optimization results can be converted to rules-based algorithms. Global Optimization algorithms uses a look-ahead of what the vehicle is going to encounter in the future and optimizes the vehicle performance for the entire horizon.

Global Optimization must be done real-time and requires huge computational power

but these algorithms have the largest potential to save energy. But in order to implement these commercially, major infrastructure developments are needed which include V2V (Vehicle to Vehicle), V2I (Vehicle to Infrastructure), and V2C (Vehicle to Cloud) communication.

1.1 The NEXTCAR Project

The work presented in this report is part of Advanced Research Projects Agency - Energy's (ARPA-E) NEXTCAR project (Next-Generation Energy Technologies for Connected and Automated On-Road Vehicles) funded by the Department of Energy (DoE). The project's aim is to reduce the energy consumed by individual, group or entire fleet of vehicles through the use of vehicle connectivity to optimize powertrain and vehicle dynamics performance [12]. The ultimate goal of this project is to develop vehicle technologies that would improve fuel efficiency by 20% and electric range by 6%. The idea is to use real-time road and traffic data for a foreseeable future, obtained through V2X communication, and use that data for energy optimization using Optimal Mode Selection, Eco Approach and Departure at traffic lights and stops, Optimal Powersplit Mode, Eco Routing, Optimal Engine On/Off Strategies and Vehicle Platooning.

The Michigan Tech NEXTCAR team is working with General Motors to achieve

these goals for HEVs and for this, a fleet of four Chevrolet Gen II Volts have been instrumented with dSpace MicroAutoBox II – "a real-time system for performing fast function prototyping" [13], to tap into the vehicles' bus signals for obtaining real-time data as well as sending control signals. The MicroAutoBox was interfaced with laptops on-board the vehicles through dSpace ControlDesk – a flexible software that can be used for synchronized data collection and instrumentation [14].

1.2 Chevrolet Gen II Volt

The Chevrolet Volt II is a Plug-in HEV (PHEV), which has the capability to run as a BEV with full vehicle capabilities until the batteries are drained. Compared to the first generation of Volts, the new Volts have a larger battery pack of 18.4 kW-hr energy which translates to increased EV range.The propulsion system of the Volts is made up of two motor-generators and an Engine connected to the axle via two planetary gear-sets. One of the motors and engine is connected to the first planetary gear and the second motor is connected to the second gear-set. Both these gear-sets are connected to the axle of the vehicle and there are clutch three clutches – one of which is used to connect or disconnect the engine from the gear-set. One is used to ground the ring gear of the second gear-set and the other one is used to connect or disconnect the sun gear of the 1st set with the ring gear of the second. This combination of motors, engine and gear-sets allows the vehicle to operate in five

different modes. Since, the Drive Ratio between the wheels and the engine is not fixed, the engine is independent of the wheels to operate at an efficient region [2].

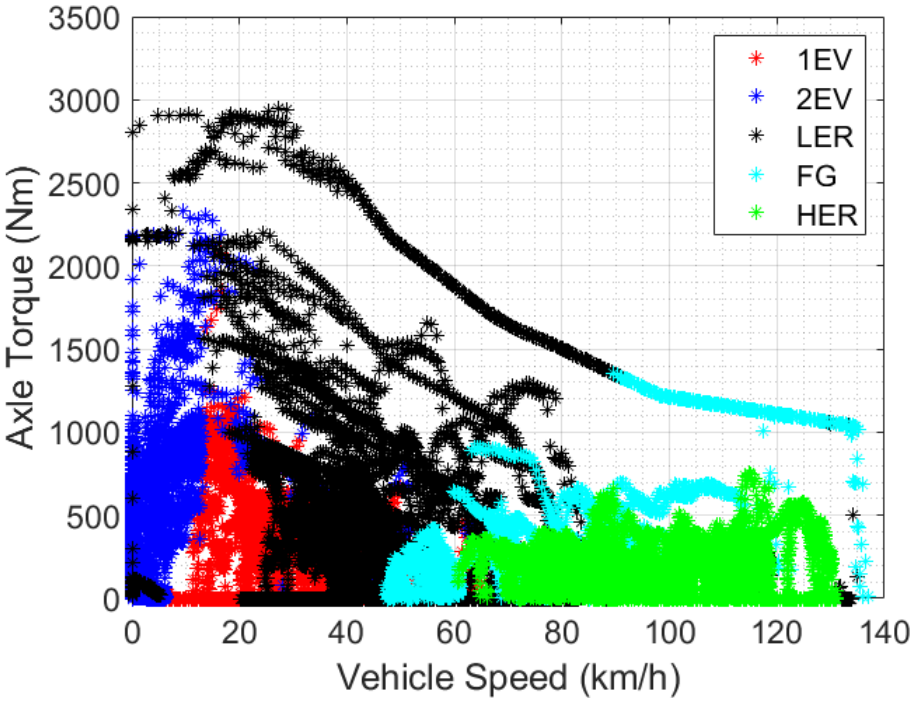

Figure 1.3: VOLT II operating modes in Charge Sustaining mode operation obtained during vehicle testing [2] [3]

The different operating regions of each mode during the Charge Sustaining Operation are are shown in Figure 1.3 Two of the five modes are EV modes and the rest are blended modes. Each of these modes are designed to operate the propulsion system at high efficiency for different driving scenarios. The 1-motor-EV mode is used when the vehicle is operating under light load conditions. When the load is higher in EV mode, the second motor will kick in to assist the first one . The rest of the three modes are reserved for charge sustaining operation when the engine is ON. The Low Extended Range (LER) Mode is used when a high axle torque is required at lower

vehicle speeds. One of the motor acts as a generator in this mode. The Fixed Gear Ratio Mode is selected for moderate axle loads and moderate speed conditions. In this mode, one of the gears in each planetary gear-set is grounded providing a fixed gear reduction. One of the motor is grounded and the other can act as a motor or generator depending on the driving conditions. The last mode is called High Extended Range (HER), which is used when the axle load demand is low and vehicle which is typical highway cruising. In this mode,the engine primarily provides the power to the wheels and the speed of one of the motors can be adjusted to maintain the engine at an optimal speed and torque [2].

The rest of the report discusses what the major technologies being developed in this field are and the methods that they follow, the experiments conducted as part of this research and the setups used, the results of the experiments conducted and conclusions and opportunity for improvement in this field.

The studies explained in this report can be divided into four.

1. First, the development and energy consumption analysis of a Real-World Drive Cycle is reported. I was involved in testing and processing the data collected from these tests.

2. Next, a preliminary investigation into the energy savings potential of vehicle platooning is conducted. In this study also, I was involved with conducting the

tests and processing and analyzing the data collected. A more detailed study in this section will be conducted in the future.

3. The next part deals with the testing of a route based blended mode optimizer. The optimizer was developed by students who were previously involved with the NEXTCAR project at Michigan Technological University. My job was to extract the Optimal Control Matrix from the optimizer and implement it in the vehicles as a lookup table with distance travelled and SOC as the breakpoints. In previous years, the output of the optimizer was input as a 1-D vector with only distance as the breakpoints. After this task was completed, on-road testing was conducted.

4. Finally, the report discusses the development of two kind of Engine Start-Stop Optimizers and its testing on different routes for energy savings.

Chapter 2

Literature Review

Connected Vehicle Infrastructure and Technologies are developing at a fast rate worldwide. The greatest advantage of vehicle connectivity is that the vehicle will be aware of the conditions it is about to encounter and can prepare for that ahead of time. One of the major application of Connected Vehicle Technology is its use to reduce the energy consumption of HEVs by coming up with an Energy Management Strategy using the road conditions and traffic data ahead of it.

2.1 Blended Mode Optimization in HEVs

Most of the research related to Connected Vehicle Technology focuses on optimal blended mode operation of engine and e-motors. In case, a look ahead of the driving conditions is not available, a control strategy of instantaneous optimization has to be adopted. Such a method is discussed in [15]. In this method, cost function is developed as a function of the sum of fuel energy and electrical energy. The electrical energy has a weighting factor called equivalence factor to make it equivalent to fuel energy. The equivalence factor is modelled as a variable which depends on the probability of charging or discharging and current driving conditions. The Equivalent Consumption Minimization Strategy (ECMS) is applied using the equivalence factor to the find the optimal operating points. If a look ahead of the driving conditions are available, this method can be extended to a Global Optimization level.

If the vehicle have limited connectivity like GPS location, another type of Energy Management Strategy can be applied as discussed in the literature [16]. It is to use Dynamic Programming to find the operating cost of the powertrain at all instances, when the driving conditions is divided into four kinds on the basis of average speed of the vehicle and congestion on the road. For each of these condition and based on the distance to be driven, optimal control strategies are extracted from the output of DP. The current driving condition is determined using a method called K-means

clustering and GPS data is used for to find the distance to the end of the trip. With these two inputs an optimal control strategy is selected which controls the the gear ratio, engine torque output and motor torque output for maximum efficiency. This method of optimization can be applied wherever a modern connectivity infrastructure does not exist. The only external data this algorithm requires is the GPS location of the vehicle and the distance to its destination. The method does not take in to account the terrain of the road ahead, which is a major contributing factor.

A forward looking algorithm is described in [17], in which Pontryagin's Minimum Principle (PMP) is applied to a global optimization problem to obtain a locally optimized solution. The cost function is defined as the sum of CO_2 emitted, from I.C Engine emissions as well as that from electrical energy used from the grid. A Hamiltonian function is derived from the cost function and its minimization leads to optimal solution of the problem. But this method is very computationally demanding and implementing it real-time will be a challenge. As in other cases, with prior knowledge of the driving conditions, optimal control maps can be obtained and implemented in the vehicle.

A different approach to developing an Energy Management Strategy can be found in [18]. This paper proposes a non-model based development of Energy Management Strategy using Artificial Neural Network (ANN). It uses the Pontryagin's Minimum Principle (PMP) to derive the Equivalent Consumption Minimum Strategy (ECMS).

The authors used randomly selected velocity profiles of a particular route to train the neural network with three input variables – the power demand, state of charge and the ratio of distance to be travelled to the total distance. The network was trained for different initial SOCs.The neural network came up with a co-state factor that would determine the power distribution between the motor and the engine. Once, these networks were trained for a particular route, it could provide the co-state values at each instant based on the inputs. Once the neural networks are trained, this method will be faster than Dynamic Programming. The downside of this method is that it cannot adapt to unforeseen changes in traffic conditions. In this method also, the road is assumed to be flat and elevation is ignored.

Using the Dynamic Programming Approach to implement real-time optimal control strategy was considered impractical due to the computational load and lack of predictability of future driving conditions. But with the recent developments of vehicle control units and V2X technologies, these restrictions can be overcome. A method for real-time application of DP to extract optimal control strategy is discussed in [19] using prior knowledge of the drive cycle. The idea in this paper is to use DP to extract an SOC trajectory against distance travelled based on future route speeds and elevation information. Once this SOC trajectory is known, the vehicle's controller will optimize the operating points of engine and e-motor to follow the desired SOC trajectory. The control strategy can be updated real-time if there is a change in the predicted drive cycle.

With a preview of the drive cycle available to the controller, another method is illustrated in [20]. The proposed method is to use the ECMS approach to find the instantaneous optimal operating points. The equivalence factor used for local ECMS at each instant will be determined by processing the future driving conditions. Two methods are proposed to determine the Equivalence Factor. One is to use backward DP and the other is to use backward ECMS with the final SOC set at desired SOC and working backwards to find the equivalence factor to follow the desired SOC trace.

The paper [21], describes the development of a real-time control policy using Dynamic Programming and Linear regression process to come up with optimal operating controls for the engine and two motors for a power-split PHEV like Toyota Prius. The first part of the study is to use the Dynamic Programming method to come up with optimal control trajectories so that the combined cost of electrical and fuel energy is minimized for a given drive cycle. Once, the optimal solution is obtained, the control states (Torque of engine and the two motors) are formulated as a linear combination of the demanded force and the system states. The coefficients of these states are then determined using a process called least squares minimization. In this process, the coefficients are adjusted such that the difference between values of the control variables from the linear regression model and those from the optimal solution obtained from Dynamic Programming, is minimum. Once, the coefficients are determined this linear model is used to obtain the near optimal solution based on the demanded power and system states.

2.2 Speed Harmonization and Vehicle Platooning

At higher vehicle speeds, aerodynamic drag is the largest contributor to the resistive forces faced by the vehicle. A major contributing factor to this drag is the shape of the car. More streamlined cars face lesser aerodynamic drag. If one vehicle is closely following another vehicle, this aerodynamic drag is greatly reduced for the trailing vehicle. Also, a region of high pressure is formed between these two vehicles, which slightly assist the leading vehicle in its motion. This phenomenon is the principal idea behind vehicle platooning for energy savings. To implement this technology into the market, the vehicles in the platoon needs to be communicating regularly among each other about the vehicle status. All the vehicles would also need information about the driving conditions ahead to prepare for driving maneuvers it will encounter in the future.

A social problem may also arise during vehicle platooning, which is addressed in [22]. Since, different cars have different dimensions, the savings may not be equally distributed. Also, vehicles at different positions in the platoon will have different savings. [22] describes a method to allocate savings to all vehicles in a platoon equally in order to avoid conflict of interest.

Since CACC, introduces a level of autonomy into the vehicles, a lot of control problems

needs to addressed. Protocols and control algorithms are needed for creation of a platoon, leaving a platoon, preparing for unforeseen scenarios etc. [23]. The literature [23] presented a two stage controller by which cars can join a platoon by reducing the gap between vehicles and once the vehicles have approached the desired gap a gap regulation controller takes control and maintains the gap. Instead of following a fixed gap for all speeds, a constant time-gap between vehicles is maintained by the controller. This means that the gap between two vehicles will be a function of speed and the set time. This system uses vehicle connectivity to communicate between vehicles in the platoon about the target speeds of the leading vehicle and desired gaps and the controller ensures platoon stability using this knowledge. The authors have also implemented and successfully tested these controls on four production cars.

Another study [24], presents a Cooperative Adaptive Cruise Controller based on non-linear Model Predictive Control approach which optimizes the gap reduction between vehicles and velocity profile smoothing to minimize the energy consumption. Most CACCs try to follow a reference trajectory, but, in this literature a trade-off between following a reference trajectory rigorously and maintaining a less gap between vehicles are achieved. A rigorous following of a reference velocity trajectory will lead to losses in the powertrain. The Model Predictive Controller, has a lookup of the lead vehicle velocity trajectory which is smoothed to reduce transients and but maintains the vehicle within a safe distance to reduce energy consumption due to aerodynamic losses.

A similar study to [24], is found in [25]. In this study, the NMPC model is applied to 2-vehicle platoon of Battery Electric Vehicles to minimize the energy consumption. This study tries to optimize velocity tracking and gap maintaining to maximize savings. The authors also investigate the effect of the length of prediction horizon provided to the controller on savings compared to a global optimal solution obtained from Dynamic Programming. The results of the study shows that this velocity smoothing is very effective in reducing energy consumption in low and irregular speed scenarios, since the target velocity profile is smoothed to avoid sudden transients, while at high or constant speeds, the reduction in inter-vehicular gap is preferred by the controller. But the NMPC is still less efficient compared to the Global optimal solution in transient situation. In high speed, non-transient scenarios the solution of NMPC is closer to Global Optimality. As the prediction horizon of the NMPC increases the efficiency also increases. The study suggests that the eco-CACC will be able to provide upto 40% energy savings compared to using traditional Adaptive Cruise Control Systems. This number should not be confused with the energy savings numbers of other studies, since the energy savings reported in the other studies are for constant and high speed maneuvers which does not have large and sudden velocity transients.

When it comes to energy consumption of vehicle platoons, most of the investigation of energy savings in CACC has been conducted in the case of trucks. Since, aerodynamic drag is directly proportional to the frontal area of the body in motion, trucks have a larger potential to save energy in platoons than streamlined cars. One such study is

presented in [26], where the energy savings of a 3-vehicle truck platoon was investigated under different scenarios. The energy consumption analysis were conducted at different gaps from as far as 87m to as close as 4m, while travelling at 65 mph. The tests were conducted on a test track with all the trailing trucks under CACC. The study found out that the middle truck saved the most, upto 17% at close gaps while the trailing vehicle saved the most, upto 13% at moderate gaps of 10 to 20m. On a platoon-wide scale, a maximum savings of 13% was achieved at the closest gap of 4m. The study also looked into energy consumption during variation of speed and found upto 2% reduction in energy savings in these cases. Another scenario tested was the effect of other vehicles entering and leaving the platoon, which was found to have no considerable effect on energy consumption.

A similar study was conducted in Japan for reducing CO_2 emissions [27]. In this study, a 3-truck platoon under automated control was tested at a gap of 10m travelling at 80 km/h (50mph) on an empty expressway. Along with longitudinal control, lane changing maneuvers were also conducted which led to a 14% reduction in energy consumption. Another interesting finding in this study is that the CFD simulations of the trucks travelling at a gap of 4m and 80km/h, the co-efficient of Drag for the middle vehicle is found to decrease by 50%, which would significantly reduce drag. This lines up with the findings presented in [26].

2.3 Engine Start/Stop Optimization in HEVs and PHEVs

The third section in this chapter discusses the research activities in the field of optimization of the engine starts and stops in an HEV or a PHEV through vehicle connectivity to maximize efficiency.

The article [28], proposes a control algorithm for optimizing the energy consumption of a vehicle platoon on a hilly road. The control system is divided into two layers for computational efficiency since each vehicle has five states - vehicle velocity, travelled distance, battery energy and engine state. The top layer tries to optimize the vehicle velocity and SOC trajectory for minimum energy consumption for the entire platoon on the hilly terrain using convex optimization. The top layer outputs the target velocity and battery co-state which is like an equivalence factor for battery energy. The bottom layer deals with the individual vehicles. The bottom layer optimizes the discrete control variables, which are the engine on/off state, optimal gear selection and e-motor torque, based on the output of the top layer. The bottom layer is optimized using Dynamic Programming. The bottom layer formulates a Hamiltonian based on the power split between the engine and motor. This Hamiltonian will be the cost function at each state and Dynamic Programming is used to minimize the cost. The

output of the DP will yield an optimal engine on/off strategy for each vehicle along with optimal gear selection.

In [29], an engine start/stop control strategy is described as part of a controller used to optimize the energy consumption of an HEV using Model-Based Predictive Control. The controller uses a cost function with motor and engine operating points as control variables. The MPC uses the the future speed trajectory and vehicle gear state to optimize the operating points of motor and the engine. Based, on the predicted operating points certain rules are developed to determine whether the engine should stop or start. If the required torque from an engine is less than a threshold torque for a preset period of time, the engine would be turned off. Once the engine is turned off it will remain turned off for preset time period which is determined by the engine's idling power requirement and restart energy. Similarly, once the engine is turned on it will not be turned back off until a preset time. All these control decisions can be overridden if it affects the safe operation of the vehicle.

Another study, that came out of Colorado State University uses "Nonlinear Autoregressive Artificial Neural Network" to predict the future velocity profile of the vehicle based on current GPS location and previous driving information [30]. Real World Driving data is used to train the Neural Network. During the optimization process, the GPS data and past vehicle speeds are inputted into the Neural Network which

provides a future velocity profile. This profile is inputted into a Dynamic Programming Controller which optimizes the engine operating points for the predicted velocity period. The DP controller populates a table of optimal engine power demand which is a function of time and SOC. The vehicle controller uses this table to control the engine operating points. If the optimal engine operating power demand is zero, the engine is turned off and it is turned back on only if the demanded power is above a certain threshold. The literature does not talk about assigning any penalty for turning on the engine or any time delay between an engine on and off. The time step for the simulation was one second. There is also a trade-off between the powertrain controller and the neural network. The longer the prediction horizon, more is the error in predicted velocity. But a longer prediction horizon provides a better control output from the powertrain controller. As a trade-off between these two factors, the authors chose 30 seconds as the optimal prediction horizon for the controller.

Another way of using Dynamic Programming to achieve a optimal solution is described in [31]. The authors use SOC and final gear ratio as the state variables and also assigned penalties for engine starting as a function of rotational engine speed at two consecutive time-steps. Penalties are assigned for shifting gears as well. The motor torque and selectable gear ratio is taken as the control variables. In order to ease the computational demand, the optimal solution only at reachable region of the SOC, when the initial and final SOC was fixed, was calculated. The results say that around 15% reduction in fuel consumption can be achieved with this controller.

Chapter 3

Test Setup

All the tests pertaining to this report were conducted on Gen II Chevrolet Volts. The Michigan Tech NEXTCAR team has a fleet of four instrumented Volts. These vehicles were instrumented by Pilot Systems LLC. Each vehicle was equipped with GPS sensors,four thermocouples (two for the cabin and two for the engine bay), LIDAR, anemometer and a tri-axial accelerometer for sensing road, vehicle and environmental conditions. There was also a provision for measuring the electrical load for traction and auxiliary load separately. dSpace MicroAutoBox was used for recording the CAN (Low Speed, High Speed and Powertrain Expansion Bus) signals along with time synchronous data from all the other sensors and sending it to an on-board laptop computer. The on-board laptop computer used dSpace ControlDesk to save the received data and also could display the desired vehicle parameters in real-time [4].

Among the parameters displayed, using a Human Machine Interface (HMI), the driver was also able to visualize the gap between one's car and the car infront of it, using the output from a set of LIDAR sensors. This was utilized for maintaining the vehicle to vehicle gap during Speed Harmonization Testing. The ControlDesk could also be utilized to send signals to the MicroAutoBox for switching the vehicle from Normal Mode to Hold Mode for implementing the Blended Mode Optimizer Controller.

3.1 Reverse MTUDC

Reverse Michigan Technological University Drive Cycle (R-MTUDC) is a Real-World Drive Cycle designed for the NEXTCAR project local to Michigan Technological University. This Drive Cycle is a successor to the Michigan Technological University Drive Cycle (MTUDC), which was developed as a Real World Drive Cycle to encompass different driving characteristics like change in traffic lights, congestion, also for the NEXTCAR project. The R-MTUDC as the name suggests, traverse the MTUDC in the reverse direction. Even though the driving route is the same, the road features encountered by the two drive cycles are different. Figure 3.1 shows the direction and route used for the R-MTUDC. The color of the route is indicative of the speed limits at those sections. A colorbar is provided on the right side for speed limit reference.

The R-MTUDC, Figure 3.1, starts off with Highway Driving from the APS Labs on

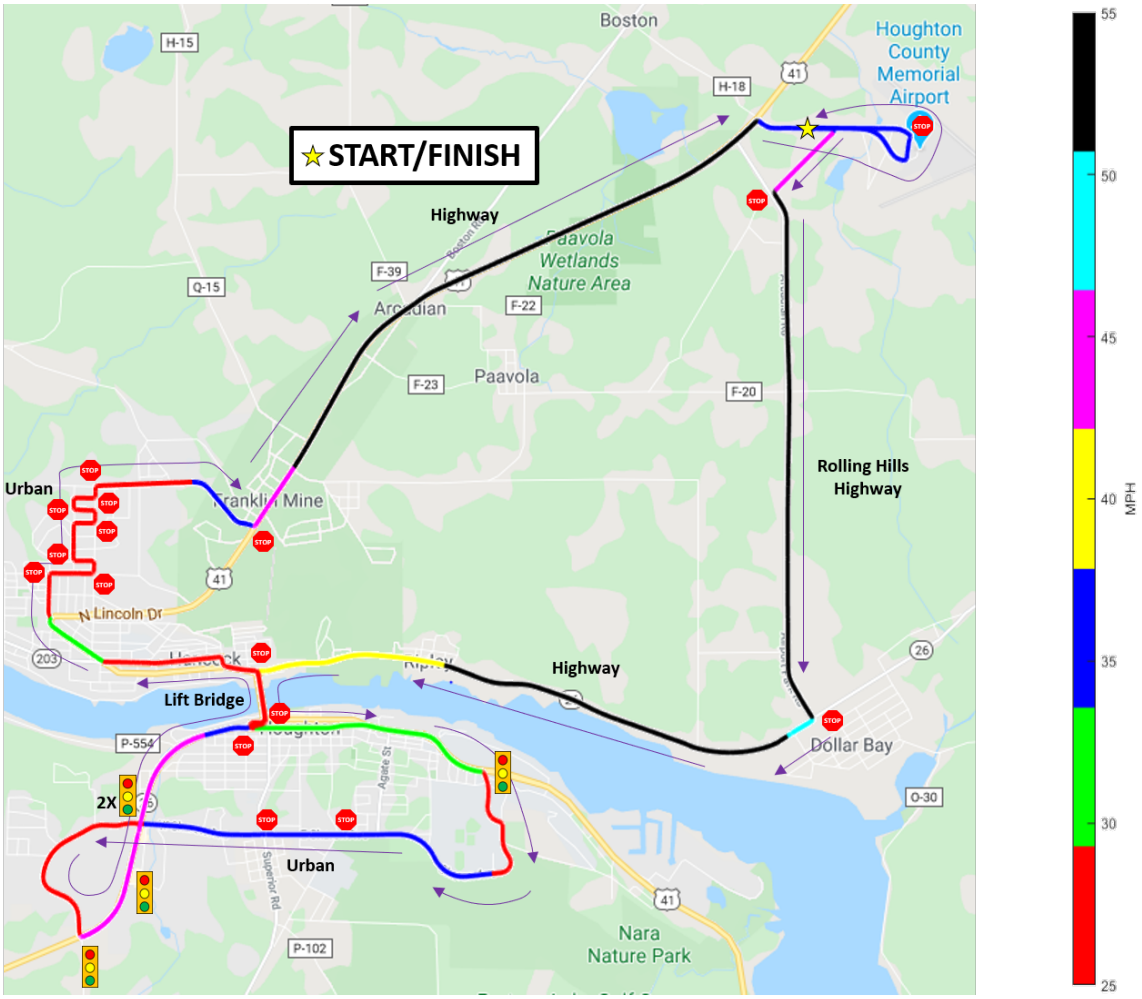

Figure 3.1: Reverse MTU Drive Cycle overlaid on a map with directions and speed limits of each section

to a 45 mph (72 km/h) to 55 mph (89 km/h) highway route. This route is a route with rolling hills which eventually ends with a downhill slope. After that, the route is of 55 mph (89 km/h) highway driving which drops down to 40 mph (64 km/h). This Highway phase is about 11 km long. After this the car crosses the lift bridge into the city of Houghton and then to Michigan Technological University where there is a traffic signal. The speeds for this region vary from 25 mph (40 km/h) to 30 mph (48 km/h). From the traffic signal the route proceeds to a residential area at

25(40 km/h) mph and then to a commercial area, with two stop signs at 35 mph (57 km/h) until it reaches another traffic signal. From this traffic signal the route goes up a hill at 25 mph and comes back down to another traffic signal on US-41. This entire urban driving is around the 20.5 km mark.

Table 3.1
Reverse MTU Drive Cycle Route Statistics

Total Distance	38.8 km
Maximum Speed	55 mph
Minimum Speed	25 mph
Maximum Elevation	362.5 m
Minimum Elevation	185.2 m
Maximum Uphill Grade	8 %
Maximum Downhill Grade	15 %
No. of Stop Signs	16
No. of Traffic Lights	5

From the traffic signal, the route goes into another commercial section at 45 mph (72 km/h), which has two traffic signals. The speed then drops to 35 mph and then to 25 mph as it crosses the bridge again, at 23.5 km, to enter the city of Hancock. On its way to the bridge, the route crosses a loop called Yooper loop which has two stop signs, once before the crossing and one after the crossing. Once in Hancock, the route proceeds at 25 mph (40 km/h) and then to 30 mph (48 km/h) and enters a residential area with multiple stops and large elevation changes at 25 mph (40 km/h). Once out of the residential area, the route continues at 25 mph(40 km/h) and then to 35 mph (57 km/h) as it reaches the stop sign on US-41 again at the 30 km mark. From there, it is purely highway driving at 55 mph (89 km/h), till it has

to turn to Airpark Boulevard at 36 km. This road has a speed limit of 35 mph (57 km/h) which has a stop sign and then ends back at the APS labs.

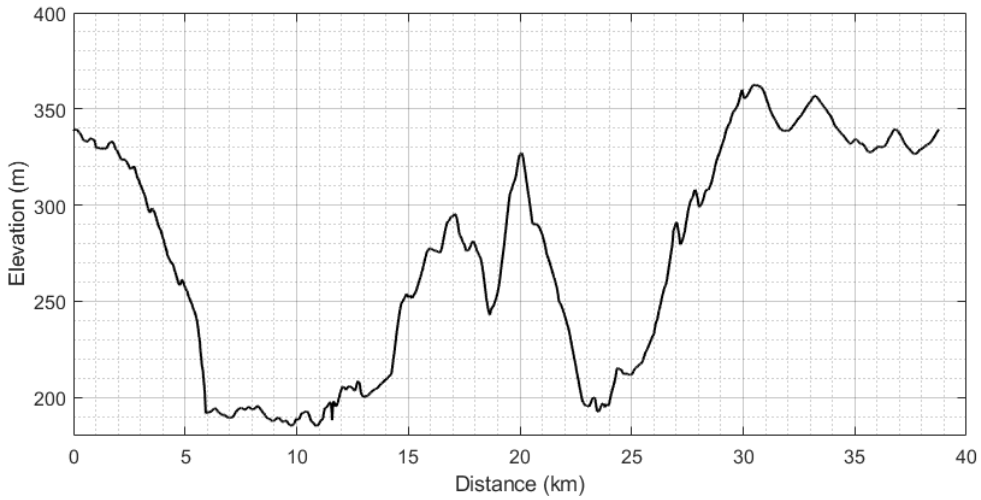

Figure 3.2: Reverse MTU Drive Cycle elevation trace traced against distance

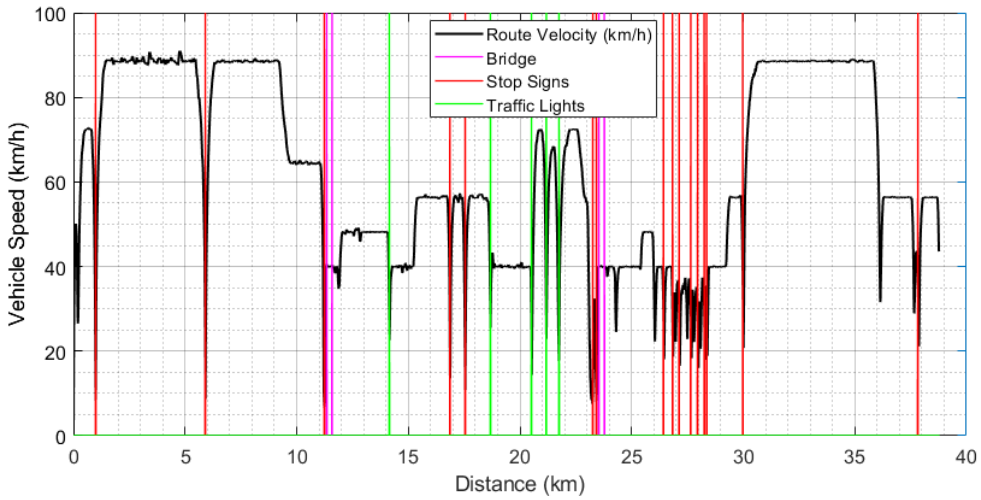

Figure 3.3: Reverse MTU Drive Cycle speed trace overlaid with traffic signals, stop signs and lift bridge gates

The typical drive cycle characteristics of the R-MTUDC is provided in Table 3.1. From the elevation and grade data, it can be inferred that a considerable amount of

gradient change occurs on the route which can also be observed in Figure 3.2. The speed trace, Figure 3.3, also confirms that the drive cycle is an inclusive one, with numerours stops, highway driving and low speed driving. The only limitation of the Drive Cycle is that it does not represent very high speed ($>$ 55 mph) highway driving. This is because none of the roads in the Houghton locality has speed limit greater than 55 mph.

The energy consumption of the vehicle can be divided into two parts – the energy consumed from the battery which can be positive (traction) or negative (Regenerative) and the energy consumed from Fuel energy. The instantaneous power from the battery can be determined using Equation 3.1.

$$P_{Batt} = (V_{Batt} \times I_{Batt}) \tag{3.1}$$

where, V_Batt and I_Batt are the instantaneous bus voltage and current of the High Voltage Battery.

The instantaneous power derived from fuel can be determined using Equation 3.2.

$$P_{Fuel} = (\dot{m}_f \times LHV_f) \tag{3.2}$$

where ($\dot{m}_f$ is the instantaneous fuel flow rate and LHV_f is 41.28 MJ/kg, which is the lower heating value of pump gasoline with an octane number of 87 [32].

The total energy consumed by the vehicle will be the sum of the battery power and the fuel power summed over the entire drive cycle time as given in Equation 3.3.

$$E_{Total} = \sum_{0}^{t_f} (E_{Batt} + E_{Fuel}) \tag{3.3}$$

Finally, the equivalent miles per gallon (MPGe) is calculated using the Equation 3.4.

$$MPG_e = \frac{Distance\ Travelled\ in\ Miles\ \times\ (31.79 * 3600)}{E_{Total}} \tag{3.4}$$

where E_{Total} is the total energy consumed in kJ.

In order to get a baseline energy consumption of the Volts on R-MTUDC and extract an average velocity profile, 30 runs on the test route was conducted. These 30 runs had the same start and end location at the APS Labs. Another set of 5 runs were also conducted, which used the same route but had five different start and end locations along the route. The different starting locations are shown in Figure 3.4, with numbers 1 to 5.

Among the 30 runs that started at APS labs, ten runs were conducted with an initial

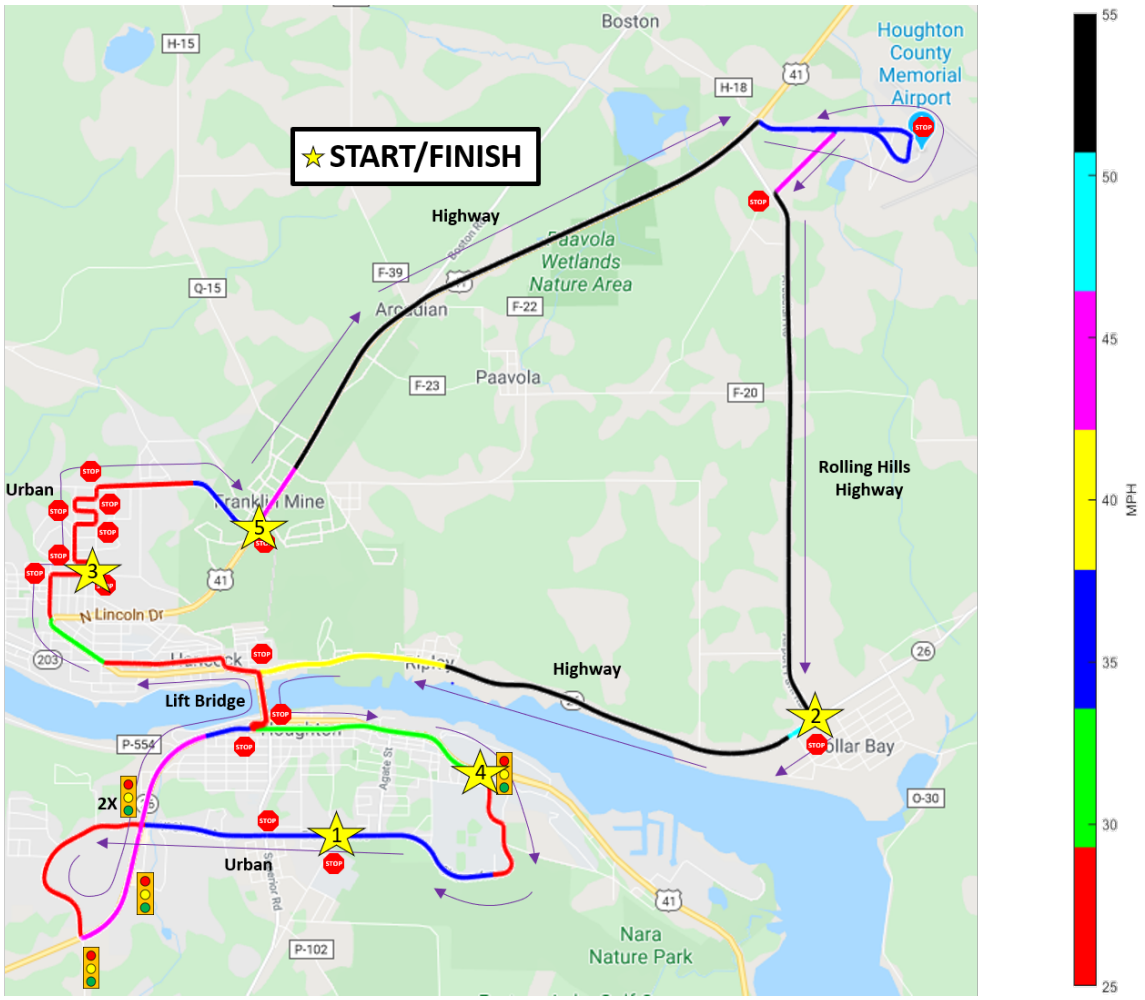

Figure 3.4: Reverse MTU Drive Cycle overlaid on a map with different start locations marked on it for Varied Start Tests

SOC between 92% and 55%, so that the car would be able to complete the entire drive cycle in EV mode. Ten runs were conducted with an initial SOC of around 16.5%, so that the car would be in Charge Sustaining Mode during the entire vehicle operation and the rest of the ten runs were conducted with an initial SOC of around 31%, so that the vehicle would be in Charge Depleting mode, around half of the time, and in Charge Sustaining Mode, the rest of the time. All the five runs that had five different starting location had an initial SOC of 31%. Another set of 10 runs were conducted

in the forward MTUDC direction with an initial SOC of 31% for comparison with the R-MTUDC CD-CS runs. These tests were conducted between 22nd May and 17th June of 2019, where the ambient temperature was between 8^{o}C and 26^{o}C and the atmospheric conditions varied between sunny, cloudy or light showers. The cars' interior and propulsion system were fully warmed up before each day's testing. The HVAC system was set to keep the cabin temperature at 22^o C (72^o F).

3.2 Speed Harmonization and Vehicle Platooning

A preliminary investigative study on energy savings potential for electric vehicles was conducted. For this, three of the four instrumented Volts (Beta 1, Beta 2 and Beta 3),shown in Figure 3.5, were used. Beta 3 had a roof rack installed on it. In order to minimize the effect of roof rack, Beta 3 was running at the end of the platoon unless necessary. The study was conducted on a nearly flat, 900 m straight stretch of road on M-203 near McLain State Park, Michigan.The test route and elevation profile of the road is shown in Figure 3.6 and Figure 3.7, respectively. The data collected for the experiments were part of the experiments conducted at the Advanced Power Systems Laboratory at Michigan Technological University.

It is evident from the map of the route that the section is a straight section and the maximum difference between the elevation of the lowest point and the highest point

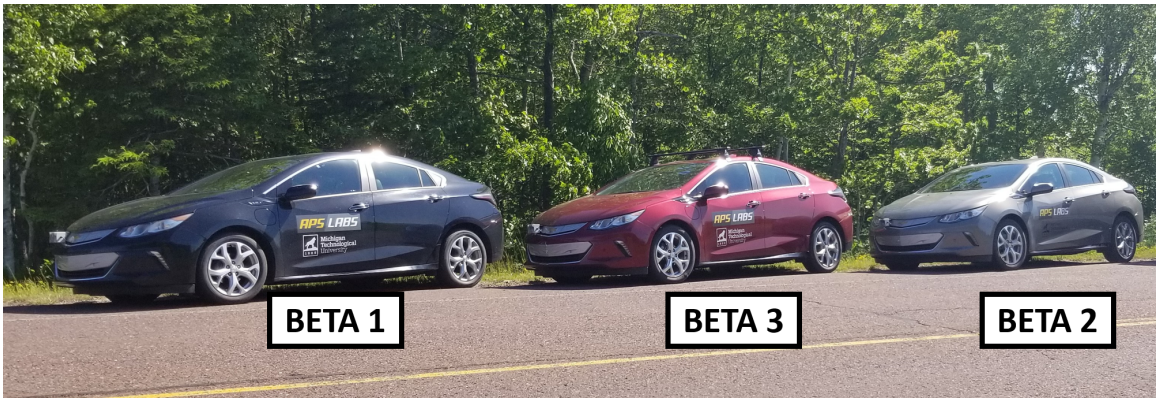

Figure 3.5: The three instrumented Volts used for Vehicle Platoon testing. From left: Beta 1, Beta 3 and Beta 2.

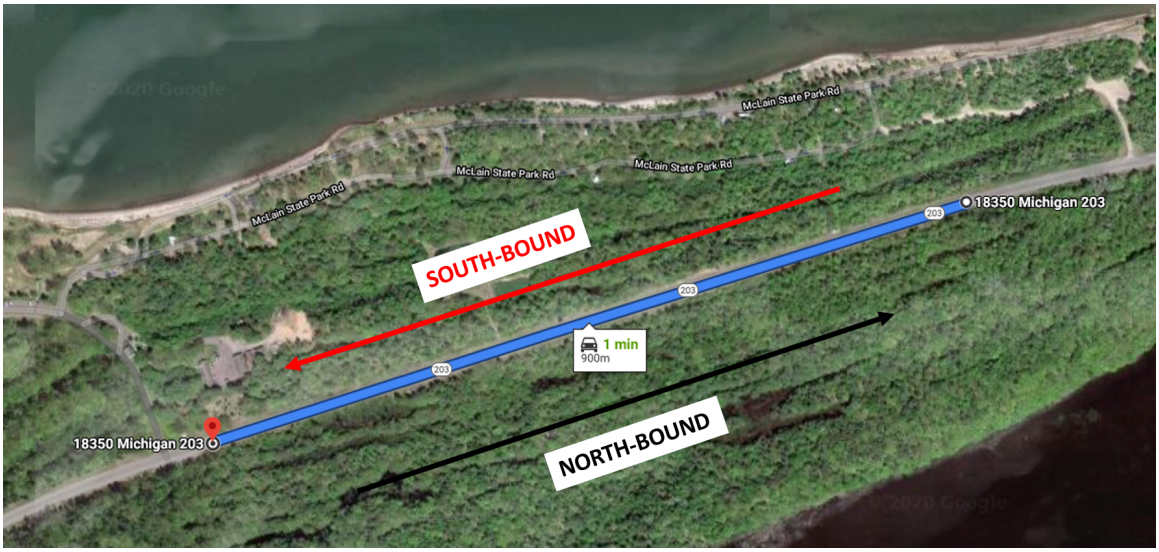

Figure 3.6: 900 m long route selected for Vehicle Platoon Testing on M-203 near McLain State Park

on the route is 0.8 m. Data was recorded for the experiment in both directions of the route - southbound and northbound - as indicated in Figure 3.6. The influence of various factors on energy consumption during vehicle platooning was investigated. The effect of vehicle gap, effect of vehicle speed, effect of the lateral position of the vehicle in a platoon and the effect of an aero-modifier on top of one of the cars were investigated.

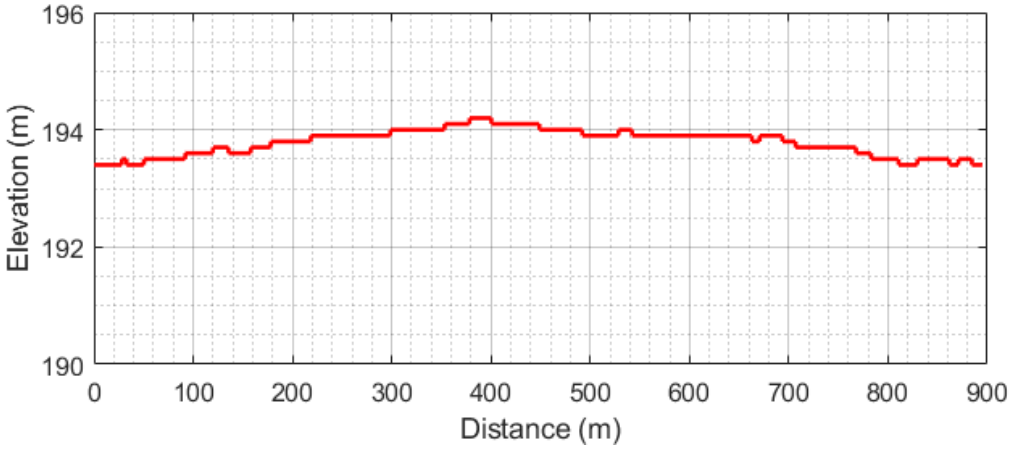

Figure 3.7: Elevation Trace of the 900 m long route selected for Vehicle Platoon Testing on M-203 near McLain State Park

The car at the front ran at a pre-defined speed using the vehicle's cruise control. The speed of the trailing vehicles were controlled by the drivers in those vehicles, as the trailing vehicles' cruise control system was not operational at the vehicle gaps we required. There were eight LIDAR sensors at the front of each car, which relayed the vehicle gap between it and the vehicle in front, in real-time through an HMI display screen visible to the driver. The driver could get a feedback on the vehicle gap and make necessary corrections to maintain the speed and gap at desired levels. All three vehicles were under radio communication at all times during testing and the tests were conducted when no other vehicles were on the route.

All the tests were conducted in Charge Depleting (CD) Mode, between the months of May and July 2019, with ambient temperatures ranging from 8° C to 28 ° C. In order to minimize the effect of this variation in ambient temperature, all the tests were run with the HVAC system off and the vehicle was sufficiently warmed up before

the tests. Moreover, an independent vehicle runs and control tests were conducted at regular intervals for consistency in results.

The vehicles started off at a distance before the actual starting point of the test route. By the time it reached the route starting point, the vehicles would have lined up at the required gap and speed. The cars would be maintained at this gap and speed for the entire test route. Once the test run is complete, the vehicles would separate out and come to a stop. Data recording was started before the vehicles started moving and was stopped once it came back to rest. The data for the test route was trimmed based on the vehicle's GPS coordinates and analyzed.

3.2.1 Vehicle Platooning Studies

The different investigations in vehicle platooning is explained in this section.

3.2.1.1 Vehicle Gap Study

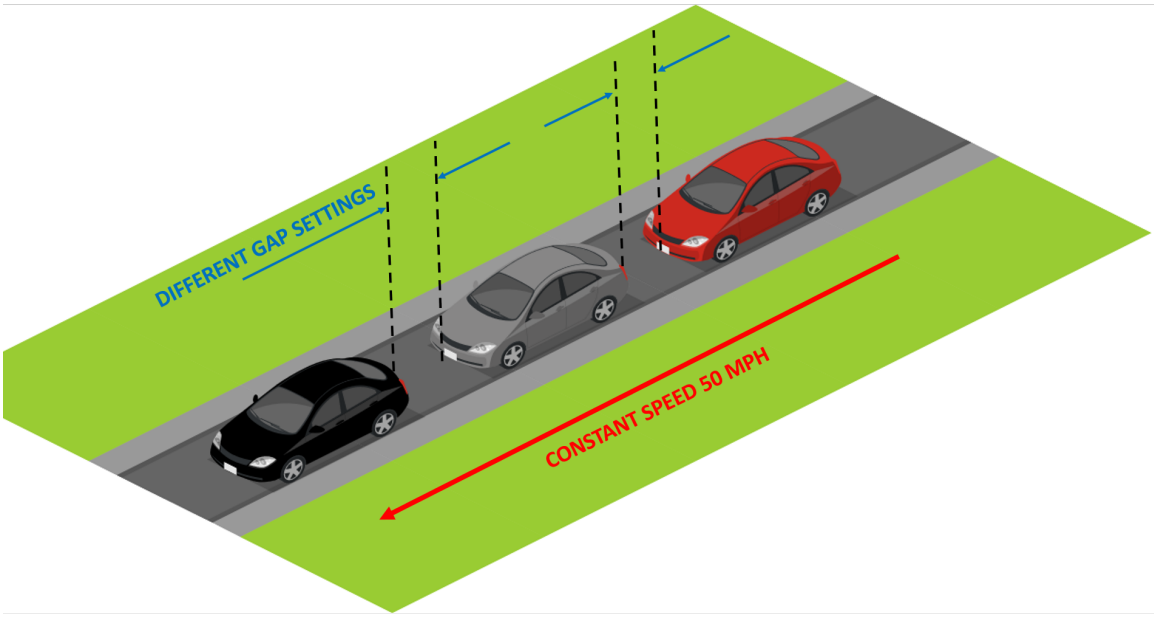

Figure 3.8: Figure showing the vehicle configuration in gap study

The energy savings of a vehicle platoon at different vehicle gaps of 6m, 9m, 12m and 15m is investigated in this study. The 6m runs were repeated 4 times.The 12m, 15m runs were repeated twice in each direction and the 9m run was repeated thrice.Two independent runs were also run in each direction to set baseline energy consumption for each vehicle. All the gap tests were run at a constant vehicle speed of 50 mph as shown in Figure 3.8.

3.2.1.2 Vehicle Speed Study

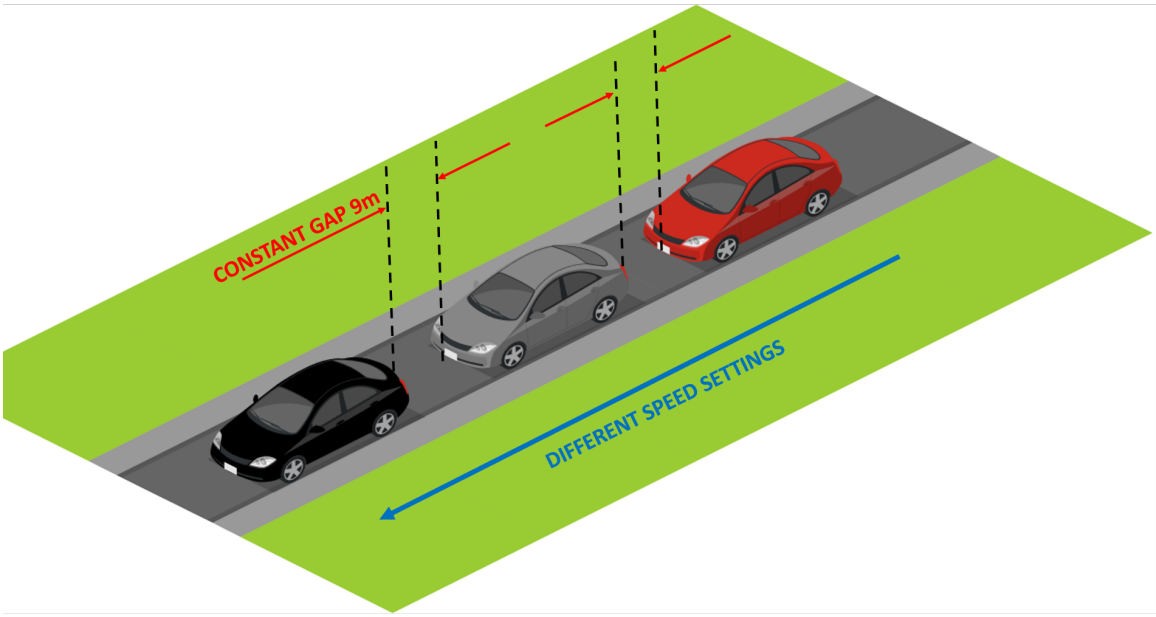

Figure 3.9: Figure showing the vehicle configuration in speed study

The energy savings of the vehicle platoon at different vehicle speeds from 30 mph to 60 mph with increments of 10 mph is investigated in this study. Runs at all speeds except 50 and 60 mph were were repeated twice in each direction. The 60 and 50 mph test was repeated thrice in each direction. One independent run was also run in each direction at all speeds except 50 mph to set baseline energy consumption for each vehicle. The independent 50 mph run was repeated twice.

3.2.1.3 Lateral Offset Study

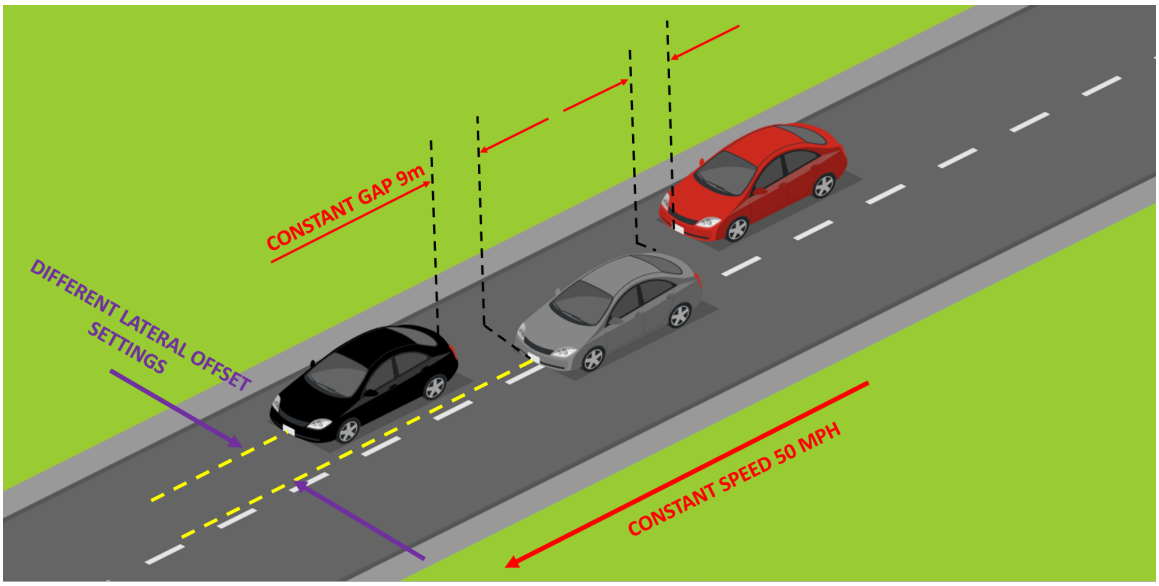

Figure 3.10: Figure showing the vehicle configuration in lateral offset study

In lateral offset study, the middle vehicle (Beta 2) was offset laterally by 1 ft, 2ft and 3ft from the center-line of the platoon. Each condition was repeated twice in each direction. Another set of tests with the offset vehicle (Beta 2) shifted to rear of the vehicle was also conducted with 1 ft offset. This was repeated twice in each direction. All these tests were conducted at 50 mph and 9m gap. Therefore, the independent runs of vehicle gap study can be used for comparison.

3.2.1.4 Location of vehicle with Aerodynamic modifier study

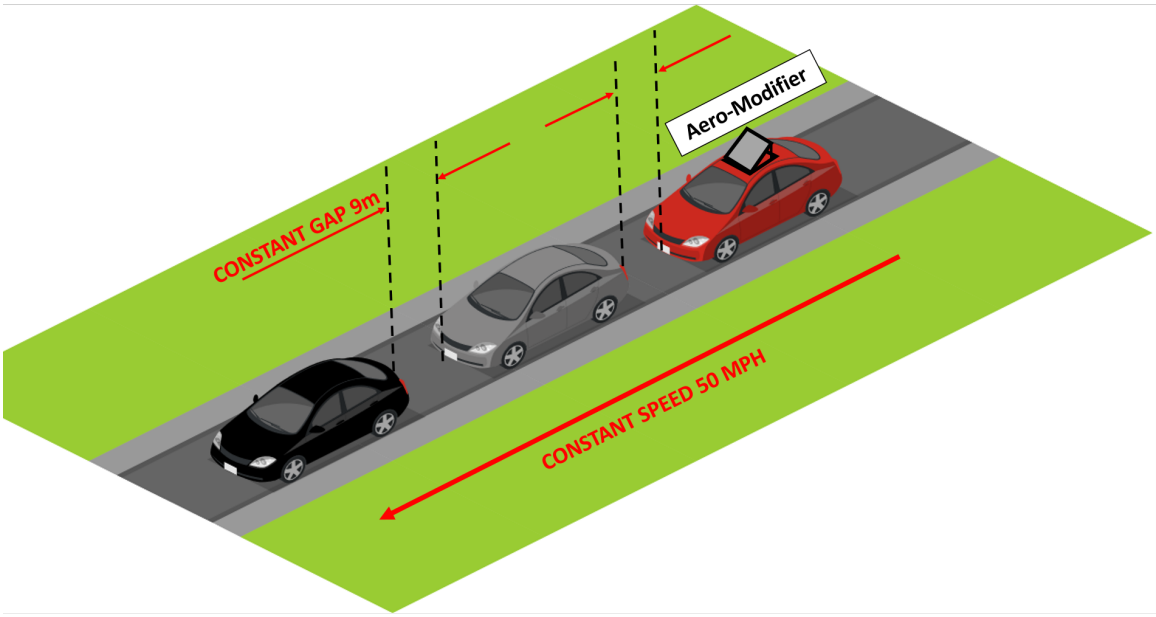

Figure 3.11: Figure showing the vehicle configuration and aero-modifier in location of vehicle with aero-modifier study

Beta 3 of the platoon was fitted with an aerodynamic modifier on the roof rack. This test was to see how the energy savings would be affected when items are placed on roof of a vehicle. Energy consumption analysis was done with Beta 3 at the front, middle and rear of the vehicle once in each direction. These tests were also conducted at 9m gap and 50 mph speed.

3.3 Route Based Blended Mode Optimizer

Most of the PHEVs currently in the market employs a Charge Depleting - Charge Sustaining (CD-CS) strategy where the engine is started only after the Battery has been depleted. The blended mode optimizer outputs a new control strategy where the engine will be turned on before the battery is completely discharged with the aim of getting the battery SOC to its lowest limit by the end of the trip. The optimizer is built so as to operate the engine when a lot of transients are not present and at its peak efficiency point. A detailed explanation of the optimizer and its features can be found in [33]. The work presented in this report concerning the blended mode optimizer is a continuation of the earlier work conducted as part of the same project by Neeraj Rama, Huanqing Wang, Joshua Orlando, Darrell Robinette and Bo Chen. A brief explanation of the optimizer is made in this report.

The Chevrolet Gen 2 Volts have 4 driver selectable modes – Normal, Sport, Mountain and Hold. In Normal Mode the vehicle operates under normal CD-CS strategy, in which the vehicle operates in CD mode when the SOC is between 90% and 16.5% and operates in CS mode once the SOC drops to around 16.5%. In Sport mode the vehicle operates under the same strategy but the vehicle will be more responsive to accelerator pedal changes. In Mountain mode, if the SOC is less than around 25%, the controller uses the engine to charge the battery back up to around 25%. In Hold

mode, the controller will try to hold the SOC at which the mode is selected by shifting to CS operation instantly.

The optimizer makes use of the normal mode and the hold mode to cycle between CD and CS operation, to turn the engine on whenever it is necessary. The optimizer uses a Reduced-Order Powertrain Model to estimate the energy consumption of the vehicle to complete specific velocity and elevation profiles. A detailed explanation of the reduced-order powertrain model can be found in [3]. The powertrain energy consumption model takes the velocity and elevation data as inputs and estimates the energy consumed by the vehicle depending on the starting SOC. The powertrain energy consumption model utilized actual vehicle data collected under different scenarios to come up with rules and mimic the performance of various systems in the powertrain. The axle torque at the wheels was predicted from velocity profile and elevation data using a longitudinal vehicle dynamics model using Equation 3.5 [33].

$$T_{Axle}(t) = (F_0 + F_1 V_{kph}(t) + F_2 V_{kph}(t)^2 + mgsin(\theta(t)) + I_{eff}\alpha_{Axle}(t) + m\frac{dV_{m/s}(t)}{dt})r_{tire} \tag{3.5}$$

In Equation 3.5, T_{Axle} is the axle torque at a particular time, F_0, F_1, F_2 are the road load coefficients of the vehicle. The Environmental Protection Agency (EPA) publishes these coefficients for all the cars released in the US. But, as the vehicle is

put to use, these coefficients is found to change and the accuracy of the axle torque highly depends on these values. For, this part of the project, the coefficients were adjusted to make the estimated axle torque data match the actual axle torque data trace. V_{kph} is the instantaneous velocity of the vehicle. The next term $mgsin(\theta(t))$ is the force term related to the road grade. $\theta(t)$ is calculated from the road elevation data. m is the mass of the vehicle in kilograms and g is the acceleration due to gravity in m/s^2. The next term $I_{eff}\alpha_{Axle}(t)$ is the force term associated with the rotational inertia of the car's wheels. I_{eff} is the moment of inertia of the wheels and $\alpha_{Axle}(t)$ is the rotational acceleration. The last term $m\frac{dV_{m/s}(t)}{dt}$ is the force associated with vehicle acceleration, where V is the velocity of the car in m/s. The sum of these forces when multiplied by the radius of the tire (r_{tire}) is the torque experienced by the vehicle at its axle.

Once the axle torque is determined, based on the battery SOC, the decision to operate in CD or CS mode is made. If the vehicle is operated in CD mode, the energy consumption for that instant is calculated from a response surface equation generated from actual vehicle data. The general form of the response surface equation is given in Equation 3.6 [33].

$$y = b_0 + \sum_{i=1}^{k} b_i x_i + \sum_{i=1}^{k} b_{ii} x_i^2 + \sum_{i=1}^{k-1} \sum_{j=1+1}^{k} b_{ij} x_i x_j \tag{3.6}$$

If the decision is to operate the vehicle in CS mode, similar response surface equations are used to determine the mode of operation (LER, FG or HER) and based on the mode, the operating points of the engine and e-motors are determined and finally the energy consumed is calculated from a response surface equation. Once, the energy is computed the new battery SOC is determined and this SOC value is sent again to the controller to process the next time step.

In the optimizer, once the velocity profile and elevation data is received, it uses the powertrain model to estimate whether the trip can be completed in pure EV mode. If it can, then the entire trip will be completed in Normal mode. If the powertrain model predicts that the battery is going to be depleted before reaching the trip destination, then the optimizer divides the entire trip into segments of equal time intervals. For this study, the trip is divided into 30 second segments. A method called backward induction algorithm is used to determine the optimum hold mode matrix, which is a matrix which holds information of whether to force the vehicle to be in normal or hold mode based on the current SOC and drive segment.

In the backward induction algorithm, the cost-to-go is calculated from the last segment. The formula used for estimating the cost-to-go is given in Equation 3.7 [33].

$$J(n, SOC_n) = \min_u \left[J\left\{ n+1, \left(SOC_n - \frac{E_b(n, u_n)}{Q_0} \right) \right\} + E(n, u_n) \right] \quad (3.7)$$
$$u \in (Normal, Hold)$$

subject to

$$J(n_f, SOC_f) = \begin{cases} 0 \; if \; SOC_f = SOC_0 \\ \infty \; if \; SOC_f \neq SOC_0 \end{cases} \quad (3.8)$$

and

$$SOC_n \in (SOC_{min}, SOC_{max}) \quad (3.9)$$

In Equation 3.7, J is the minimum energy required to go from the nth segment to the end of the drive cycle if the SOC at the nth segment is SOC$_n$. The cost-to-go from the final segment is calculated backwards iteratively till the first segment. For each state the cost-to-go will be the sum of the energy utilized in that segment and the cost-to-go of the next segment where the SOC would end up if the control u_n is applied. The controller is trying to minimize the energy utilized to go to the end for each segment. Based on the chosen control u_n, an optimum control mode matrix is populated for each segment and SOC level. The whole cost-to-go and optimal mode matrices are populated such that the constraints in Equation 3.8 and 3.9 are always satisfied. The constraint in Equation 3.8 forces the final state of the SOC to be near the charge

sustaining SOC, so that all of the electrical energy in the batteries are used. The constraint in 3.9, makes sure that the battery SOC stays within its operating range.

3.3.1 Modifications to the Blended Mode Optimizer and Implementing it in MicroAutoBox

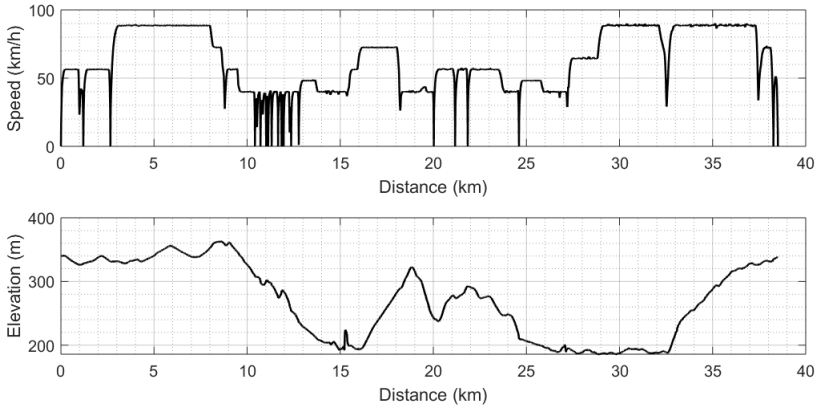

Figure 3.12: MTU Drive Cycle Speed and Elevation Inputted into the Optimizer

In the earlier versions of the optimizer, the Optimal Mode Matrix was inputted into the vehicle as a function of the distance travelled only. The trouble with this implementation was that the starting SOC of the car had to exactly match the starting SOC mentioned in the Optimizer to obtain maximum savings. Also, if there was an unforeseen variation between the optimal SOC profile generated by the optimizer and the actual SOC trace of the car, the hold mode vector would be rendered ineffective. In order to tackle this problem, the optimum control matrix was extracted from the

optimizer as a function of SOC and Distance travelled. Now, the hold mode vector generated from this matrix will automatically account for any variation in the initial SOC or SOC change along the route. The optimum control matrix was stored as a function of SOC and drive segments. In order to implement it in the vehicle, the matrix had to be interpolated with respect to distance. The distance travelled by the vehicle at each of the segment time was assigned to that segment number. After that, the optimum control matrix was interpolated to include the distances in between the segment distances. A figure depicting the Optimal Mode Control Matrix interpolated this way is shown in Figure 3.13, along with the velocity and elevation data inputted into the optimizer represented in Figure 3.12. The interpolated matrix was large in size and had difficulty in compiling it into C code. This matrix then had to be decimated based on distance while accounting for the transfer time it took to change the mode in the car. Then, the decimated optimal control matrix was input into a 2-D Lookup table in a vehicle controller model with SOC and Distance as break-points. The output of the table will be a Hold or Normal mode signal, based on the distance travelled and current SOC. This model was then built into the ControlDesk environment, where it would run real-time during vehicle operation.

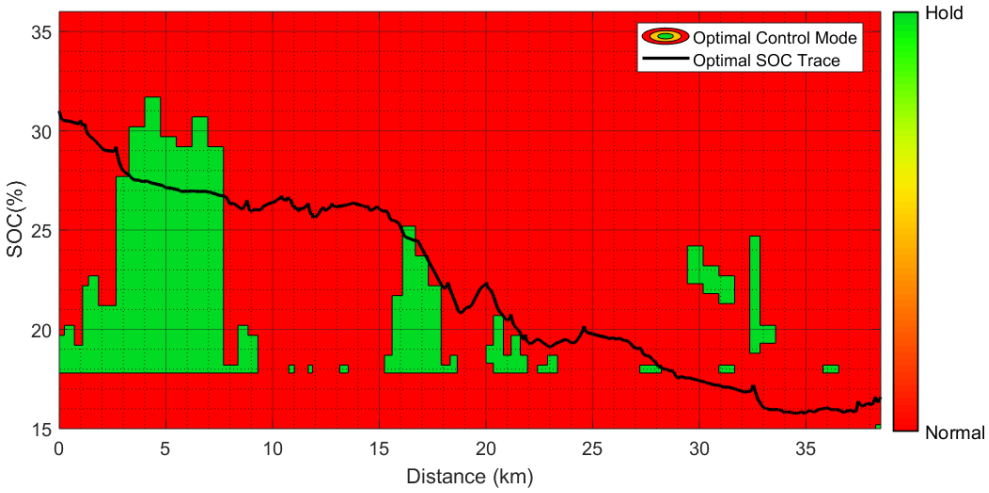

Figure 3.13: Optimal Mode Control Matrix that was inputted into the vehicle overlaid with the predicted optimal SOC trace

3.3.2 Vehicle Testing

Once, the controller was set up, the cars went out for testing. Testing was done on Forward MTUDC and R-MTUDC. In the first five test runs on Forward MTUDC, the cars went out in pairs. One car was in normal CD-CS mode and the other was running the Optimizer. In the rest of the tests, the car ran in blended strategy after it completed one run in normal mode. Both the vehicles started off with an initial SOC of 31%. Figure 3.14 shows the MTUDC overlaid on a map. The route characteristics of MTUDC is provided in Table 3.2 [4]. The route characteristics of the R-MTUDC is described in Section 3.1.

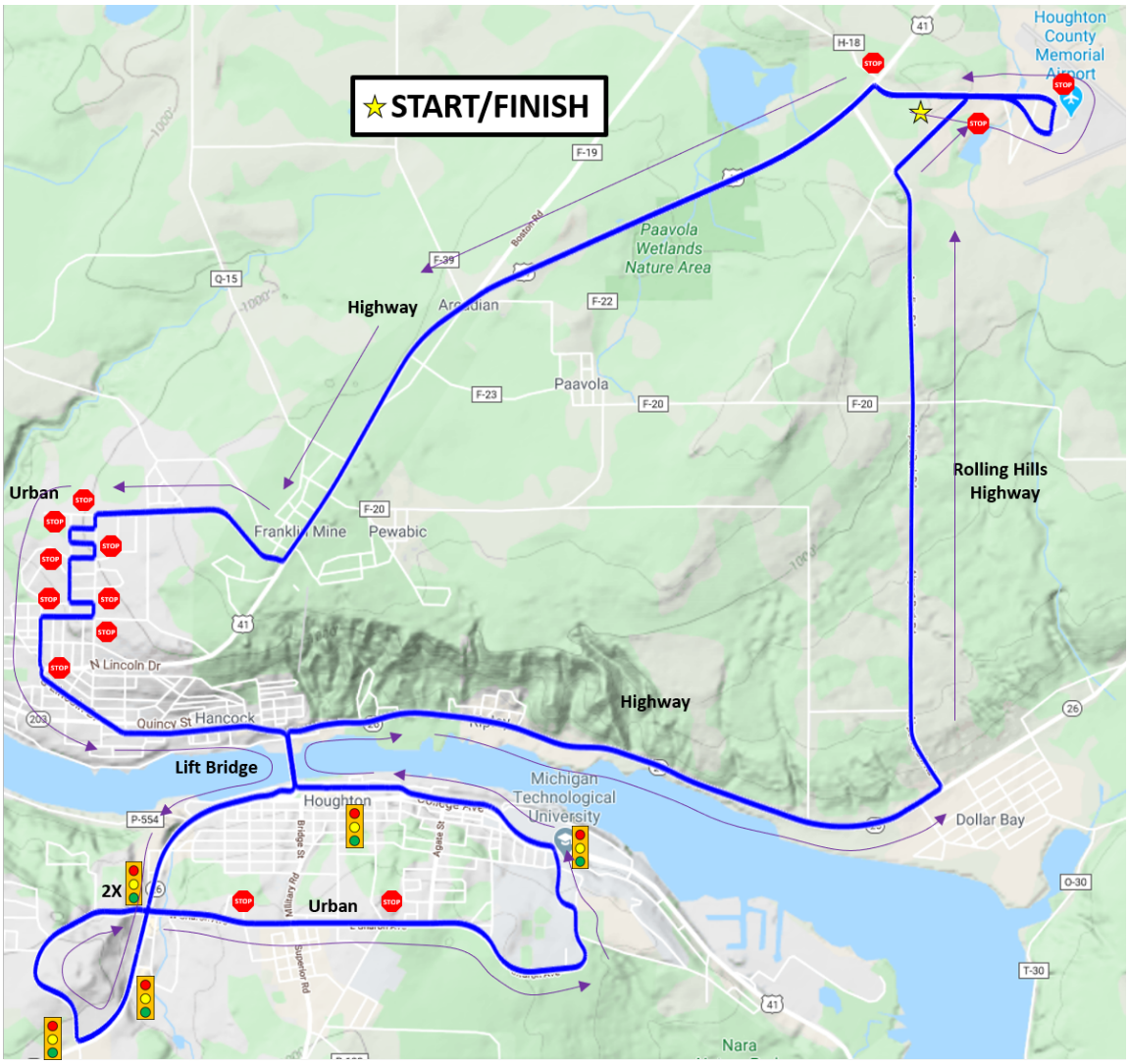

Figure 3.14: MTU Drive Cycle route overlaid on a map with directions, stop signs and traffic signals

3.4 Engine Start-Stop Optimizer

In Gen II Volts, even in Charge Sustaining mode, based on the vehicle driving conditions and battery SOC level, the controller can choose to turn off the engine to save energy. The possible conditions for turning off the engine is when the required

Table 3.2
MTU Drive Cycle Route Statistics [4]

Total Distance	38.6 km
Maximum Speed	55 mph
Minimum Speed	25 mph
Maximum Elevation	362.5 m
Minimum Elevation	185.2 m
Maximum Uphill Grade	7 %
Maximum Downhill Grade	8 %
No. of Stop Signs	13
No. of Traffic Lights	6

axle power is low or when the battery SOC is at a higher level. Since, the vehicle controller does not have a look ahead of the velocity profile, the controller can make decisions to turn the engine on or off based on calibration tables, but it may have to reverse its decision soon because of a change in velocity profile or elevation about which the controller did not have prior information. Such a case is shown at the top of Figure 3.15, where the controller decided to turned the engine off but had to restart it within seconds and at the bottom of Figure 3.15, where the controller turned on the engine for only a short while. With availability of prior knowledge about the route and traffic, these situations can be avoided using an Engine Start-Stop Optimizer.

Two kinds of Engine Start-Stop Optimizers are discussed in this section. One is based on predicting the engine start/stop from the actual vehicle controller and the other one is based on finding a path of least cost using Dynamic Programming using Backward Induction algorithm similar to the Route Based Blended Mode Optimizer

described in Subsection 4.3. The two kinds of Optimizers are discussed in detail.

3.4.1 Engine Start-Stop Optimizer using Predicted Engine Start and Stops

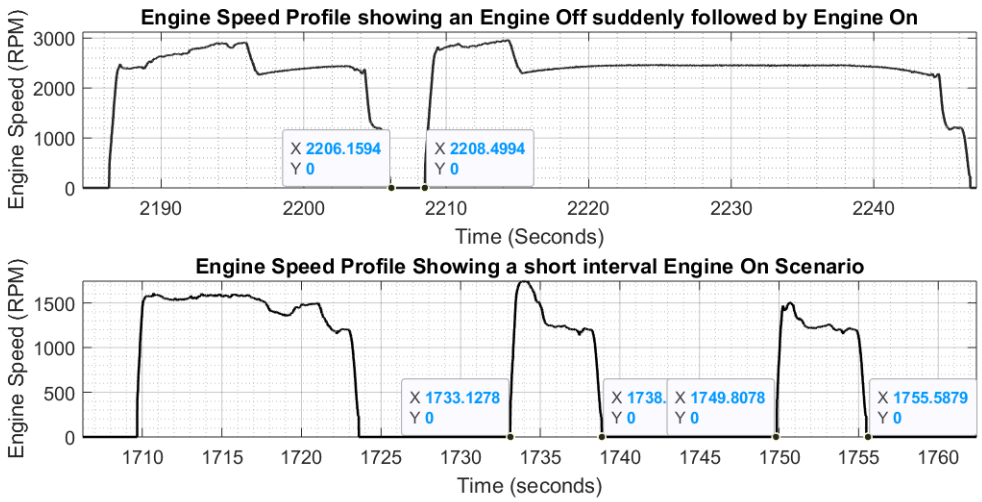

Figure 3.15: A trace of Engine Speed showing the short-coming of the vehicle controller, where the engine is turn off and then suddenly turned back on (top) and the engine being turned on for a short-interval (bottom)

The control flowchart for the proposed Engine Start-Stop Optimizer is shown in Figures 3.17 and 3.18. The Optimizer has two parts. The part to be executed depends on the status of the Engine Start-Stop signal of the vehicle controller. When the vehicle controller gives a signal that the engine needs to be turned off, the controller referred in Figure 3.17 is executed. The cost function associated with each instance of signal to turn on engine is given in Equation 3.10. The SOC is the state variable in equation which changes based on the control variables which are Engine ON, Engine

OFF and DEFCO.

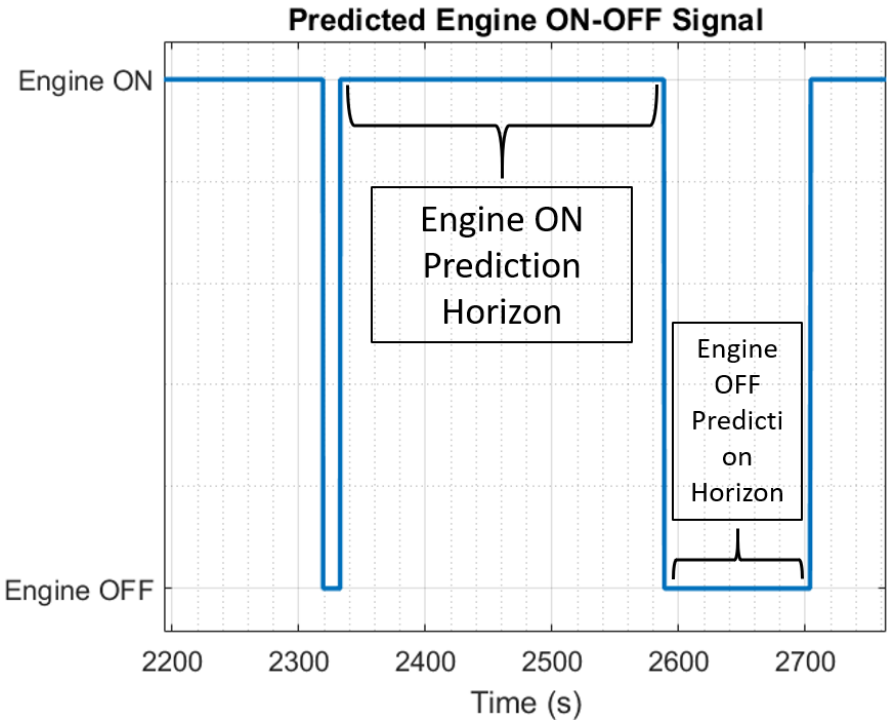

Figure 3.16: A snip of the predicted engine ON-OFF signal zoomed in to show the optimizing horizon

The optimizer uses a model to predict the engine ON-OFF signal using the route velocity profile and elevation data. A rudimentary rule based model was developed which used the Axle Torque profile from the route characteristics and future battery SOC trace to predict when the engine would turn ON and OFF. An example of such a predicted Engine ON-OFF signal is shown in Figure 3.16. Whenever an Engine ON event comes up, the engine ON-OFF signal predictor predicts the next Engine OFF. This period is marked as Engine ON Prediction horizon in Figure 3.16.The optimizer chooses the control for this period based on energy comparison. Similarly, whenever an Engine OFF event comes up, the engine ON-OFF signal predictor predicts the

next Engine ON. This period is marked as Engine OFF Prediction horizon in Figure 3.16. The prediction horizon does not have a constant time or distance horizon but varies depending on the engine ON-OFF signal.

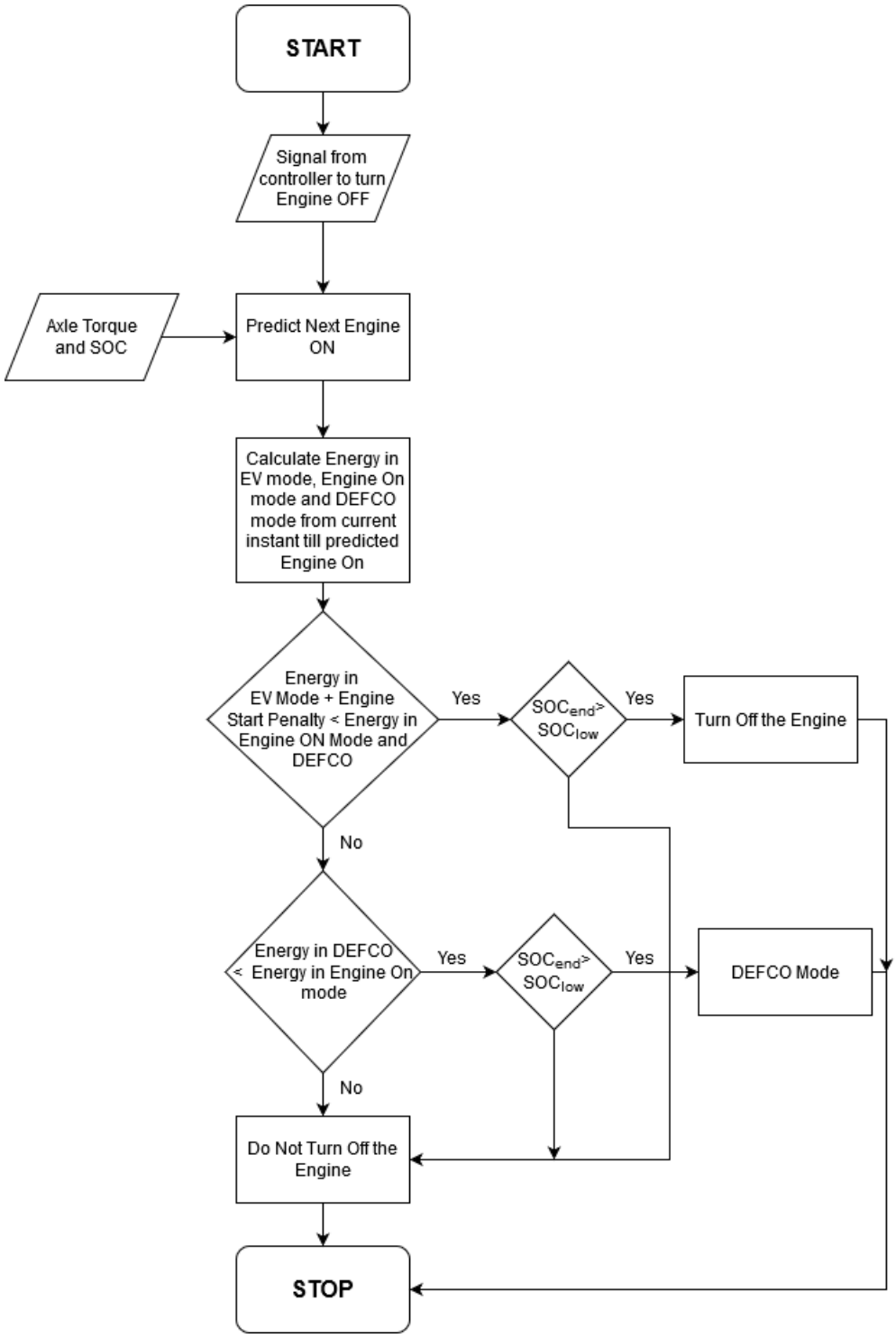

Figure 3.17: Engine Start-Stop Control Flowchart when the vehicle controller signals the engine to turn OFF

$$J(n) = \min_{u} \left[\sum_{i=1}^{k} E_{ui} \right] \tag{3.10}$$
$$u \in (Engine\ Off,\ Engine\ On,\ DEFCO)$$

subject to

$$J(n) = \infty\ if\ SOC_k < SOC_{LB}\ and\ u = Engine\ Off$$

$$J(n) = \infty\ if\ SOC_k < SOC_{LB}\ and\ u = DEFCO \tag{3.11}$$

and

$$SOC_n \in (SOC_{LB}, SOC_{UB}) \tag{3.12}$$

Once the signal to turn OFF the engine is received, the controller uses a model to predict when the engine would need to turn on later, using the route velocity profile and elevation data. Once, the period of predicted engine off is available, the controller uses the Reduced-Order Powertrain model [3] to predict the energy that would be needed by the vehicle to operate during the period. The look ahead horizon for this optimizer is the period between the time at which the Engine ON signal is generated to the predicted Engine OFF instant. Energy needed for this period

for EV only mode, Engine On mode and DEFCO mode are calculated. DEFCO stands for Deceleration Fuel Cut Off, where the fuel supply to the engine is cut off but the engine is kept spinning by the motor until it needs to draw power from the engine again. A response surface was used to predict the energy needed to keep the engine running based on the engine speed. To calculate the energy consumed in EV mode, the axle torque, velocity and current SOC data is sent to a model which uses a response surface to predict the energy consumed. This energy consumed is then used to predict the SOC at the end of the period. To calculate the Engine On energy, the same axle torque and velocity profile is sent to another model which predicts the mode (LER, FG or HER) to operate the vehicle using response surfaces. Once the mode is selected, the engine operating points are determined using response surfaces and these operating points are used to determine the energy consumed by the vehicle when engine is On.The motor operating points are determined based on the engine operating points and gear ratios of planetary gearsets. From this, the energy drawn or sent to the battery is determined and thus the SOC at the end of period is determined. If the engine has to be turned off, whenever it needs to be turned back on again, a fuel penalty is added to the energy consumed. This fuel penalty depends on the Axle Power, vehicle velocity and battery SOC at the time of engine start. A response surface, whose form is provided in Equation 3.16, was fitted with available engine start data to predict the engine start penalty. In Equation 3.16,$E_{startKJ}$ is the energy required to start the engine in kJ, P_{axle} is the axle power in kW, SOC

is the SOC of the vehicle and V_{kph} is vehicle velocity in km/h. Once, the energy in the three control modes have been determined, the control with the least energy is selected, which is the cost, represented in Equation 3.10, subject to the constraints given in Equations 3.11 and 3.12. The constraint in Equation 3.11, makes sure that the Engine off or DEFCO decision is not taken if the final SOC (SOC_k) of the section, is less than allowed lower limit of SOC (SOC_{LB} (15.3%)). This part of the controller helps remove the scenario where the engine turns off and then suddenly turns back on.

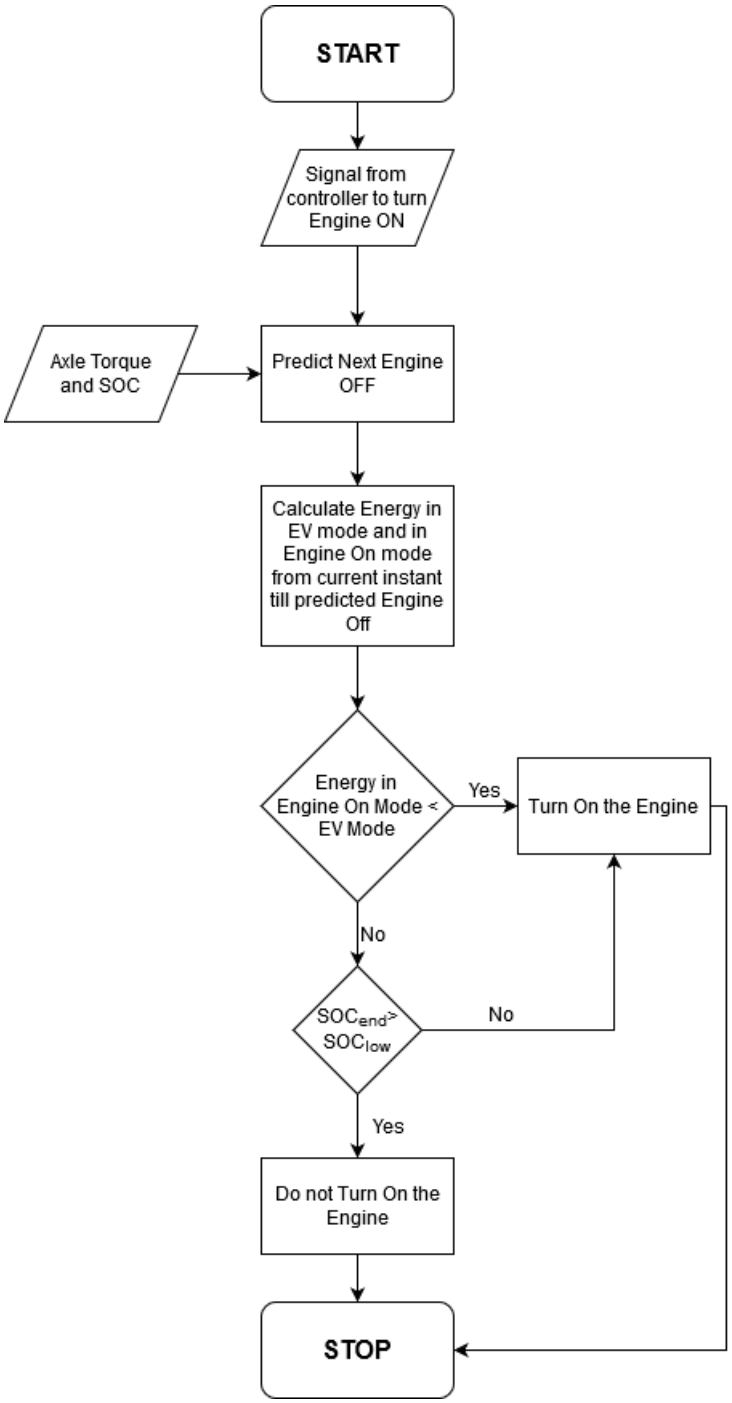

Figure 3.18: Engine Start-Stop Control Flowchart when the vehicle controller signals the engine to turn ON

$$J(n) = \min_{u} \left[\sum_{i=1}^{k} E_{ui} \right] \tag{3.13}$$
$$u \in (Engine\ Off,\ Engine\ On)$$

subject to

$$J(n) = \infty\ if\ SOC_k < SOC_{LB}\ and\ u = Engine\ Off \tag{3.14}$$

and

$$SOC_n \in (SOC_{LB}, SOC_{UB}) \tag{3.15}$$

The second part of the controller, shown in Figure 3.18, is executed when the controller decides to turn the engine on. Another model is used to predict when the engine will turn off. Once, the period of engine on is available, the energy needed to operate the vehicle in both EV mode and Engine on mode are calculated and the control with the minimum energy is selected as shown in Equation 3.13, as long as the constraints in Equation 3.14 and 3.15 are satisfied. The look ahead horizon for this optimizer is the period between the time at which the Engine OFF signal is generated to the predicted Engine ON instant. This part of the controller helps remove the scenario where the engine turns on for a short period and then suddenly turns back off.

3.4.1.1 Determining the Engine Start Penalty

During engine start, the e-motor of the car cranks the engine upto the required speed and once the speed is reached, fuelling starts. Figure 3.19 shows the engine speed profile and the fuel flow rate during an engine start. A slight delay in fuelling and start of engine speed can be observed. The engine is cranked up to speed during this delay period using battery energy. To calculate this energy, the output power at the axle of the vehicle is subtracted from the total energy drawn from the battery. To account for the accessory loads and powertrain losses, the same energy drawn from the battery for the same period as the engine start period is determined. The difference between the calculated energies during engine start period and the same time period just before the engine start should be the energy required to start the engine. It is assumed that the accessory loads and the powertrain losses during the engine start period and the period just before engine start remains a constant. The axle power, SOC and vehicle speed are recorded at the start of different engine starts and these values are used to create a response surface equation shown in Equation 3.16, that would predict the engine start penalty.

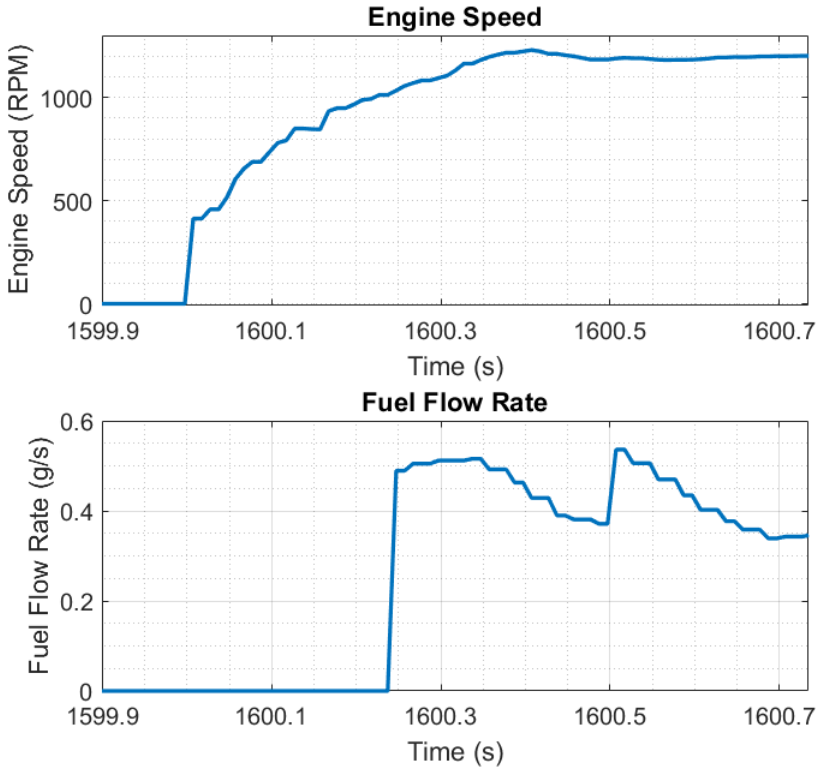

Figure 3.19: Plot showing the relative difference between instant of engine cranking and start of fuelling

$$E_{startKJ} = 681 + 1.87\ P_{axle} - 2.31\ V_{kph} - 76.6\ SOC + 2.13\ SOC^2 + 0.14\ V_{kph}SOC \tag{3.16}$$

3.4.2 Engine Start-Stop Optimizer using Dynamic Programming

The main difference between this optimizer and the one mentioned in Section 3.4.1, is that this optimizer optimizes the entire drive cycle by dividing it into segments, while the one mentioned in section 3.4.1, optimizes a section based on the predicted engine start and stop. Once the optimizer receives the proposed route velocity and elevation data, it splits the entire drive cycle into 10 second segments. The optimizer selects the optimal control for this 10 second period. Each drive segment is divided into different SOC levels from the lower SOC limit to the upper charge sustaining SOC limit with increments of 0.1%. The SOC is the state variable and the Engine ON and Engine OFF are the control variables. The optimizer calculates the energy required by the last segment for both the Engine On and Engine Off condition using the same Reduced Order Powertrain model as explained in Subsection 3.4.1. Once the energy values are calculated, the optimizer chooses a mode which has the least cost subject to the constraints mentioned in Equation 3.18. After that the optimizer does the same for the drive section before the last section and computes the path with the lowest energy to go to the end of the drive cycle.

$$J(n, SOC_n) = \min_u \left[J\left\{ n+1, \left(SOC_n - \frac{E_b(n, u_n)}{Q_0} \right) \right\} + E(n, u_n) \right] \tag{3.17}$$
$$u \in (Engine\ On,\ Engine\ Off)$$

subject to

$$SOC_n \in (SOC_{LB}, SOC_{UB}) \tag{3.18}$$

In Equation 3.17, J is the minimum energy required to go from the nth segment to the end of the drive cycle, if the SOC at the nth segment is SOC$_n$. The cost-to-go from the final segment is calculated backwards iteratively till the first segment. For each state the cost-to-go will be the sum of the energy utilized in that segment and the cost-to-go of the next segment where the SOC would end up if the control u_n is applied. The controller is trying to minimize the energy utilized to go to the end for each segment. Based on the chosen control u_n, an optimum Engine On/Off matrix is populated for each segment and SOC level. The whole cost-to-go and Engine On/Off matrices are populated such that the constraints in Equation 3.18 are always satisfied. The constraint in Equation 3.18, makes sure that the battery SOC stays within its operating range (15.3% to 17.65%). If the battery SOC falls below the lower bound of SOC, the optimizer is programmed keep the engine ON until the SOC goes above the lower bound. Also, if the shortest path includes going from an engine OFF section to an engine ON section, an Engine Start Penalty is added to the engine off section.

Since, the segments were 10 seconds long, the control of DEFCO was not added to the optimizer because the penalty for being in DEFCO for 10 seconds would be more than the Engine start penalty.

Chapter 4

Results and Discussions

This chapter presents the results and discussions of the different tests mentioned in Chapter 3.

4.1 Reverse MTUDC

4.1.1 Charge Depleting Mode Tests

Figure 4.1 shows the instantaneous power consumption of the car at each point on the route. It can be observed that most of the route draws only a moderate amount of power from the motors. The high power demand sections and sections that allow

maximum regeneration can also be identified from the map.

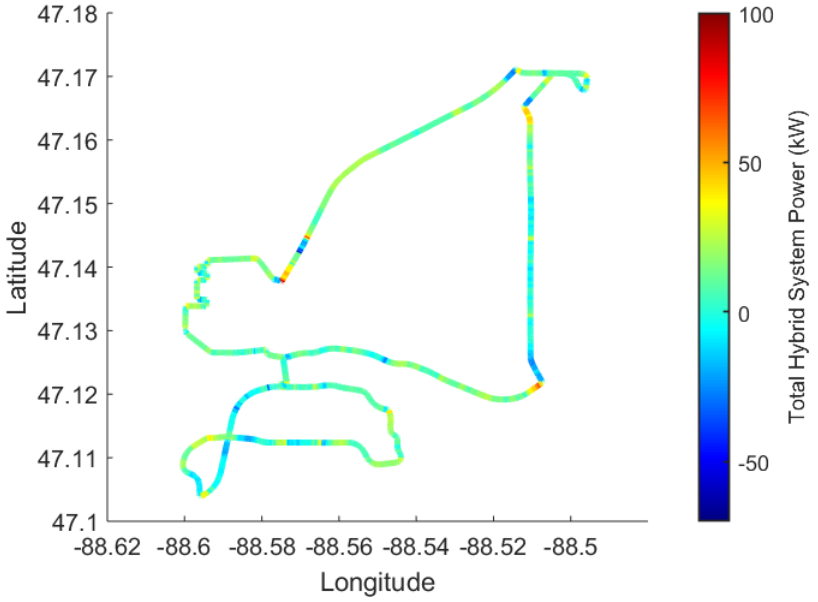

Figure 4.1: The Instantaneous power consumption of the Volts plotted at each point on the route.

The results of the ten Charge Depleting Mode runs are provided in Table 4.1. A comparison of the summary of results with forward MTUDC is shown in Table 4.2.The drive cycle is 38.8 km long. The Volts on average uses up 21.3 MJ of energy with 0.6 MJ of standard deviation to complete the R-MTUDC. This standard deviation in energy adds up to 2.9% of the total energy. The drive cycle also uses up 31.7% of SOC to drive all-electric on the R-MTUDC with a standard deviation of 1.4. The R-MTUDC took any time between 46 and 52 minutes to complete with an average cycle time of 49.3 minutes. Finally, the equivalent fuel consumption came up to be 129.7 MPGe, which was higher than the EPA rated MPGe of 106.

Table 4.1
Reverse MTU Drive Cycle Charge Depleting Mode Result Summary

CD Mode	Time	Distance	Initial SOC	SOC % used	Total Energy Consumed	Fuel Energy	Battery Energy	Equivalent Fuel Consumption
Run #	mins	km	%	%	MJ	MJ	MJ	MPGe
1	51.2	38.8	92.0	-31.6	21.9	0.0	21.9	126.3
2	46.9	38.8	62.8	-33.1	21.5	0.0	21.5	128.5
3	46.0	38.8	91.4	-31.2	21.2	0.0	21.2	130.3
4	49.8	38.8	59.6	-33.5	21.5	0.0	21.5	128.2
5	47.1	38.8	90.4	-30.3	20.5	0.0	20.5	134.3
6	51.7	38.8	88.5	-31.4	22.0	0.0	22.0	125.7
7	51.8	38.9	55.8	-34.0	22.3	0.0	22.3	124.0
8	50.6	38.8	90.5	-30.0	20.6	0.0	20.6	134.1
9	49.8	38.8	60.0	-31.6	20.9	0.0	20.9	132.4
10	48.4	38.8	89.0	-30.1	20.8	0.0	20.8	133.0
Mean	**49.3**	**38.8**	**78.0**	**-31.7**	**21.3**	**0.0**	**21.3**	**129.7**
Std Dev	**2.1**	**0.0**	**16.0**	**1.4**	**0.6**	**0.0**	**0.6**	**3.7**
Min	**46.0**	**38.8**	**55.8**	**-34.0**	**20.5**	**0.0**	**20.5**	**124.0**
Max	**51.8**	**38.9**	**92.0**	**-30.0**	**22.3**	**0.0**	**22.3**	**134.3**
% of Average	**4.3**	**0.1**	**20.5**	**-4.5**	**2.9**	**-**	**2.9**	**2.9**

Figure 4.2 shows the evolution of energy consumption as the drive cycle progresses along the route. It can be observed that all the energy traces for the individual runs follow the mean energy trace quite closely, even though various factors can affect the car during a real world drive cycle. The normalized SOC trace shown in Figure 4.3, also show a similar trend with each individual runs closely following the mean SOC trace.

In comparison to the data collected from MTUDC, the R-MTUDC, on average, takes 2.8 minutes more than MTUDC to complete the cycle and is 400 m longer. This

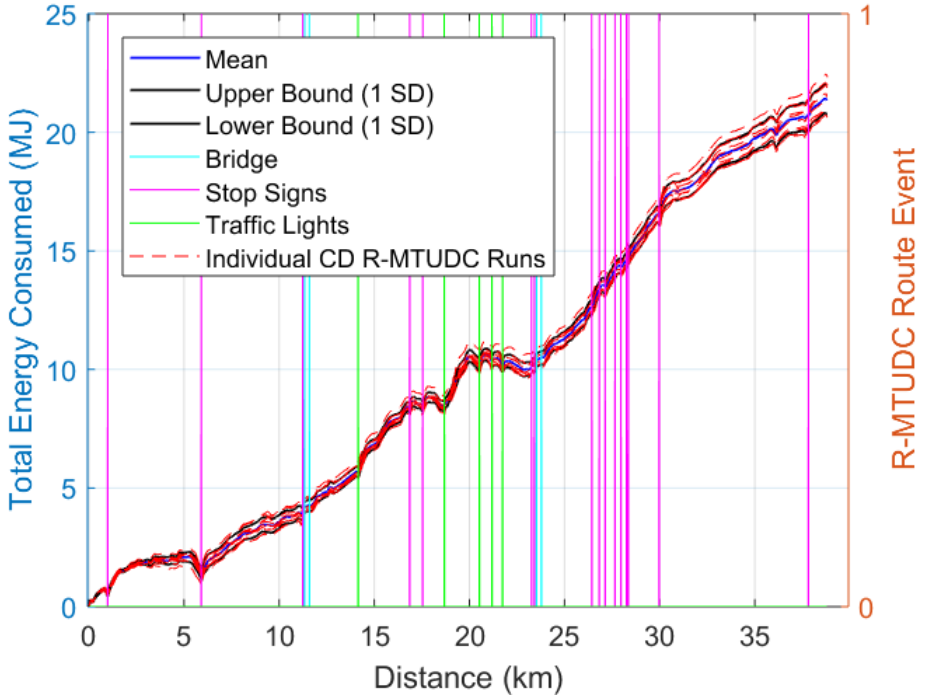

Figure 4.2: Average Energy Consumption and its standard deviation in CD mode on R-MTUDC with individual energy traces

difference in distance is only 1% of the total distance of the route but the tests on R-MTUDC,on average, used up 9.8% more energy than those on MTUDC. This could be attributed to more number of stop signs on the route. Between the MTUDC and R-MTUDC, the standard deviation in the energy consumption is 2.9% for both, which points to the fact that the variation in energy consumption of Real World Drive cycles can be predicted with some level of confidence. The equivalent fuel consumption showed an 8% decrease in R-MTUDC, compared to MTUDC.

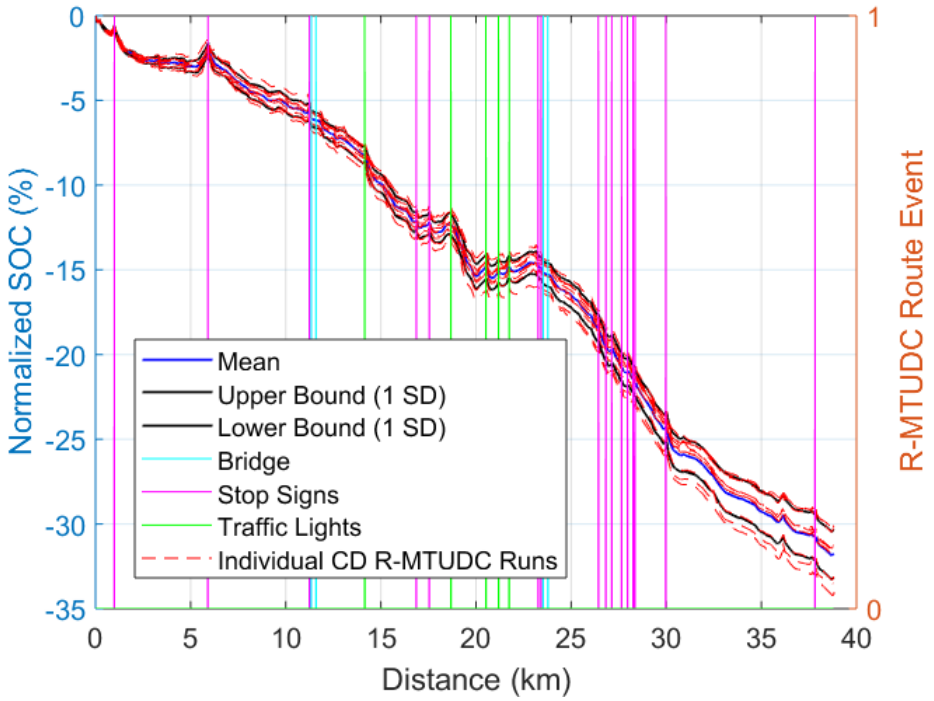

Figure 4.3: Normalized SOC trace and its standard deviation in CD mode on R-MTUDC with individual SOC traces

4.1.2 Charge Sustaining Mode Tests

The charge sustaining mode tests were conducted with an initial SOC of around 16%. The results of the tests in Charge Sustaining mode is given in Table 4.3.The average time taken to complete the route is 50.5 minutes with a standard deviation of 2.1 minutes, which is similar to the CD case. The mean SOC used is positive (0.9%), which means that the battery gained some energy when compared to the start of the drive cycle. On an average 0.7 MJ of energy is stored in the battery after a cycle. The total energy used for the entire trip is 61.1 MJ, almost three times the

Table 4.2
Comparison of statistics summary of R-MTUDC and MTUDC in CD mode

		R-MTUDC					MTUDC				
Charge Depleting Mode		**Mean**	**Std Dev**	**Min**	**Max**	**% of Mean**	**Mean**	**Std Dev**	**Min**	**Max**	**% of Mean**
Time	Minutes	49.3	2.1	46.0	51.8	4.3	46.5	5.6	43.0	62.4	12.1
Distance	km	38.8	0.0	38.8	38.9	0.1	38.4	0.0	38.3	38.4	0.1
Initial SOC	%	78.0	16.0	55.8	92.0	20.5	75.1	15.3	58.9	91.6	20.4
SOC Used	%	-31.7	1.4	-34.0	-30.0	-4.5	-28.5	1.1	-30.4	-26.5	-4.0
Total Energy Consumed	MJ	21.3	0.6	20.5	22.3	2.9	19.4	0.6	18.5	20.1	2.9
Fuel Energy	MJ	0.0	0.0	0.0	0.0	-	0.0	0.0	0.0	0.0	-
Battery Energy	MJ	21.3	0.6	20.5	22.3	2.9	19.4	0.6	18.5	20.1	2.9
Equivalent Fuel Consumption	MPGe	129.7	3.7	124.0	134.3	2.9	141.0	4.1	135.9	147.5	2.9

CD energy usage, with a standard deviation of 1.7 MJ, which comes out to be 2.7% of the average. This 2.7% of standard deviation in energy lines up closely with the standard deviation of 2.9% for CD mode. The equivalent energy consumption for the route came up to be 45.2 MPGe, which is higher than the EPA rated MPGe of 42.

Figure 4.4 shows the evolution of energy consumption over distance on the R-MTUDC. As with the CD runs, all the individual energy traces are closely spaced to the mean energy trace, which is also reflected in the energy standard deviation.The variation in energy gets larger as the drive cycle approaches its end. The SOC traces, shown in Figure 4.5 also follows a similar trend showing that the drive cycle can be repeated without a lot of variability.

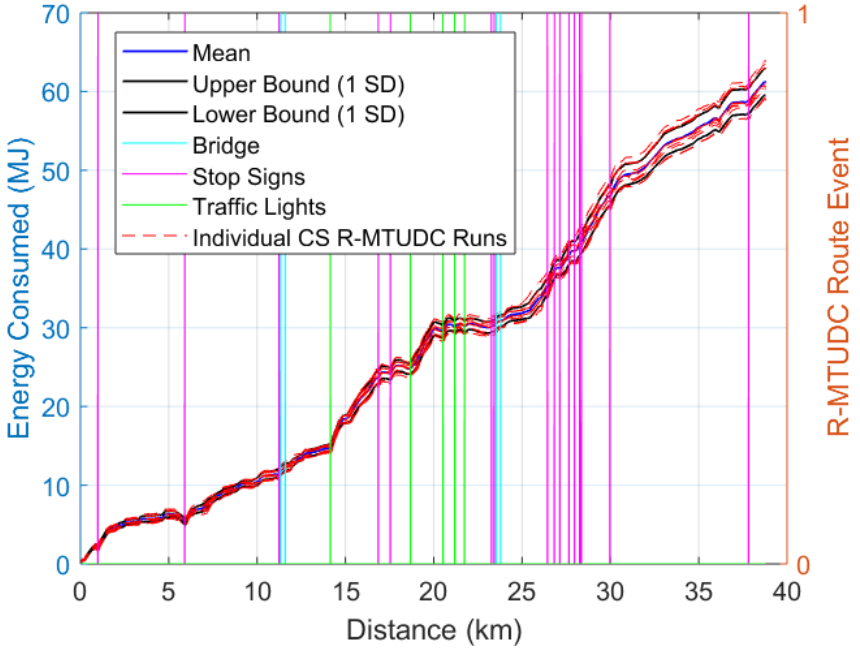

Figure 4.4: Average Energy Consumption and its standard deviation in CS mode on R-MTUDC with individual energy traces

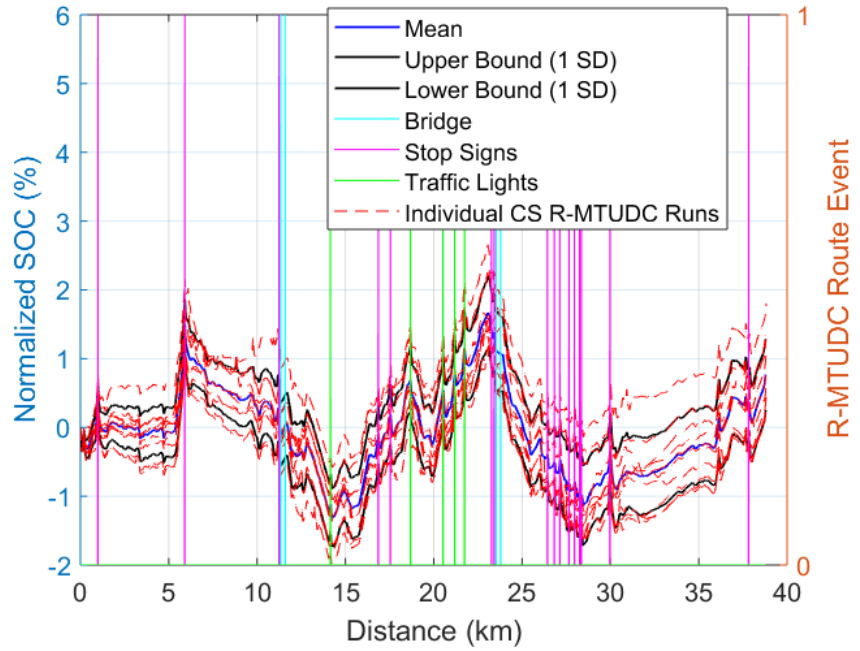

Figure 4.5: Normalized SOC trace and its standard deviation in CS mode on R-MTUDC with individual SOC traces

Table 4.3
Reverse MTU Drive Cycle Charge Sustaining Mode Result Summary

CS Mode	Time	Distance	Initial SOC	SOC % used	Total Energy Consumed	Fuel Energy	Battery Energy	Equivalent Fuel Consumption
Run #	mins	km	%	%	MJ	MJ	MJ	MPGe
1	50.2	38.8	16.3	1.3	62.9	63.9	-1.0	43.9
2	48.3	38.8	15.9	1.3	61.0	61.9	-0.9	45.2
3	50.1	38.8	16.8	0.4	63.4	63.8	-0.4	43.6
4	50.1	38.8	17.0	0.4	63.8	64.3	-0.5	43.3
5	46.5	38.8	17.2	0.2	60.7	61.1	-0.4	45.5
6	52.7	38.8	16.3	1.1	60.2	61.1	-0.9	45.9
7	52.6	38.8	15.5	1.8	60.5	61.9	-1.4	45.7
8	52.1	38.8	16.4	0.8	58.9	59.6	-0.7	46.9
9	52.4	38.9	16.6	0.7	61.0	61.6	-0.6	45.3
10	49.6	38.8	16.6	0.5	59.1	59.7	-0.6	46.7
Mean	**50.5**	**38.8**	**16.4**	**0.9**	**61.1**	**61.9**	**-0.7**	**45.2**
Std Dev	**2.1**	**0.0**	**0.5**	**0.5**	**1.7**	**1.7**	**0.3**	**1.3**
Min	**46.5**	**38.8**	**15.5**	**0.2**	**58.9**	**59.6**	**-1.4**	**43.3**
Max	**52.7**	**38.9**	**17.2**	**1.8**	**63.8**	**64.3**	**-0.4**	**46.9**
% of Average	**4.1**	**0.1**	**2.9**	**60.4**	**2.8**	**2.7**	**-41.2**	**2.8**

Table 4.4, compares the MTUDC and the R-MTUDC in charge sustaining mode. The R-MTUDC took 4.8 minutes more than the MTUDC in CS operation. In CS mode also, the variability in time to complete the R-MTUDC (4.1%) is lesser than that of MTUDC (6.6%). The average energy used by R-MTUDC is only 0.49 % greater than that used up by the MTUDC, while it was 9.8% in CD mode. One of the reasons for the decreased usage of energy in R-MTUDC could be that, the initial battery SOC for R-MTUDC runs (16.4%) were at a higher value than those for the MTUDC runs (15.7%). Another reason for the increased consumption of energy in forward MTUDC can be attributed to a 7% uphill gradient towards the end of the drive cycle. On this

uphill gradient, a considerable amount of battery energy is used up by the car to accelerate and drive uphill. This will lower the battery SOC considerably. When the SOC level drops considerably, the vehicle controller tries to actively recharge the battery to bring the SOC back to its normal level. For this, the vehicle is operated in Fixed Gear Mode. This would cause considerable increase of energy in forward MTUDC making the energy consumption similar to R-MTUDC. This problem is not encountered in CD mode operation as the engine won't be trying to recharge the battery. The equivalent fuel consumption for R-MTUDC is 45.2 MPGe compared to 44.9 MPGe of MTUDC.

4.1.3 Charge Depleting - Charge Sustaining Mode Tests

The Charge Depleting - Charge Sustaining Test (CD-CS) runs were carried out with a starting SOC of around 31%, so that the vehicle will be in EV mode for half of the drive cycle and in Charge Sustaining Mode for the other half. The results of these tests are provided in Table 4.5. The average time taken for these tests are 48.3 minutes with a standard deviation of 2.6 which is consistent with the other tests. The average starting SOC is 30.8 % with a standard deviation of 0.2. The percent of SOC used is also consistent with an average of -13.5% with a standard deviation of 0.2. The total energy consumption is 42.8 MJ with a 3.7% standard deviation is higher than the 2.9% of CS and CD runs. This can be expected due to the variability

Table 4.4
Comparison of statistics summary of R-MTUDC and MTUDC in CS Mode

		R-MTUDC					MTUDC				
Charge Sustaining Mode		Mean	Std Dev	Min	Max	% of Mean	Mean	Std Dev	Min	Max	% of Mean
Time	Mins	50.5	2.1	46.5	52.7	4.1	45.7	3.0	43.8	54.0	6.6
Distance	km	38.8	0.0	38.8	38.9	0.1	38.3	0.0	38.3	38.4	0.0
Initial SOC	%	16.4	0.5	15.5	17.2	2.9	15.7	0.5	14.8	16.4	3.4
SOC Used	%	0.9	0.5	0.2	1.8	60.4	0.5	0.6	-0.4	1.4	109.4
Total Energy Consumed	MJ	61.1	1.7	58.9	63.8	2.8	60.8	2.2	56.4	64.2	3.5
Fuel Energy	MJ	61.9	1.7	59.6	64.3	2.7	61.1	2.2	56.6	64.5	3.5
Battery Energy	MJ	-0.7	0.3	-1.4	-0.4	-41.2	-0.3	0.5	-1.1	0.4	-151.9
Equivalent Fuel Consumption	MPGe	45.2	1.3	43.3	46.9	2.8	44.9	1.6	42.5	48.4	3.6

in drive cycle where the engine starts because of the CD-CS operation. The CD-CS mode puts the equivalent fuel consumption for R-MTUDC at around 64.6 MPGe.

On looking at the Total Energy Consumption trace along the distance of R-MTUDC in Figure 4.6, it is seen that the energy traces are closely bound in EV mode. Once, the vehicle changes to EV mode, the variability increases, with the maximum variability near the point where the mode changes from CD to CS. This is because, in every run,

Table 4.5
Reverse MTU Drive Cycle Charge Depleting - Charge Sustaining Mode
Result Summary

CD-CS Mode R-MTUDC	Time	Distance	Initial SOC	SOC % used	Total Energy Consumed	Fuel Energy	Battery Energy	Equivalent Fuel Consumption
Run #	mins	km	%	%	MJ	MJ	MJ	MPGe
1	49.1	38.8	30.8	-13.3	42.9	34.7	8.2	64.3
2	45.2	38.8	31.1	-13.6	41.1	32.9	8.2	67.2
3	51.6	38.8	30.8	-13.4	42.7	34.7	8.1	64.6
4	52.4	38.9	30.9	-13.5	40.4	32.2	8.2	68.5
5	46.4	38.8	30.6	-13.3	40.9	32.7	8.1	67.5
6	48.4	38.8	30.9	-13.8	42.2	33.9	8.3	65.4
7	50.0	38.8	30.9	-13.7	44.4	36.2	8.2	62.2
8	44.9	38.8	30.2	-13.0	44.4	36.5	7.9	62.1
9	49.0	38.8	31.0	-13.6	44.5	36.4	8.1	62.1
10	46.0	38.8	30.7	-13.5	44.1	35.6	8.5	62.6
Mean	**48.3**	**38.8**	**30.8**	**-13.5**	**42.8**	**34.6**	**8.2**	**64.6**
Std Dev	**2.6**	**0.0**	**0.2**	**0.2**	**1.6**	**1.6**	**0.1**	**2.4**
Min	**44.9**	**38.8**	**30.2**	**-13.8**	**40.4**	**32.2**	**7.9**	**62.1**
Max	**52.4**	**38.9**	**31.1**	**-13.0**	**44.5**	**36.5**	**8.5**	**68.5**
% of Average	**5.4**	**0.1**	**0.8**	**-1.8**	**3.7**	**4.6**	**1.8**	**3.8**

the mode doesn't change from CD to CS at exactly the same point in the Drive cycle. In some runs, the mode change happens later, which will keep the cars running in CD mode longer, using up less energy. We can see that this variability decreases after some time and after that, most of the energy traces are near the standard deviation trace. The same is also true for the SOC trace, Figure 4.7, which diverge from each other near the mode shift region but converges towards the end of the drive cycle.

Since the CD-CS runs were not conducted on Forward MTUDC, this study also conducted 10 runs on MTUDC in CD-CS strategy. The results of those runs are

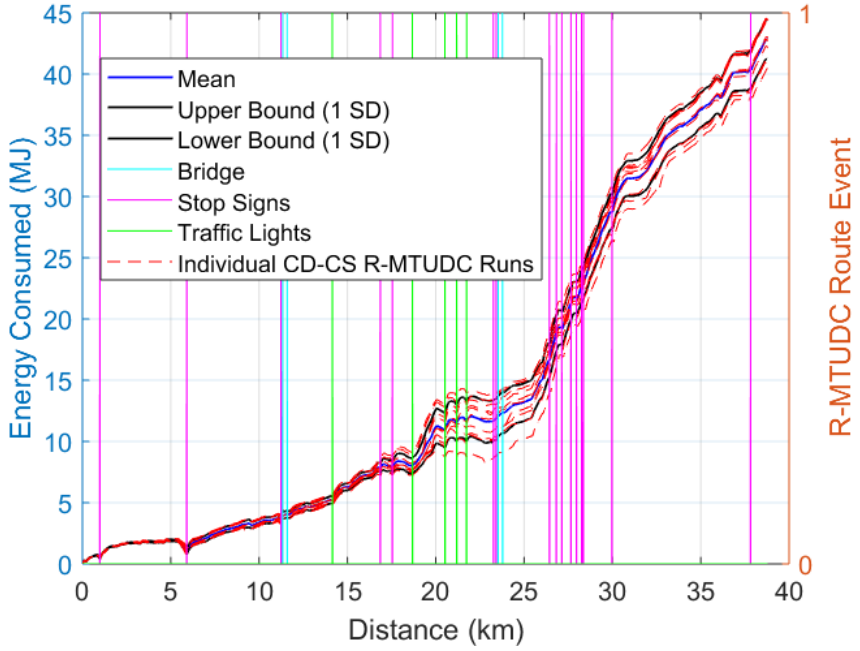

Figure 4.6: Average Energy Consumption and its standard deviation in CD-CS mode on R-MTUDC with individual energy traces

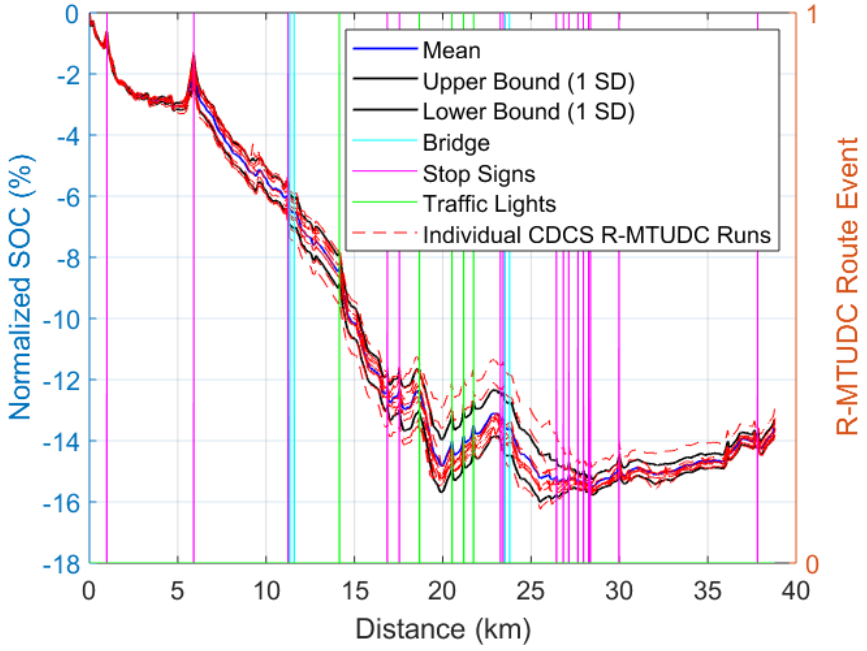

Figure 4.7: Normalized SOC trace and its standard deviation in CD-CS mode on R-MTUDC with individual SOC traces

summarized in Table 4.6

Table 4.6
Forward MTU Drive Cycle Charge Depleting - Charge Sustaining Mode
Result Summary

CD-CS Mode MTUDC	Time	Distance	Initial SOC	SOC % used	Total Energy Consumed	Fuel Energy	Battery Energy	Equivalent Fuel Consumption
Run #	mins	km	%	%	MJ	MJ	MJ	MPGe
1	43.9	38.4	30.3	-13.6	41.7	34.0	7.7	65.4
2	43.4	38.4	31.0	-14.4	35.5	27.1	8.4	77.0
3	45.2	38.4	30.8	-14.6	38.7	29.8	8.9	70.5
4	46.3	38.4	31.5	-14.9	38.7	29.4	9.3	70.5
5	45.3	38.4	31.2	-15.1	38.4	29.1	9.2	71.2
6	45.9	38.4	30.7	-14.1	39.1	30.1	9.0	69.9
7	43.9	38.4	30.8	-14.3	37.9	28.8	9.1	72.0
8	45.1	38.4	30.9	-14.5	37.1	27.9	9.2	73.5
9	43.0	38.4	30.6	-14.0	41.3	33.1	8.2	66.1
10	43.8	38.4	30.5	-13.8	40.9	32.6	8.2	66.8
Mean	**44.6**	**38.4**	**30.8**	**-14.4**	**38.9**	**30.2**	**8.7**	**70.3**
Std Dev	**1.1**	**0.0**	**0.4**	**0.5**	**1.9**	**2.3**	**0.5**	**3.5**
Min	**43.0**	**38.4**	**30.3**	**-15.1**	**35.5**	**27.1**	**7.7**	**65.4**
Max	**46.3**	**38.4**	**31.5**	**-13.6**	**41.7**	**34.0**	**9.3**	**77.0**
% of Average	**2.5**	**0.0**	**1.2**	**-3.3**	**5.0**	**7.6**	**6.2**	**5.0**

The Forward MTUDC CD-CS runs' average time of 44.6 minutes aligns with the that of the CD and CS runs. For the reverse CD-CS runs, the time taken was more than this. The average initial SOC of the MTUDC CD-CS runs were 30.8% which is the same as that of R-MTUDC, but with a greater variability of 0.4. The R-MTUDC consumed 10% more energy than MTUDC, but MTUDC also used up 6% more battery energy on average than R-MTUDC. This can account for a slightly higher than normal energy usage for R-MTUDC. The equivalent fuel consumption from MTUDC is 70.3 MPGe, while for R-MTUDC it is 64.6 MPGe. This justifies

argument that the usage of energy from the battery was more during the forward MTUDC runs.

4.2 Speed Harmonization and Vehicle Platooning

The vehicle platooning experiments were conducted with three cars, Figure 4.8 and the Figure 4.9, shows the speed profile of three cars travelling at 50 mph with 6m gap in between them. The front car was on cruise control and the trailing cars were controlled using the accelerator pedal. The cars were tried to be held at ±2 km/h.

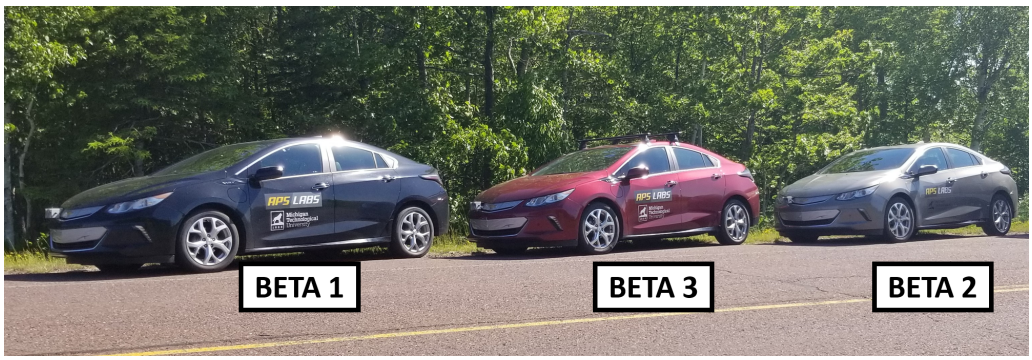

Figure 4.8: The three instrumented Volts used for Vehicle Platoon testing. From left: Beta 1, Beta 3 and Beta 2.

The results of various studies are presented below.

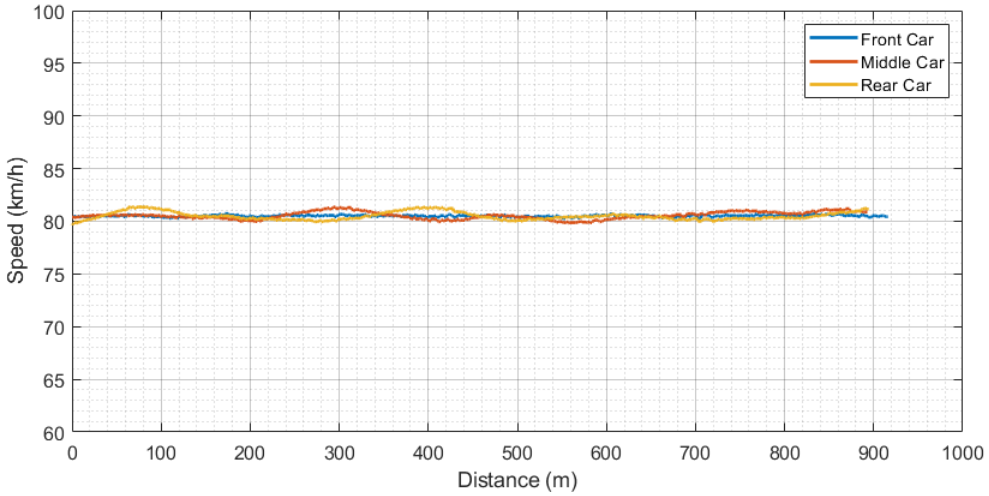

Figure 4.9: The Speed vs Distance of the three Volts running on M-203 at 50 mph and 6m gap

4.2.1 Vehicle Gap Study

The cars were run at 50 mph under gaps of 6m, 9m, 12m and 15m, the results of which are given in Table 4.7 and plotted in Figure 4.10. The rows in the table are color coded to be similar to the color of the respective cars and the BETA 1, BETA 2 and BETA 3 are abbreviated as B1, B2, B3 respectively. In the table, the left most column shows the gap at which the vehicles were running. 'INDEPENDENT' represents the data collected when the vehicles were running independently. The average energy consumption of each vehicle in that particular configuration for both northbound and southbound are shown in column three. The final column shows the energy savings of each car while running in a platoon to when it ran independently. In Figure 4.10, the bars represents the average energy consumption of each vehicle

and the number on top of each bar represents the percent energy savings of each car while in a platoon when compared to running independently.

For tests under all gaps, it can be observed in Figure 4.10 that the middle vehicle consumed the least power in the platoon, while the rear vehicle consumed more energy and the front vehicle consumed the most energy. This is because of the aerodynamics of the platoon, where the middle vehicle does not have a high pressure at the front because of another car in front and the trailing vehicle gives a kind of push to the middle vehicle. A slight increase in the energy consumption of Beta 3 (Rear vehicle in this case) is expected because it was attached with roof rails which could increase the drag. Still, the energy consumption is lesser than the front vehicle. The rear vehicle shows more percent energy savings when compared to independent runs at 9m and 15m gaps.

When the entire platoon is considered, the energy savings is presented in Figure 4.11. Contrary to expectations, the most savings for the platoon is achieved at 9 m gap. Conventional thinking would make us think that the most savings will be achieved at 6m gap compared to 9m. At 6m gaps some other aerodynamic phenomenon might be occurring which increases the platoon energy consumption. Another reason could be that, at very close gap of 6m, the drivers' instincts might have made them react to even small changes in gap which would result in speed transients and hence increased energy consumption. To clear the this question, future tests will have to take the

Table 4.7
Summary of Results for Gap Study

Gap (m)	Car	Average Energy (kJ)	Savings (%)
6	B1	445.1	0.9
	B2	403.4	10.1
	B3	434.7	8.5
9	B1	448.8	0.1
	B2	397.7	11.4
	B3	412.4	13.2
12	B1	448.6	0.1
	B2	407.8	9.2
	B3	436.8	8.0
15	B1	443.7	1.2
	B2	409.2	8.9
	B3	429.9	9.5
INDEPENDENT	B1	449.2	-
	B2	448.9	-
	B3	475.0	-

driver out of the equation and adaptive cruise control systems operable at very close gaps should be used.

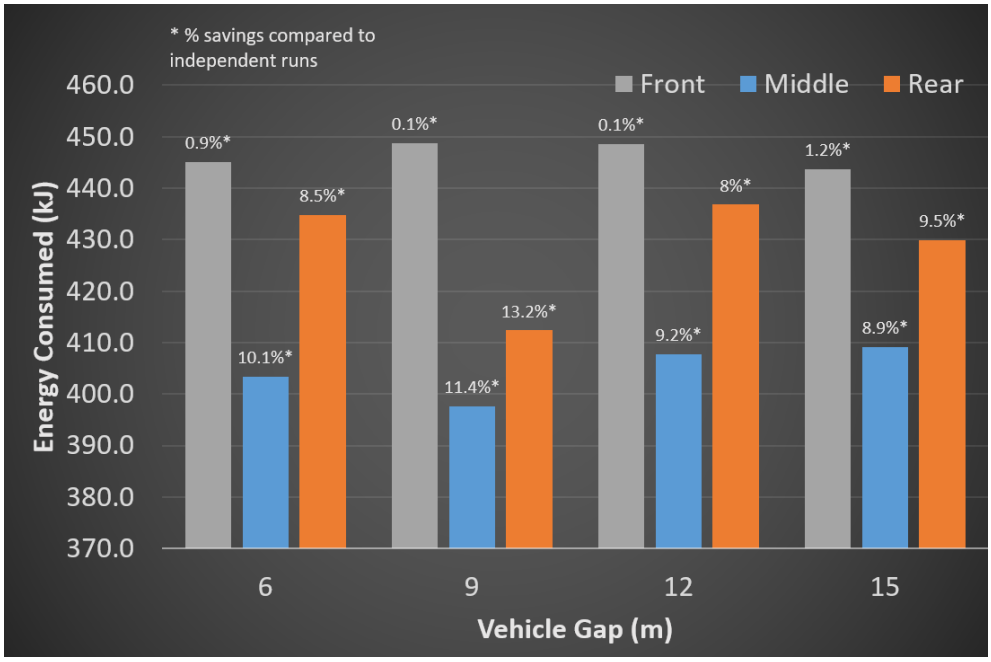

Figure 4.10: The average energy consumption of the three cars running at 50 mph and gaps of 6m, 9m, 12m and 15m

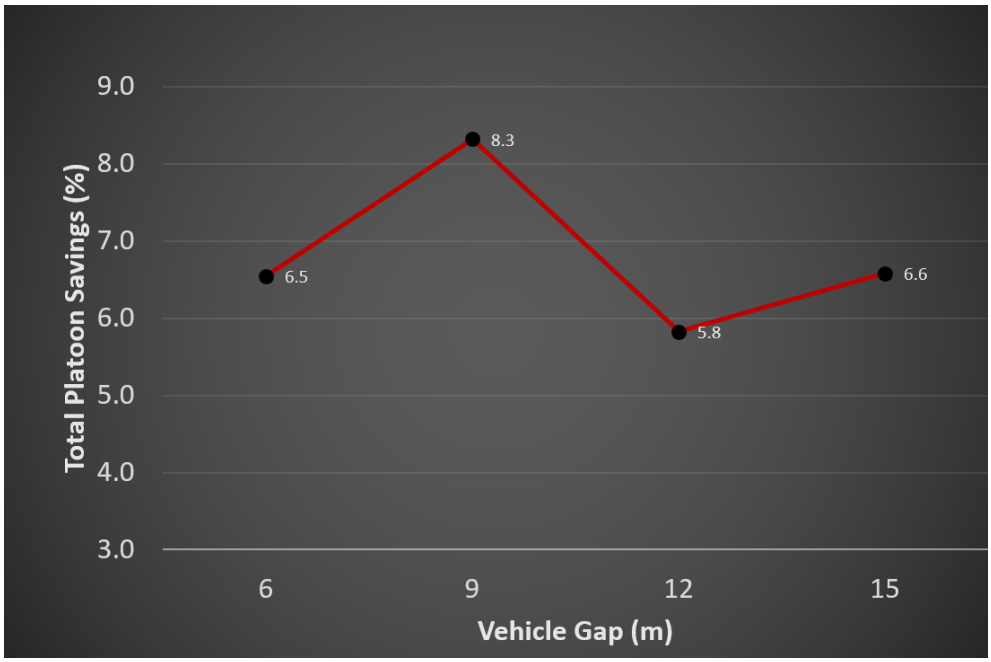

Figure 4.11: The average energy savings of the whole platoon running at 50 mph and gaps of 6m, 9m, 12m and 15m

4.2.2 Vehicle Speed Study

In this study, the cars were run at different speeds of 30 mph, 40 mph, 50 mph and 60 mph at a constant gap of 9m. The average results of the study is tabulated in Table 4.8. Independent runs were also carried out at each speed. The data in the table is shown in Figure 4.12. As the speed increases the energy consumption also increases with least amount of energy at 30 mph runs. Similar to the gap study, the trailing vehicles consume lesser energy, with the middle vehicle consuming the least. But when percent savings are compared, the middle vehicle saves the most at a low speed of 40 mph compared to running independently, while the rear vehicle saves the most at all other speeds.

The savings of the entire platoon is shown in Figure 4.13. The savings should increase with speed but there is a dip in the savings at 40 mph. This could be due to the fact that one of the 40 mph run was done on a cooler day. The savings drastically increases for 50 mph but then decreases again for 60 mph. This dip could be due to environmental factors or some aerodynamic phenomenon that has a greater effect at higher speeds. The platoon shows the highest savings of 8.3% at 50 mph.

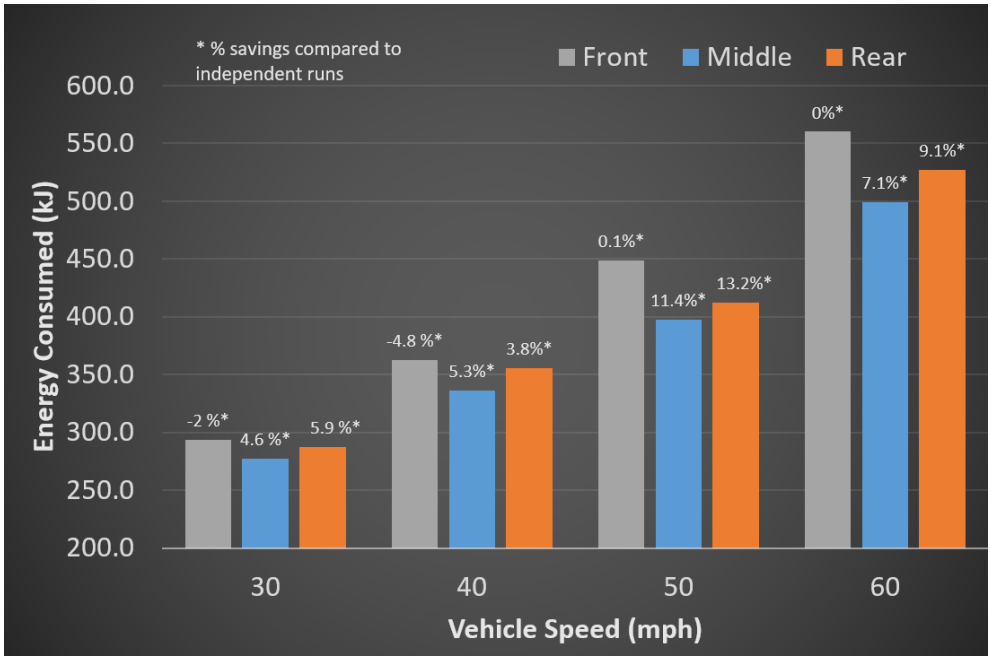

Figure 4.12: The average energy consumption of the three cars running at 9m gap and speeds of 30 mph, 40 mph, 50 mph and 60 mph

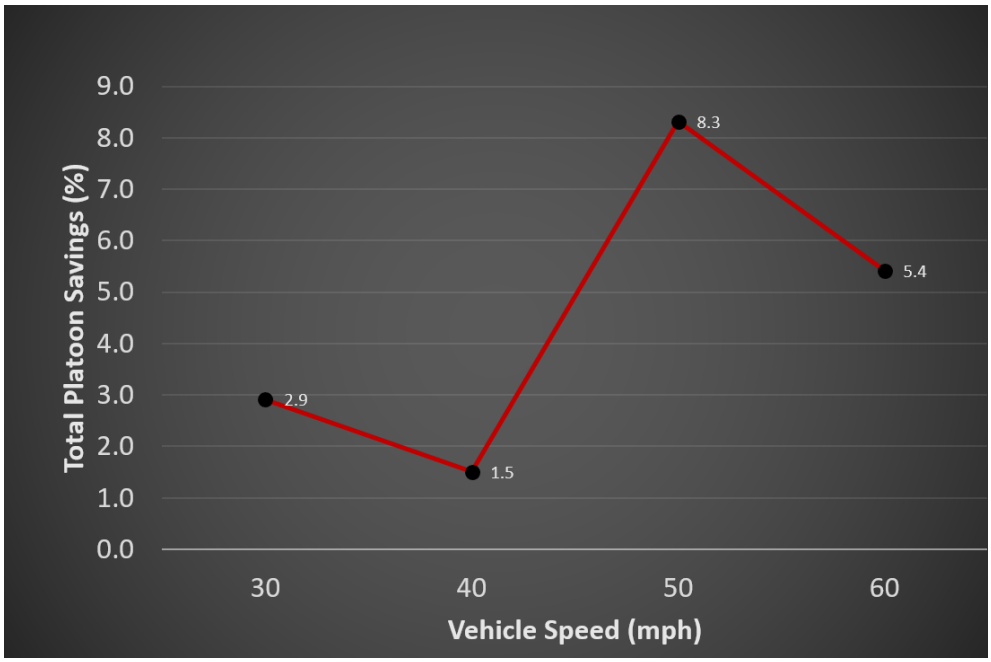

Figure 4.13: The average energy savings of the whole platoon running at 9m gap and speeds of 30 mph, 40 mph, 50 mph and 60 mph

Table 4.8
Summary of Results for Speed Study

Speed (mph)	Car	Average Energy (kJ)	Savings (%)
30	B1	293.6	0.9
	B2	277.3	10.1
	B3	287.3	8.5
40	B1	362.4	0.1
	B2	336.4	11.4
	B3	355.5	13.2
50	B1	448.8	0.1
	B2	397.7	9.2
	B3	412.4	8.0
60	B1	559.9	1.2
	B2	498.9	8.9
	B3	526.9	9.5
30 (INDEPENDENT)	B1	287.8	-
	B2	290.8	-
	B3	305.3	-
40 (INDEPENDENT)	B1	345.6	-
	B2	355.2	-
	B3	369.6	-
50 (INDEPENDENT)	B1	449.2	-
	B2	448.9	-
	B3	475.0	-
60 (INDEPENDENT)	B1	559.9	-
	B2	536.8	-
	B3	579.7	-

4.2.3 Lateral Offset study

The purpose of this study was to investigate how the energy consumption would be affected if all the vehicles in the platoon were not aligned. For this, one of the Volts (Beta 2), which ran in the middle of the pack three times out of the four test scenarios, was offset by a distance on 1 ft, 2 ft and 3 ft. In the last scenario, Beta 2 was shifted to the rear of the pack and ran at an offset of 1 ft.

The results of the study are provided in Table 4.9 and plotted in Figure 4.14. When the offset vehicle is in the middle, the energy consumption of the middle vehicle increases with increasing offset as expected. This is because as the offset of the vehicle increases, it will have to overcome more aerodynamic drag. There is no large difference in energy consumption for the rear vehicle when the offset is 1 ft or 2 ft, but the energy consumption of the rear vehicle also increases when the middle vehicle is offset by 3 ft. When Beta 2 is at the rear of the platoon, Beta 3 has more energy savings as it can take full advantage of the vehicle in front.

When it comes to the entire platoon, the savings drop as the offset increases as seen in Figure 4.15. The maximum savings (7.3%) is when the offset vehicle is at the rear of the pack, since it does not affect the aerodynamics of the other vehicles in the platoon. When, the vehicle in middle of the platoon, is offset, the platoon energy

Table 4.9
Summary of Results for Vehicle Lateral Offset Study

Lateral Offset (B2) ft	Car	Average Energy (kJ)	Savings (%)
1	B1	396.5	-0.5
	B2	370.0	7.8
	B3	395.7	11.9
2	B1	406.1	-2.9
	B2	381.7	4.9
	B3	393.3	12.4
3	B1	407.9	-3.4
	B2	387.8	3.3
	B3	407.0	9.4
1 (B2 Rear)	B1	405.8	-2.8
	B2	357.8	10.8
	B3	390.0	13.1
INDEPENDENT	B1	394.7	-
	B2	401.2	-
	B3	449.1	-

savings vary from 6.6% to 3.4%.

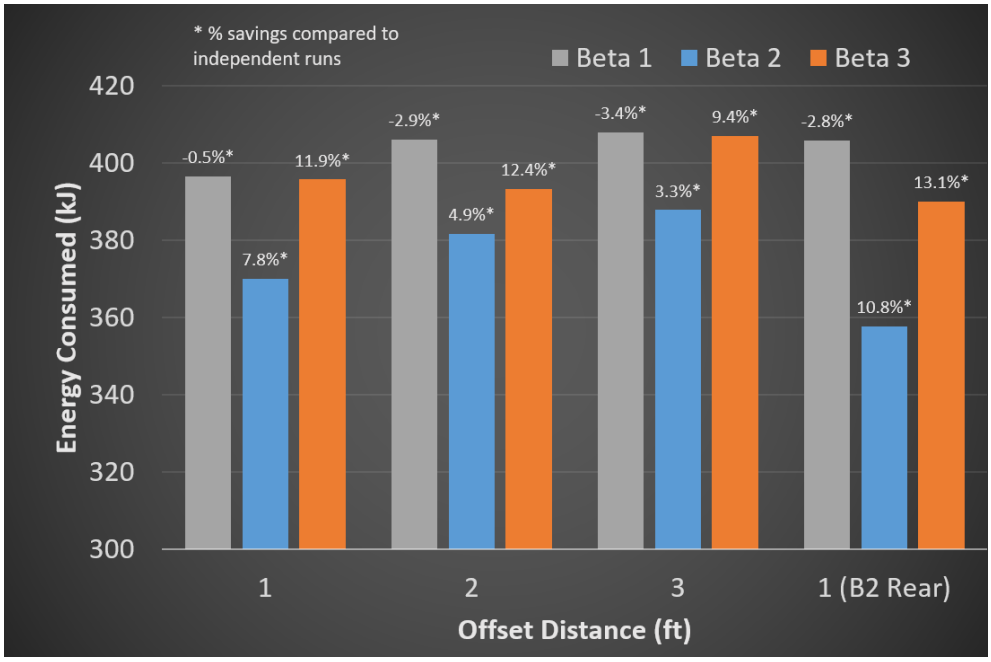

Figure 4.14: The average energy consumption of the three cars running at 9m gap and Beta 2 offset laterally by 1 ft, 2 ft and 3 ft

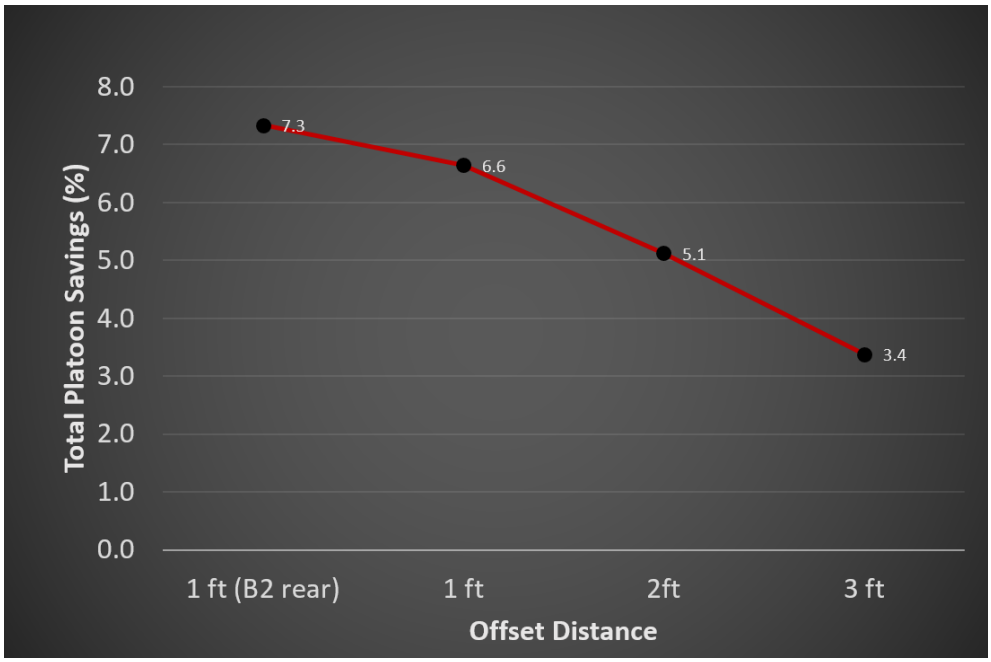

Figure 4.15: The average energy savings of the platoon running at 9m gap with the Beta 2 offset laterally by 1 ft, 2 ft and 3 ft

4.2.4 Location of vehicle with aero-modifier study

An aero-modifier was fixed to the top of Beta 3 and the variation in energy consumption at different vehicle locations in the platoon were analyzed. All the tests were carried out at 9m gap and 50 mph. The average energy consumption data for the study is provided in Table 4.10 and plotted in Figure 4.16. A considerable increase in energy consumption of Beta 3 is noticed compared to energy consumption with no aero-modifier. This is indicative of how even a small change in the shape of the car can increase the energy consumption. There is an energy savings for Beta 3, even when it runs at the front of the platoon. The reason for this could be that Beta 3 was running on cruise control when it ran at the front of the platoon, but it was running on accelerator pedal at all other times, even when running independently.

The savings of the whole platoon shown in Figure 4.17, indicates that the most energy savings is achieved when the vehicle with the aero-modifier is present at the front of the platoon. Once the vehicle moves to the middle or rear, the savings of the platoon remains constant.When Beta 3 is at the front of the platoon, the total energy consumption of the platoon is 1241 kJ. While for a platoon running in the same speed and gap configuration but without the aero-modifier, the average total energy consumption is 1259 kJ. In a platoon wide view, there is not much difference in energy but the front vehicle in the first case had an additional load on its roof.

Table 4.10
Summary of Results for location of vehicle with Aero-Modifier Study

Location of car with aeromodifier (B3)	Car	Average Energy (kJ)	Savings (%)
Rear	B1	404.1	-2.4
	B2	346.3	13.7
	B3	513.8	11.2
Middle	B1	393.7	0.2
	B2	358.7	10.6
	B3	513.0	11.3
Front	B1	360.9	8.6
	B2	337.0	16.0
	B3	543.1	6.1
INDEPENDENT	B1	394.7	-
	B2	401.2	-
	B3	578.6	-

These numbers can also be because of the atmospheric conditions, because the tests were conducted on two different days but it is worth investigating further.

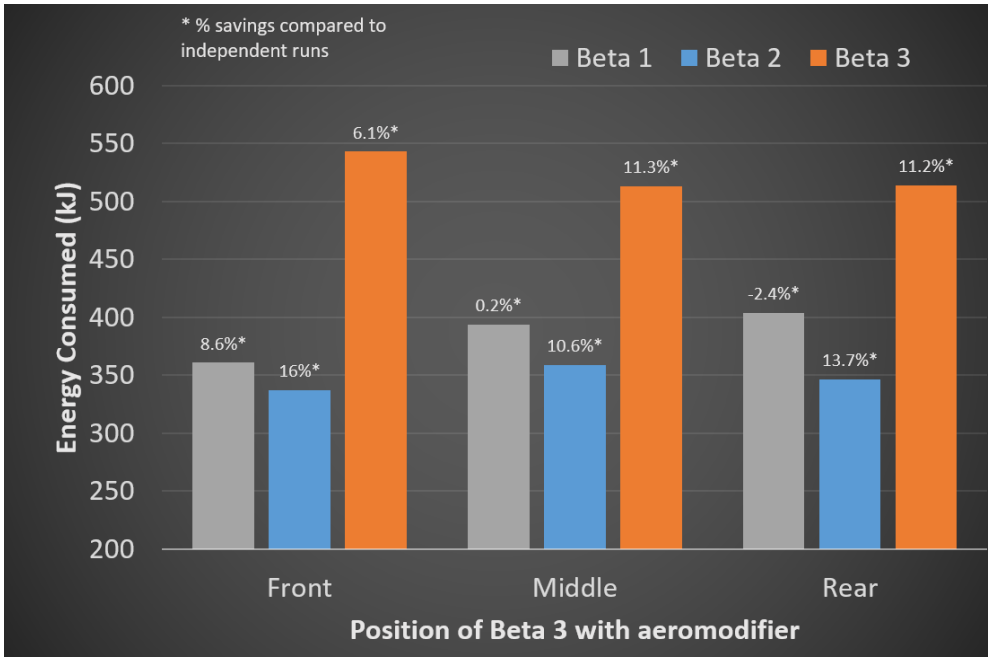

Figure 4.16: The average energy consumption of the three cars running at 9m gap with the vehicle with aero-modifier running at different locations in the platoon

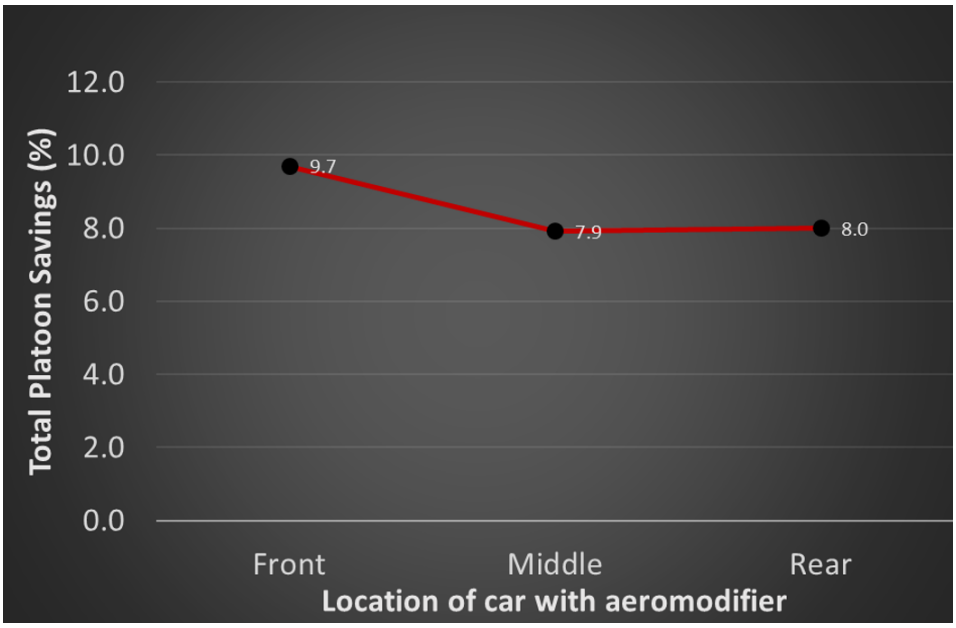

Figure 4.17: The average energy savings of the platoon running at 9m gap with the vehicle with aero-modifier running at different locations in the platoon

4.3 Route Based Blended Mode Optimizer

The cars were run under normal CD-CS strategy and also with the optimal control matrix from the Blended Mode Optimizer. Figure 4.18 shows the fuel power used on the MTUDC when the vehicle controller is following the Hold Mode matrix generated from the blended mode optimizer, while Figure 4.19, shows the section of the route where the engine was ON, when the vehicle was running under normal CD-CS operation.

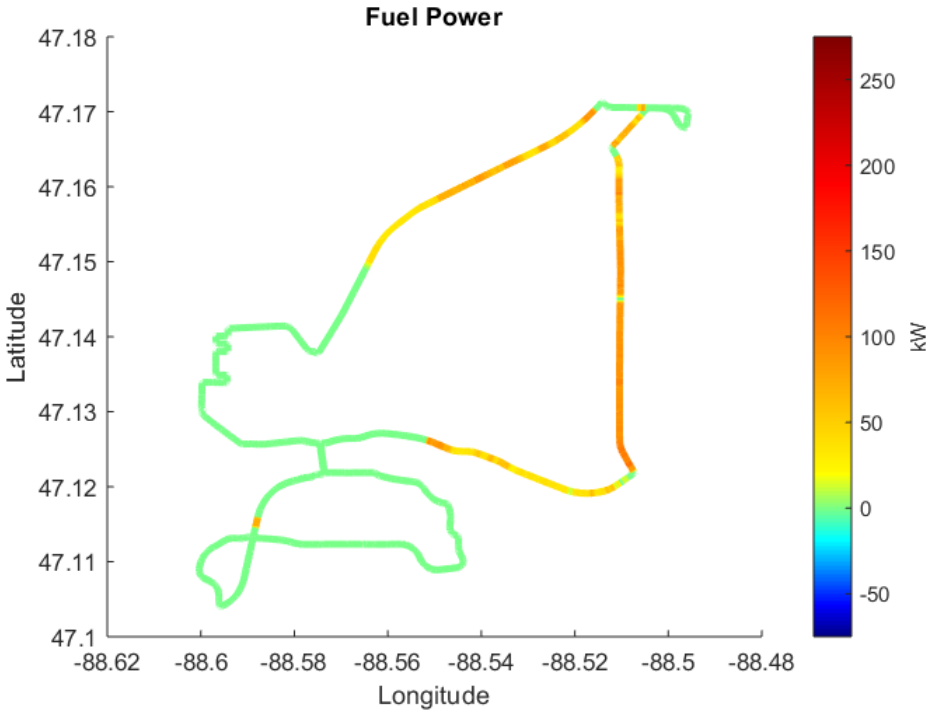

Figure 4.18: Energy from fuel used on the section of the MTUDC when the cars are following the Hold Mode Matrix

It can be seen in Figure 4.18, that, by using the Hold Mode Matrix, the engine turns

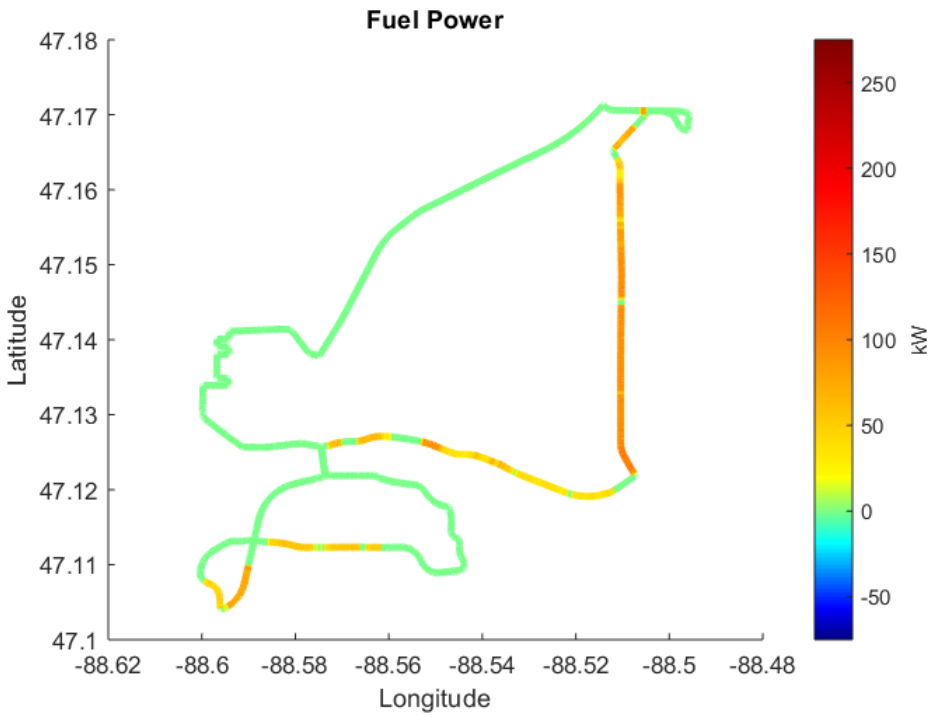

Figure 4.19: Energy from fuel used on the sections of the MTUDC when the cars are following the Normal CD-CS strategy

on only at sections of the Drive cycle where the power demand is constant and vehicle is travelling at higher and constant speeds, improving the fuel economy. While, the fuel energy consumption map of the vehicle in Normal CD-CS strategy, Figure 4.19, shows that, the engine turns on at sections on the Drive Cycle where the vehicle speed is low and varying, with stop signs and traffic signals. This will lead to transients in engine operation and decrease in fuel economy.

Figure 4.20 shows the optimal control matrix inputted into the vehicle before one of the Forward MTUDC runs. The figure is overlaid with the actual SOC trace the vehicle followed and the Hold Mode signal from the vehicle. This shows that the vehicle

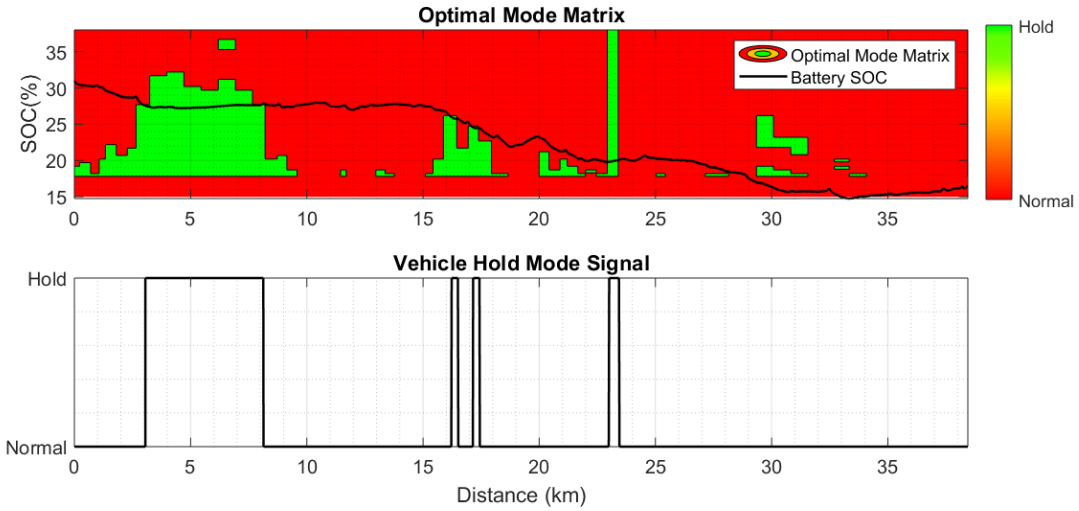

Figure 4.20: The Optimal Control Matrix input into the vehicle overlaid with the actual SOC profile of the test run along with the Hold Mode Signal generated by the car

is able to go into Hold and Normal Mode based on the inputted Optimal Control Matrix. Since, the optimal control matrix is input as function of SOC and Distance, the vehicle will follow the path of minimum energy consumption independent of the starting SOC. Also, because of this, even if some unforeseen circumstances cause the battery SOC to vary from the optimal SOC path predicted by the optimizer, the vehicle will follow the path of minimum energy consumption from the new SOC level to the end of drive cycle.

The results of the test runs are provided in the Table 4.11. The first 5 runs of the MTUDC test runs were carried out as pairs of cars with one car running under blended strategy and the other running under normal strategy. The rest of the test runs were conducted one at a time with the car under blended strategy running after the test run in normal strategy was completed. The savings obtained from these runs

Table 4.11
The Results of the Blended Test runs, each test running with a blended strategy is paired with a test running the normal strategy.

Drive Cycle	Run No.	Mode	Initial SOC (%)	Final SOC (%)	Total Energy (MJ)	Savings (%)
MTUDC	1	Blended	31	16.6	41.8	-1.8
		Normal	31	16.6	41.1	
	2	Blended	31	16.5	41.4	2.4
		Normal	31	16.6	42.4	
	3	Blended	31	16.4	43.7	-0.5
		Normal	31	16.6	43.5	
	4	Blended	31	16.3	44.7	5.2
		Normal	31	15.9	47.2	
	5	Blended	31	16.0	45.6	-4.2
		Normal	31	16.3	43.8	
	6	Blended	31	16.5	43.4	3.0
		Normal	31	16.8	44.7	
R-MTUDC	1	Blended	31	17.4	50.7	2.7
		Normal	31	17.4	52.1	
	2	Blended	31	17.5	51.4	-1.4
		Normal	31	17.5	50.7	
	3	Blended	33	17.7	43.8	-0.4
		Normal	33	17.5	43.6	
	4	Blended	33	17.4	45.7	-4.1
		Normal	33	17.6	43.9	

are mixed, with some runs providing a net positive energy savings while some runs providing a net negative energy savings. This shows that the actual test results are highly dependent on the testing conditions. The savings were found to be affected by the distance at which the engine turned on in the Normal runs which occurred within a 1 km window. The engine On duration and the number of engine starts also varied from run to run. The duration of engine On was lesser in blended runs compared to normal ones except for the 4th R-MTUDC run. The maximum savings of 5.2% is achieved in the 4th MTUDC run. The results of this run is shown in Figure 4.23. The least savings of -4.2% was achieved in the 5th MTUDC run. Another reason for

the negative energy savings is the variation in the route characteristics from run to run. Since, the vehicle connectivity technology has not been implemented on-road, the vehicles cannot get a real-time look up of the velocity ahead of it and adjust accordingly. An example of this defect can be seen in Figures 4.21 and 4.22. Figure 4.21 shows the optimal control matrix inputted into the vehicle controller before the 4th R-MTUDC Blended run which had a negative savings of -4.1% and Figure 4.22 shows the optimal mode matrix extracted from the actual blended run made by the car. Some differences can be observed between the two matrices and the Hold Mode signals, especially towards the end of the drive cycle. In Figure 4.21, around the 30 km mark, the vehicle SOC misses the Hold region but ideally, for the drive cycle, the hold region should have extended a bit more towards 29 km. This small difference caused the SOC to drop below 18% and caused a drop in SOC to around 16% and the vehicle controller was not able to shift modes because once the SOC drops below 18%, the option to select Hold mode gets disabled and the vehicle runs according to its own controller, which reduces our chances to operate the vehicle in hold mode towards the end of the drive cycle. Towards the end the SOC rises back to 17% due to the engine recharging the battery. So, the run to run variation also plays a major role in determining the energy savings from blended mode optimization.

In Figure 4.23, it can be seen that the axle torque profile and the vehicle speed profile for both the normal and blended operation are similar. On looking at the energy and SOC trace, it can be observed that they diverge from each other at around the

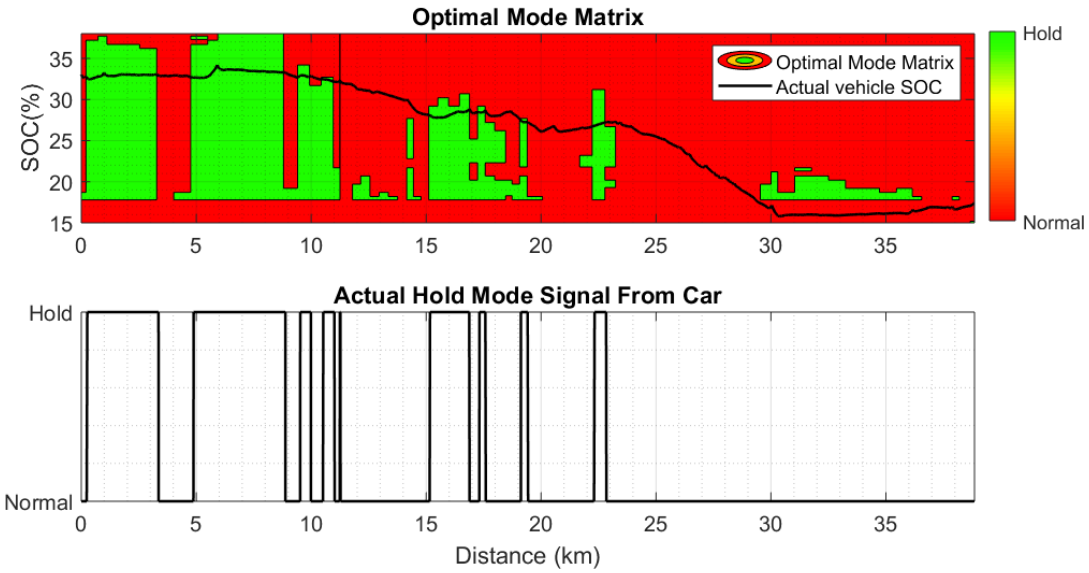

Figure 4.21: The Optimal Mode Matrix Input into the vehicle controller for the 4th R-MTUDC run, along with the actual vehicle SOC trace and Hold Mode Signal

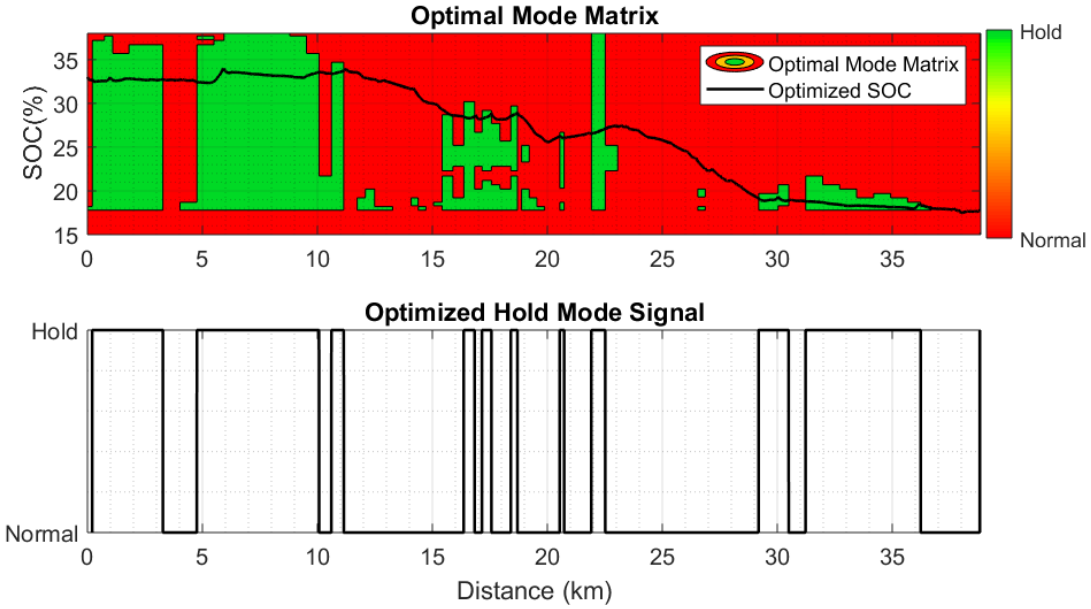

Figure 4.22: The Optimal Mode Matrix extracted from the 4th R-MTUDC Blended Run along with the predicted SOC and Hold Mode signal

3 km mark. This is where the car under blended operation turns into hold mode for the first time. After that, at around the 21 km mark, the energy traces cross over and from this point onward, the car running the blended strategy is at a net positive energy savings. The SOC traces of both the runs end at the same value confirming that the savings in the blended run is not due to more usage of electrical energy.

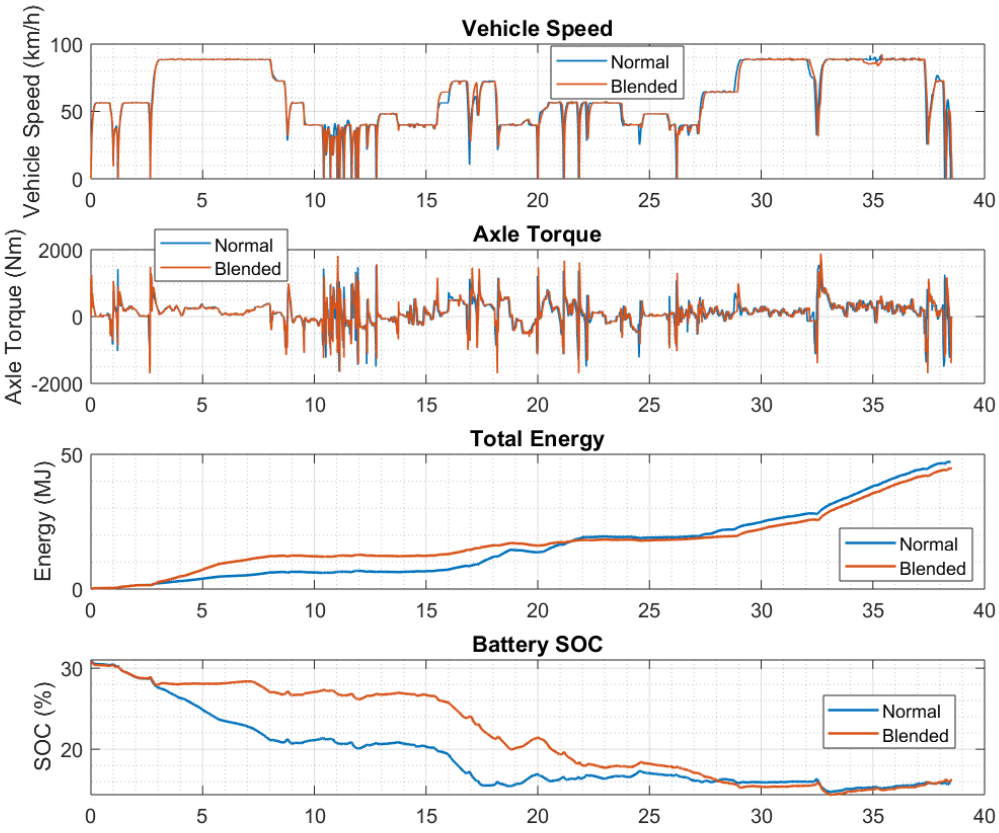

Figure 4.23: Velocity, Axle Torque, Energy and SOC trace of Normal and Blended MTUDC Run 4 with 5.2% savings

4.4 Engine Start-Stop Optimizer

4.4.1 Engine Start-Stop Optimizer using Predicted Engine Start and Stops

Since, the start-stop optimizer could not be tested on the cars, data already collected from previous tests were used to test the optimizer and obtain the energy consumption values. To maintain uniformity in the results, the energy values from the Reduced Order Powertrain Model of the Volt [3], was used to compare the energy savings from the optimizer. The data presented here for comparison was taken from a test run made on an 84 km route from Copper Harbor to the Michigan Technological University. During the run, a large number of engine start and stops were noticed which led to the development of the optimizer. The velocity and elevation profile for the route is shown in Figure 4.24, along with the actual Engine Starts and Stops. It can be seen that, the engine was turned on and off multiple times along the route.

Figure 4.25, shows the optimized results for the inputs shown in Figure 4.24. It can be seen that the optimizer successfully reduced the number of Engine Starts, and was also able to reduce energy consumption, as seen from the Energy trace. In the part of Figure 4.25 pertaining to the SOC, it can be seen that the final SOC of the optimized

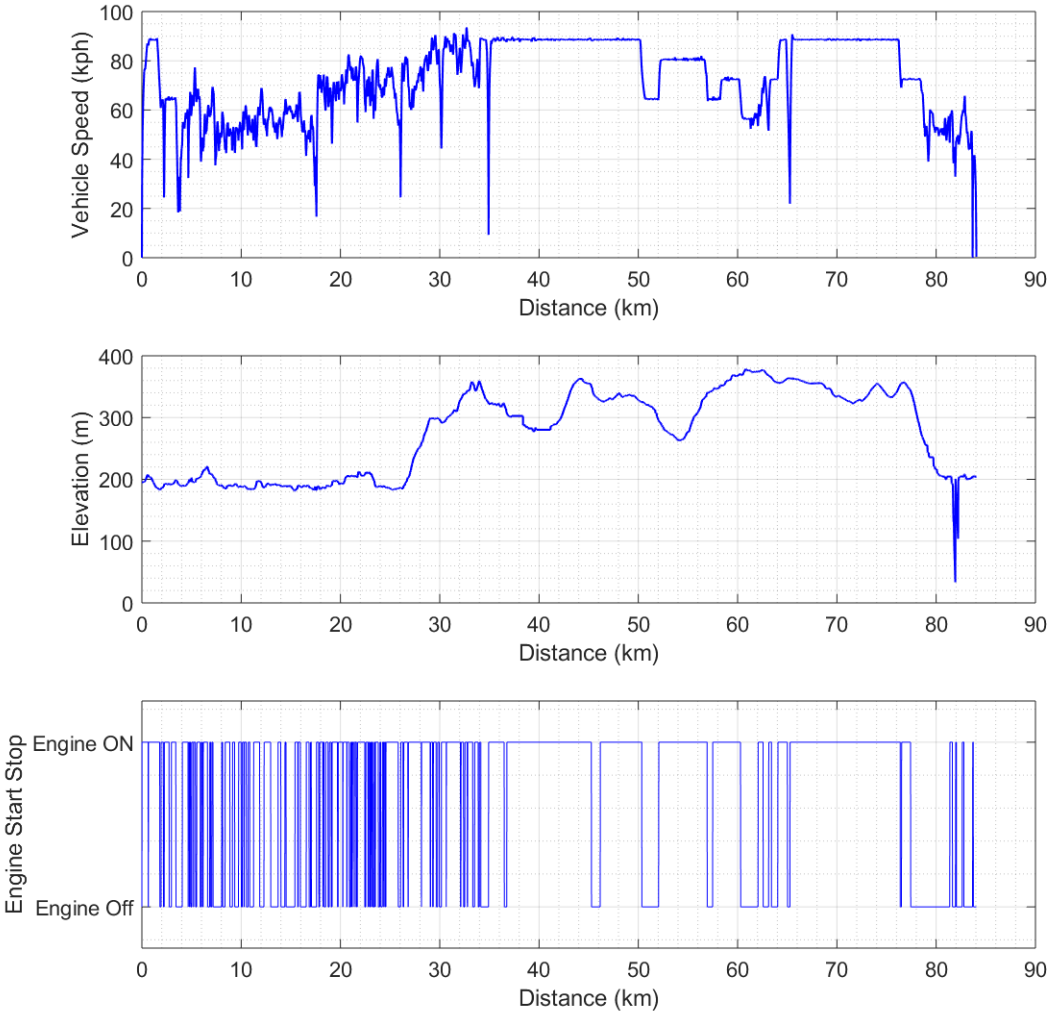

Figure 4.24: Velocity and Elevation profile of Copper Harbor to Michigan Tech University route, along with the actual Engine Start-Stop profile, used to analyze the results of Engine Start-Stop Optimizer

result is lower than the predicted final SOC. This is because the optimizer tries to utilize the maximum electrical energy available to it by the end of the route, while the normal vehicle controller tries to maintain the SOC at a higher level, to account for any high power demand maneuvers that may be required by the car since it does

not have a future look up of the route. In Table 4.12, the optimized energy refers to the total energy consumption of the route when the optimizer is allowed to end at a lower SOC. This Optimized Energy consumption has been normalized to account for the difference in final SOCs and is presented as Normalized Energy along with savings.

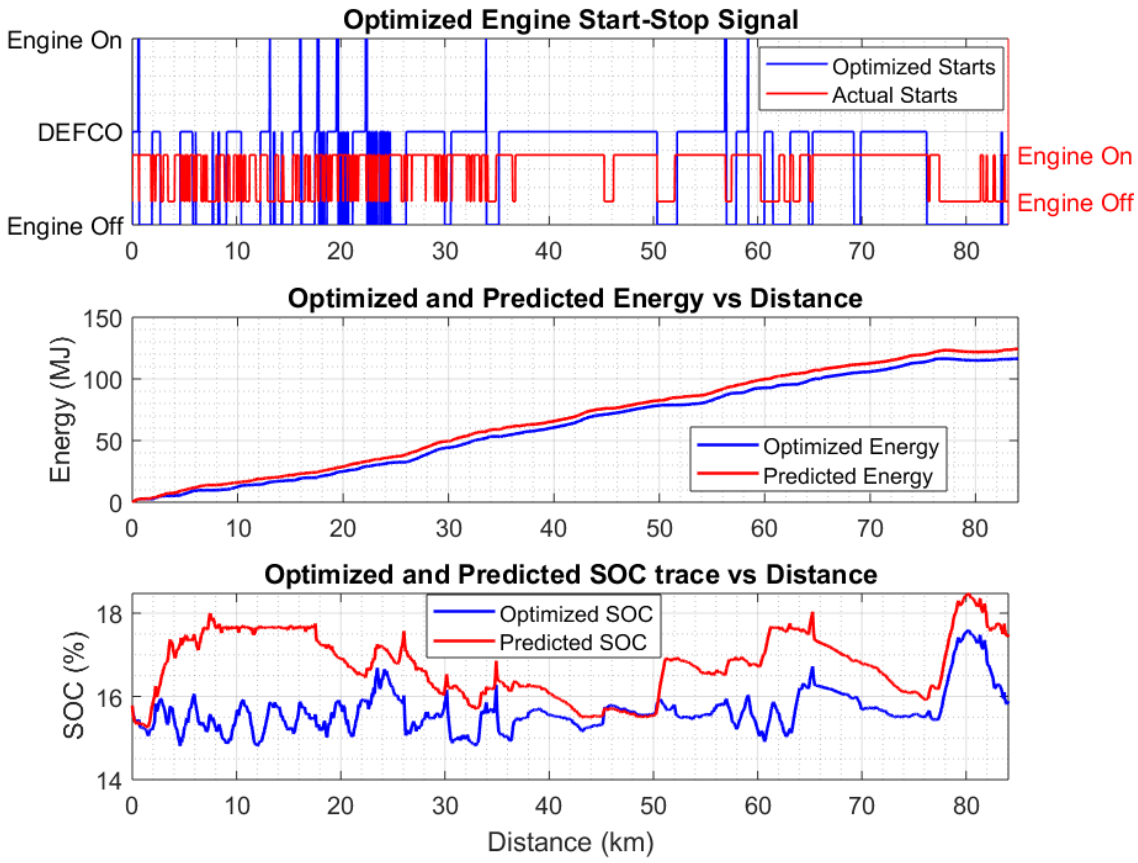

Figure 4.25: Plot of the output predicted by the Optimizer overlaid on top of Actual Engine ON/OFF, Predicted SOC and Predicted Energy

From Table 4.12, the Route 2 from Copper Harbor to MTU has the most savings of 3.8%. In all of the runs, the number of engine starts have been considerably

Table 4.12
Results showing Energy savings from optimizing the Engine Start-Stop by Engine Start-Stop Optimizer using Predicted Engine Start and Stops

Route	Normal Operation Results			Optimized Operation Results				
	No: of Engine Starts	Engine ON Time (s)	Predicted Energy (MJ)	No: of Engine Starts	Engine ON Time (s)	Optimized Energy (MJ)	Normalized Energy (MJ)	Normalized Savings (%)
Copper Harbor to MTU - Route 1	45	2826	120.2	33	2267	115.4	117.9	1.9
Copper Harbor to MTU - Route 2	**82**	**2782**	**124.2**	**48**	**2437**	**116.3**	**119.5**	**3.8**
Copper Harbor to MTU - Route 3	58	3049	128.4	35	2752	123.7	126.1	1.8
MTUDC	22	1193	69.2	10	1230	65.7	68.4	1.2
R-MTUDC	32	1623	72.7	15	1882	70.2	72.8	-0.1

reduced, while the duration of Engine On also decreased except for the MTUDC and R-MTUDC runs. In these runs, the number of Engine Starts have been considerably reduced, but due to the increase in the duration of Engine On, there is only very less savings. For Route 2, the optimizer was able to reduce the number of starts by almost 41%. The savings are highly dependent on the route as Table 4.12 suggests. Routes having considerable transients in axle torque requirements, like considerable elevation changes and rapid speed limit changes, has a huge potential for obtaining larger savings by using this optimizer.

4.4.2 Engine Start-Stop Optimizer using Dynamic Programming

The same dataset used in Section 4.4.1 is used to compare the performance of the Engine Start-Stop Optimizer using Dynamic Programming. The output of the optimizer is an Optimal Control Matrix. The matrix contains information on which mode (Engine On or Off) will be the optimal mode based on the distance travelled by the car on the predefined route and current SOC. Figure 4.26 shows the optimal control matrix for the Route 2 of the Copper Harbor to Michigan Technological University routes. Based on the optimal control matrix and the initial SOC, the optimizer also predicts the energy and the SOC trace that will be followed by the car on following this control matrix. This optimized SOC trace is also overlaid on top of the optimal control map. Basde on this SOC trace, an engine start stop trace is also shown at the bottom of the Figure 4.26. It can be seen that the the SOC remains within the required bounds of SOC.

Table 4.13 tabulates the energy savings from the optimizer when the optimizer was forced to end at the same final SOC as the final SOC predicted by the Reduced Order Powertrain model, so as to get a fair comparison. It was possible to force the optimizer to end at the desired final SOC except for the MTUDC run. This suggests that the final SOC at which the normal MTUDC run ended might have been very

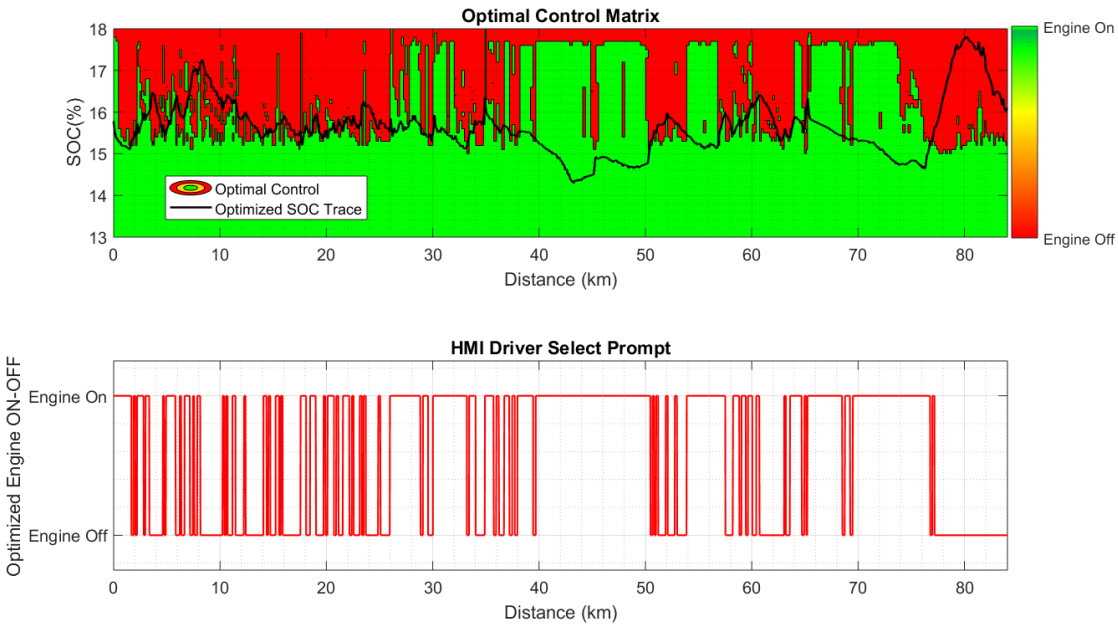

Figure 4.26: Optimal Mode Matrix output from the Engine Start-Stop Optimizer overlaid with the optimal SOC path for the actual starting SOC and the Optimized Engine Start-Stop profile overlaid on the actual Engine Start-Stop profile

costly in terms of energy consumed. The results shown in Table 4.14 data corresponds to the situation where a constraint on the final SOC was not placed and optimizer was allowed to choose the path with the least energy consumption.

For the Forced Final SOC results, by running pre-recorded routes through this optimizer, it is seen that the number of engine starts are reduced in the the Copper Harbor to MTU runs, but there is no decrease in the number of engine starts for the MTUDC and R-MTUDC runs. A similar trend is shown for the duration of engine ON, where the engine ON duration increased for the MTUDC and R-MTUDC runs, while decreased for all other runs. But, the optimizer was able to achieve a maximum

Table 4.13
Results showing Energy savings from optimizing the Engine Start-Stop by Engine Start-Stop Optimizer using Dynamic Programming when the Final SOC is forced

Route	Normal Operation Results			Optimized Operation Results (Forced Final SOC)			
	No: of Engine Starts	Engine ON Time (s)	Predicted Energy (MJ)	No: of Engine Starts	Engine ON Time (s)	Predicted Energy (MJ)	Savings (%)
Copper Harbor to MTU - Route 1	45	2826	120.2	40	2550	116.1	3.4
Copper Harbor to MTU - Route 2	**82**	**2782**	**124.2**	**58**	**2420**	**115.8**	**6.8**
Copper Harbor to MTU - Route 3	58	3049	128.4	54	2720	122.5	4.6
MTUDC	22	1193	69.2	27	1310	66.8*	3.5*
R-MTUDC	32	1623	72.7	35	1890	69.5	4.5

* Final SOC was not same as Final SOC in normal operation, hence the energy savings was normalized

savings of 6.8% for the Route 2 run compared to normal operation.

When the optimizer was not forced to end at a pre-defined final SOC, the savings improved, which is seen in Table 4.14. The 6.8% savings shot up to 8.3% when a restriction on the final SOC was not placed. The number of engine starts and duration of engine starts also decreased except for MTUDC and R-MTUDC runs. But, the savings of these runs almost doubled by not setting a target SOC.

The optimized result of the Copper Harbor to MTU Route 2 from the Dynamic

Table 4.14
Results showing Energy savings from optimizing the Engine Start-Stop by Engine Start-Stop Optimizer using Dynamic Programming when the Final SOC is not forced

Route	Normal Operation Results			Optimized Operation Results				
	No: of Engine Starts	Engine ON Time (s)	Predicted Energy (MJ)	No: of Engine Starts	Engine ON Time (s)	Final SOC (%)	Optimized Energy (MJ)	Savings (%)
Copper Harbor to MTU - Route 1	45	2826	120.2	34	2460	16.3	114.3	4.9
Copper Harbor to MTU - Route 2	**82**	**2782**	**124.2**	**53**	**2330**	**16.1**	**113.8**	**8.3**
Copper Harbor to MTU - Route 3	58	3049	128.4	51	2620	15.4	120.2	6.4
MTUDC	22	1193	69.2	27	1320	15.4	64.7	6.6
R-MTUDC	32	1623	72.7	40	1730	15.6	67.0	7.9

Programming based optimizer when the final SOC is not set, is shown in Figure 4.27. A lot of the unnecessary engine starts have been reduced and the optimized SOC trace shows a lot of oscillations compared to the predicted normal SOC trace. In the energy trace in Figure 4.27, it is seen that the maximum difference in predicted and optimized energy occurs at the first half of the drive cycle before 40 km mark. This is because there is a lot of variation is velocity in the first 40 km, Figure 4.24. This causes many unnecessary engine On-Offs. After the 40 km mark the velocity is more stable making the optimizer output similar to the in-built vehicle controller decisions.

In order to make a fair comparison of the two Engine Start-Stop Optimizers presented in this section, the results of the Dynamic Programming Optimizer when the final

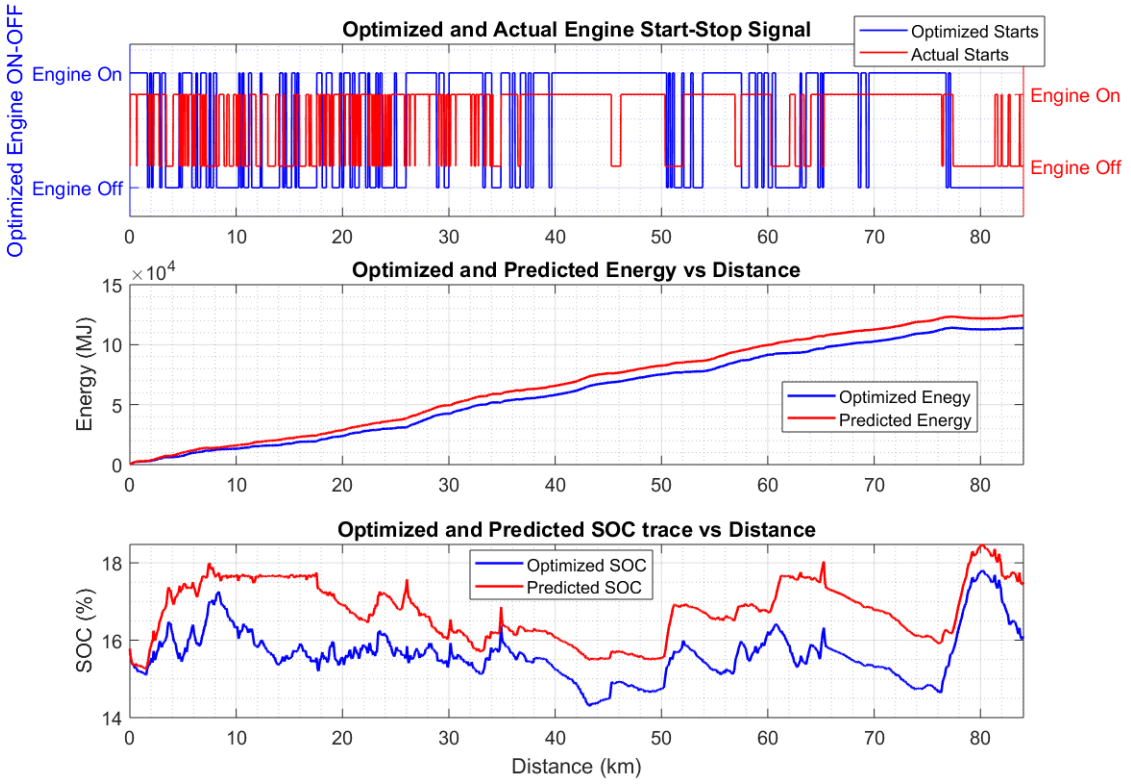

Figure 4.27: Plot of the output predicted by the Dynamic Programming based Optimizer when the final SOC is not set, overlaid on top of Actual Engine ON/OFF, Predicted SOC and Predicted Energy

SOC is forced in Table 4.13 should be compared to the results of the Engine On-Off Predictor based optimizer in Table 4.12, since the energy values are normalized. On comparison, even though the predictor based optimizer reduces the number of engine starts compared to the Dynamic Programming based one, more savings can be obtained from the Dynamic Programming optimizer in all the cases compared to the other. This is because the predictor based optimizer does not optimize for the entire drive cycle but only for the period of engine On or Engine Off predicted, while the Dynamic Programming based optimizer optimizes performance for the entire drive

cycle. But, the number of engine starts are considerably reduced in the Predictor based optimizer.

Chapter 5

Conclusions and Future Work

5.1 Reverse MTUDC

In the first part of the study, the energy consumption of a PHEV on a Real World Driving Cycle was analyzed. the Real World Drive cycle presented here has tried to encompass all of the different driving scenarios encountered by a normal person in day to day driving. From the 30 runs conducted on the Drive cycle, a baseline energy consumption map was developed, along with a mean velocity profile with a standard deviation. These values has been used for comparing the energy savings potential of a vehicle through vehicle connectivity. These tests also investigated the variability in energy consumption and found that in pure EV mode and charge sustaining mode, the

variability in energy consumption for the route is under 3%, while it is under 4% for Charge Depleting - Charge Sustaining operating strategy. The increased variability in CD-CS strategy can be attributed to the variation in the instant at which the mode changes from CD to CS in the drive cycle. From the comparison of MTUDC and R-MTUDC, it can be concluded that the R-MTUDC requires more energy to be completed and variability in time to complete the cycle is lesser.

5.2 Speed Harmonization and Vehicle Platooning

The Vehicle Platooning studies investigated the savings potential of travelling as a cohort of vehicles rather than individually to reduce the aerodynamic drag each vehicle has to face. From the Gap study, it can be concluded that the trailing vehicles has the potential to save energy. A clear conclusion as to which vehicle position saves the more energy could not be made as the vehicles at rear showed more savings at 9m (13.2%) and 15m (9.5%) gaps, while the middle vehicle showed more savings at 6m (10.1%) and 12m (9.2%) gaps. The entire platoon saved most (8.3%) at 9m gap. In the Speed study as well, the maximum savings for the platoon was achieved at 50 mph. The savings at lower speeds were less than half of the savings at 50 mph. Therefore, the vehicles need to be at higher speeds to have any considerable savings. In the study with the aero-modifier on top of a car, it was concluded that the most savings is achieved when the vehicle with the aero-modifier travels at the front of the

pack. For the Lateral Offset study, the results obtained shows that if the vehicles are not co-linear it could drastically affect the savings potential, with the savings of the entire platoon decreasing by half when the offset distance of the middle vehicle changes from 1ft to 3ft. If the vehicle needs to be offset, it should be at the rear of the platoon where it has the least effect. The platooning studies conducted had a lot of variability because of the human factor in the loop. The driver's tend to get more aggressive on the accelerator pedal at really close distance and higher speeds which could negatively affect the savings potential. For future testing getting all the cars run under cruise control will help achieve more robust results and obtain a clearer picture of the savings potential of platooning.

5.3 Route Based Blended Mode Optimizer

The Optimal Control Matrix was successfully implemented in the vehicle and the Hold Mode Signal was analyzed to make sure the vehicle was following the desired strategy based on SOC and Distance travelled. The on-road testing of Route Based Blended Mode Optimizer gave a mixed set of results ranging from positive savings of 5.2% to negative savings of -4.2%. This is because the tests are sensitive to driving conditions. More tests are needed to create a distribution of energy savings. Another scope for future work lie in getting the optimizer running automatically in the vehicle using the route data obtained by V2X communications. For testing, the optimizer was

run off-line and the optimal matrix was manually compiled into the vehicle controller. This process needs to be automated.

5.4 Engine Start-Stop Optimizer

The Engine Start-Stop Optimizer, uses the predicted velocity and elevation profile of the route to come up with an optimal mode at each section of the drive cycle to maximize efficiency. The first controller predicts the engine starts and stops using axle power, vehicle speed and SOC and then optimizes the starts and stops based on the energy consumption at each section and engine start penalty. This optimizer was able to obtain a maximum savings of 3.8% on a test route, while it was also able reduce the number of engine starts by almost 41%. The second optimizer tried to operate the engine in the most efficient sections of the route using Dynamic Programming. The route was divided into 10 second sections and a maximum savings of 8.3% was achieved for the same test route. The second optimizer has a superior energy savings potential than the first one. The second optimizer did not assign any penalty to changing the mode of engine operation. A model which assigns penalty to changing modes will provide a more closer approximation of the actual energy savings. This optimizer could not be implemented in the car as the manufacturer assistance was needed to make changes to the low level vehicle controller. Tests will have to be conducted to validate the results of the model on actual drive cycles.

References

[1] "Chart library: Passenger vehicle fuel economy." `https://theicct.org/chart-library-passenger-vehicle-fuel-economy`, 2019. [Online; accessed 03-March-2020].

[2] B. M. Conlon, T. Blohm, M. Harpster, A. Holmes, M. Palardy, S. Tarnowsky, and L. Zhou, "The next generation "voltec" extended range ev propulsion system," *SAE International Journal of Alternative Powertrains*, vol. 4, no. 2, pp. 248–259, 2015.

[3] N. Rama and D. Robinette, "Computationally efficient reduced-order powertrain model of a multi-mode plug-in hybrid electric vehicle for connected and automated vehicles," in *WCX SAE World Congress Experience*, SAE International, apr 2019.

[4] D. Robinette, E. Kostreva, A. Krisztian, A. Lackey, C. Morgan, J. Orlando, and N. Rama, "Phev real world driving cycle energy and fuel and consumption

reduction potential for connected and automated vehicles," in *SAE Technical Paper*, SAE International, 04 2019.

[5] H. He and L. Jin, "A historical review of the us vehicle emission compliance program and emission recall cases," *White paper*, April 2017.

[6] "Co2 emission standards for cars and vans: Council confirms agreement on stricter limits." `https://www.consilium.europa.eu/en/press/press-releases/2019/01/16/co2-emission-standards-for-cars-and-vans-council-confirms-agreement-on-stricter-limits/`, 01 2019. [Online; accessed 02-March-2020].

[7] A. Bandivadekar and T. Dallmann, "India bharat stage vi emission standards," report, The International Council on Clean Transportation, 04/22 2016. [Online; accessed 03-March-2020].

[8] "Vehicle and fuel emissions testing: Dynamometer drive schedules." `https://www.epa.gov/vehicle-and-fuel-emissions-testing/dynamometer-drive-schedules`, 2017. [Online; accessed 03-March-2020].

[9] B. Degraeuwe and M. Weiss, "Does the new european driving cycle (nedc) really fail to capture the nox emissions of diesel cars in europe?," *Environmental Pollution*, vol. 222, pp. 234 – 241, 2017.

[10] "Information about the emissions performance of vehicles of the mercedes-benz

cars group in real driving on the road.." https://www.mercedes-benz.com/en/vehicles/rde/. [Online; accessed 03-March-2020].

[11] "Real-driving emissions test procedure for exhaust gas pollutant emissions of cars and light commercial vehicles in europe," report, INTERNATIONAL COUNCIL ON CLEAN TRANSPORTATION, January 2017. [Online; accessed 03-March-2020].

[12] "Nextcar." https://arpa-e.energy.gov/?q=arpa-e-programs/nextcar, 2016. [Online; accessed 29-Feb-2020].

[13] "MicroAutoBox II." https://www.dspace.com/en/inc/home/products/hw/micautob/microautobox2.cfm, 2020. [Online; accessed 04-March-2020].

[14] "ControlDesk." https://www.dspace.com/en/inc/home/products/sw/experimentandvisualization/controldesk.cfm#143_25525, 2020. [Online; accessed 04-March-2020].

[15] A. Sciarretta and L. Guzzella, "Control of hybrid electric vehicles," *IEEE Control Systems Magazine*, vol. 27, pp. 60–70, April 2007.

[16] Z. Lei, D. Qin, P. Zhao, J. Li, Y. Liu, and Z. Chen, "A real-time blended energy management strategy of plug-in hybrid electric vehicles considering driving conditions," *Journal of Cleaner Production*, vol. 252, p. 119735, 2020.

[17] S. Stockar, V. Marano, M. Canova, G. Rizzoni, and L. Guzzella, "Energy-optimal control of plug-in hybrid electric vehicles for real-world driving cycles," *IEEE Transactions on Vehicular Technology*, vol. 60, pp. 2949–2962, Sep. 2011.

[18] S. Xie, X. Hu, S. Qi, and K. Lang, "An artificial neural network-enhanced energy management strategy for plug-in hybrid electric vehicles," *Energy*, vol. 163, pp. 837 – 848, 2018.

[19] H. Lee, J. Jeong, Y.-i. Park, and S. Cha, "Energy management strategy of hybrid electric vehicle using battery state of charge trajectory information," *International Journal of Precision Engineering and Manufacturing-Green Technology*, vol. 4, no. 1, pp. 79–86, 2017.

[20] C. Zhang and A. Vahid, "Real-time optimal control of plug-in hybrid vehicles with trip preview," in *Proceedings of the 2010 American Control Conference*, pp. 6917–6922, June 2010.

[21] J. A. Chekan and S. Bashash, "Dynamic programming-based approximate real-time control policies for plug in hybrid electric vehicles," in *2017 IEEE Conference on Control Technology and Applications (CCTA)*, pp. 205–210, 2017.

[22] X. Sun and Y. Yin, "Behaviorally stable vehicle platooning for energy savings," *Transportation Research Part C: Emerging Technologies*, vol. 99, pp. 37 – 52, 2019.

[23] V. Milanés, S. E. Shladover, J. Spring, C. Nowakowski, H. Kawazoe, and M. Nakamura, "Cooperative adaptive cruise control in real traffic situations," *IEEE Transactions on Intelligent Transportation Systems*, vol. 15, pp. 296–305, Feb 2014.

[24] L. Bertoni, J. Guanetti, M. Basso, M. Masoero, S. Cetinkunt, and F. Borrelli, "An adaptive cruise control for connected energy-saving electric vehicles," *IFAC-PapersOnLine*, vol. 50, no. 1, pp. 2359 – 2364, 2017. 20th IFAC World Congress.

[25] D. R. Lopes and S. A. Evangelou, "Energy savings from an eco-cooperative adaptive cruise control: a bev platoon investigation," in *2019 18th European Control Conference (ECC)*, pp. 4160–4167, 2019.

[26] B. McAuliffe, M. Lammert, X.-Y. Lu, S. Shladover, M.-D. Surcel, and A. Kailas, "Influences on energy savings of heavy trucks using cooperative adaptive cruise control," in *WCX World Congress Experience*, SAE International, apr 2018.

[27] S. Tsugawa, S. Kato, and K. Aoki, "An automated truck platoon for energy saving," in *2011 IEEE/RSJ International Conference on Intelligent Robots and Systems*, pp. 4109–4114, 2011.

[28] M. Hovgard, O. Jonsson, N. Murgovski, M. Sanfridson, and J. Fredriksson, "Cooperative energy management of electrified vehicles on hilly roads," *Control Engineering Practice*, vol. 73, pp. 66 – 78, 2018.

[29] N. Stroe, S. Olaru, G. Colin, K. Ben-Cherif, and Y. Chamaillard, "Time-varying mpc-based energy management for hev including engine stop start," in *2016 20th International Conference on System Theory, Control and Computing (ICSTCC)*, pp. 790–795, 2016.

[30] D. Baker, Z. Asher, and T. Bradley, "Investigation of vehicle speed prediction from neural network fit of real world driving data for improved engine on/off control of the ecocar3 hybrid camaro," in *WCX™ 17: SAE World Congress Experience*, SAE International, mar 2017.

[31] J. Fu, S. Song, Z. Fu, and J. Ma, "Real-time implementation of optimal control considering gear shifting and engine starting for parallel hybrid electric vehicle based on dynamic programming," *Optimal Control Applications and Methods*, vol. 39, no. 2, pp. 757–773, 2018.

[32] P. Geng, R. Furey, and A. Konzack, "Calculation of heating value for gasoline containing ethanol," may 2010.

[33] N. Rama, H. Wang, J. Orlando, D. Robinette, and B. Chen, "Route-optimized energy management of connected and automated multi-mode plug-in hybrid electric vehicle using dynamic programming," in *WCX SAE World Congress Experience*, SAE International, apr 2019.

[34] J. Pi, Y. Bak, Y. You, D. Park, and H. Kim, "Development of route information

based driving control algorithm for a range-extended electric vehicle," *International Journal of Automotive Technology*, vol. 17, no. 6, pp. 1101–1111, 2016.

[35] N. Guo, J. Shen, R. Xiao, W. Yan, and Z. Chen, "Energy management for plug-in hybrid electric vehicles considering optimal engine on/off control and fast state-of-charge trajectory planning," *Energy*, vol. 163, pp. 457 – 474, 2018.

[36] C. Morgan, D. Robinette, P. Santhosh, and J. Bloom-Edmonds, "Utilization of vehicle connectivity for improved energy consumption of a speed harmonized cohort of vehicles.," in *WCX SAE World Congress Experience*, SAE International, apr 2020.